Interpretation of UV ion mobility spectra by coupling to time-of-flight mass spectrometry

Zur Erlangung des akademischen Grades eines

Dr.rer.nat.

vom Fachbereich Bio- und Chemieingenieurwesen der Universität Dortmund
genehmigte Dissertation

vorgelegt von

Dipl.-Chem. Fang Li

aus

Changsha, V.R.China

Tag der mündlichen Prüfung: 01.02.2005

1. Gutachter: Prof. Dr. A. Manz

2. Gutachter: Prof. Dr. M. Spiteller

Dortmund 2005

Contents

Abstract

As shown by theoretical and experimental results in this thesis, a carefully designed UV-IMS[PID] coupling with oa-TOFMS was successfully self set up. It offers high transmission, simple spectrum, high speed and it is able to record the whole mass spectrum quasi simultaneously. These features make it attractive to identify ions, fragments or ion clusters in IMS and to conduct high-throughput molecular analysis of large libraries for compound confirmation and purity assessment.

By simulation with SIMION v. 7.0 it was proved that the configuration of the three stage differential pump system and the Einzel lens was suitable for an orthogonal design of an interface between atmospheric pressure and the TOFMS. The pinhole interface system to the UV-IMS [PID]-TOF was characterized by studying a two and a three stage interface. They are optimized and proved to be able to identify ions that has been ionized in IMS.

This device has been proved to have unique benefits for volatile organic compounds analysis. The utility of the UV-IMS[PID]-TOF for high-speed and high throughput analysis of different groups of chemicals, including ketones, alcohols and aromatics were studied. The detection limits are in the range of 0.8 µg/L for acetone, 8.6 µg/L for ethanol and 17.2 µg/L for benzene with direct permeation sampling. The instrument has a dynamic range of about 3 decades for all detected compounds. A wide range of applications including chemical weapon simulation substances detection as well as fungal analysis were achieved with this device. It yields simple spectra that facilitate analysis.

Compared the results of TOF spectra with UV-IMS spectra, most VOCs appearing in UV-IMS are monomer or protonated monomer ions. For the selected ketones from acetone to nonanone, the most abundant ions are protonated molecular ions and beginning from hexanone, the fragmentation is evident and can be detected in IMS. In the case of selected alcohols, not all of them have base peak corresponding to protonated molecule ions. Some of them such as 3-methyl-2-butanol and 2-hexanol the fragment ion are most abundant. These two groups of compounds all have obvious water adducts peaks because of high proton affinities. For aromatic substances the major ion is the molecular ion.

1. <u>Introduction</u>

1.1. Ion mobility spectrometry

Ion mobility spectrometry has been used for over 30 years since it was first introduced by Cohen und Karasek [1] in 1970 under the name plasma chromatography. It became commonly viewed as a technique for the selective detection of organic compounds [2,3] in the gas phase at ambient pressure. Separation is achieved through differences in mobility of ions under constant electric field and against the flow of neutral gas. Ions are formed typically by chemical ionizations initiated with reactant ions formed from radioactive ^{63}Ni β-emission. But because the principles of ion molecule chemistry and ion behavior at ambient pressure were poorly understood at that time, after first enthusiasm it developed slowly. Between 1980 and 1990s an interest in ion mobility spectrometer (IMS) was renewed, great advances in technology, design and commercialization took place. IMS has evolved into an inexpensive and powerful technique for the sensitive detection of many trace compounds such as chemical warfare agents [4], drugs of abuse [5,6], explosives [7-11] and anesthetics [12]. IMS has some unique advantages as an industry and on-site process analyzer compared to different organic molecular-based analytical techniques with respect to size, weight, power consumption and information density. It is a comparably inexpensive and compact technique, and it is extremely sensitive to many compounds at ng/L levels. In addition, IMS has continuous real time monitoring capabilities. It was used to characterize a number of wood species [13], halogenated hydrocarbons in nitrogen and in air which is of high interest for industrial and environmental applications [14,15], organophosphorus compounds [16], nicotin [17], and ammonium [18], suphur hexafluoride (SF_6) in insulated switchgears in high voltage substations [19,20], the waste gas of polymeres in semiconductive industry [21], ethanol in beer and in yeast fermentation [22] and fresh herbs detection [23]. IMS was applied in microbial and biological field too, different bacteria [24-27] were detected. Also inorganic substances including alkali salts [28] and other metal salts (Al, Mn, Pb, La, Sr et al.) [29] can be detected and separated efficiently.

Most of the ion mobility spectrometers use radioactive material like ^{63}Ni as ionization source [30-33], which is favored due to its simplicity, stability and convenience. This source has deficiencies in limited linear range, inflexible selectivity and regulatory

requirements associated with radioactive material. In recent years non-radioactive ion sources are of special interest. Including UV lamps [34-36] (ionization energy as 10.6 eV). It is a primary ionization source and consequently its linear range is not limited by reactant ion concentration, secondly, ion mobility spectra created via photoionization contain no reactant ions peak, so the complete mobility spectrum can be used for monitoring product ions. This feature is especially important for small ions with drift times near to those of the reactant ions. Corona or partial discharges [37-39] providing higher signal intensity than other sources, leading to a good sensitivity, laser ionization [40-42] and surface-ionization [43,44] are also used in recent years. With the development of electrospray ionization [45-47] for IMS, high molecular weight and non-volatile compounds could easily be analyzed, which is especially useful for biological mixtures.

Early IMS instruments from the 1970s were desk-size units and now the miniaturized IMS is a palm-size analyzer with the same analytical features compared to the normal IMS. Although the original mini-IMS was a redesign of conventional IMS technology, efforts are underway in several laboratories to make IMS analyzers on chips. Eiceman et al. developed a novel micromachined high field asymmetric waveform IMS, which has a $3 \times 1 \times 0.2$ cm^3 rectangular drift tube and a planar electrode configuration, detection of toluene at concentration as low as 100 ng/L has been demonstrated [48, 49]. Another miniaturized IMS was designed in ISAS - Institute for Analytical Sciences and G.A.S. Gesellschaft fuer Analytische Sensorsysteme mbH, Dortmund, Germany, with the use of microstructure techniques. The total length of drift unit is 6 cm and the total gas volume inside the device is 0.26 cm^3 [50].

1.2. Time-of-flight mass spectrometry

Among all types of mass analyzers, the outstanding features of time-of-flight mass spectrometers (TOFMS) were already revealed by Willey and McLaren [51]. They provide fast response and high ion transmission efficiency, all the ions over the whole m/z range can be detected almost simultaneously, in a time of less than milliseconds without scanning. A second feature is that the entire mass spectrum can be recorded from each ion packet, their mass range is unlimited, which is the great advantage for the analysis of biologic macromolecules The construction of a TOF instrument is

comparatively straightforward and inexpensive. But progress of TOF during the first decades after their advent was hindered also by the fact that their resolution and sensitivity were inferior to those of the static instruments. This was partially due to the poor level of radio frequency and pulsed technology at the time.

The construction of a TOF analyzer has been published in 1946 by Stephens [52]. The principle of TOF is quite simple: ions of different mass to charge ratio (m/z) are dispersed in time during their flight along a field-free drift path of known length. Soon increasingly useful TOF instruments were constructed [53,54] leading to their first commercialization by Bendix in the middle 1950s. These first generation of TOF instruments were designed for gas chromatography-mass spectrometry (GC-MS) coupling [55,56]. Their performance was poor compared to modern analysers, but the specific advantage of TOF over the competing magnetic sector instruments was the rate of spectra per second they were able to deliver. In GC-MS the TOF analyser soon became superseded by linear quadrupole analysers and it took until the late 1980s for their revival [57, 58].

During 1980s, at least two groups independently developed orthogonal acceleration TOFMS (oa-TOFMS), which effectively eliminates the initial kinetic energy distribution or, more precisely, the velocity distribution along the TOF axis by orthogonal acceleration of the ions in a focused ion beam. Dawson and Guilhaus [59] introduced this approach to improving the mass resolution and duty cycle for a TOF with an electron impact (EI) ion source. Ions were collimated by an electrostatic lens system and injected into an ion storage area. The ion extraction and acceleration fields then provide space focusing to the detector in a linear TOF analyzer. The predicted resolving power for the device was $m/\Delta m \approx 3800$ (FWHM). Dodonov and coworkers [60] coupled reflecting oa-TOFMS to an electrospray ionisation source (ESI) - an ion source of rapidly increasing usefulness in biomolecular analytical chemistry to achieve a resolving power of $m/\Delta m \approx 2000$ (FWHM). The work of both groups was influential in the development of a range of commercial oa-TOFMS instruments. Recently, numerous other ESI-TOF instruments have been constructed [61]. Important developments have included collisional cooling, tandem instruments, and application of similar techniques to MALDI. In addition to electrospray, orthogonal injection has been used with other types of continuous ionization, including ions from

flames [62], liquid SIMS [63], a cluster ion source [64] atmospheric pressure ionisation [65] and inductively couple plasma [66].

1.2.1. Ionization methods

Electron ionization (EI) is most useful for compounds below a molecular weight of 1000 Daltons since larger molecules tend to thermally degrade during vaporization. While electron ionization is one of the most widely used methods of ionization in mass spectrometry, the principal problem associated with it include excessive fragmentation in the ionization source, the involatility of large molecules and thermal decomposition during vaporization.

For macromolecules, fast atom bombardment (FAB) ionization [67] is very successful for the analysis of highly polar, low-volatility compounds but has the disadvantage of producing a large amount o fragmentation. Plasma desorption [68] and secondary ionization (SIMS) [69] followed. Electrospray Ionization (ESI) [70] is one of the most exciting ionization techniques which generates ions directly from solution (usually an aqueous or aqueous/organic solvent system) by creating a fine spray of highly charged droplets in the presence of a strong electric field (typically 3.5 kV). ESI allows for very sensitive analysis of small, large and labile molecules such as peptides, proteins, organometallics, oligosaccharides, and polymers, and it has made liquid chromatography mass spectrometry routine.

Matrix-assisted laser desorption/ionization (MALDI) [71] has its biggest impact on the field of protein research. The efficient and directed energy transfer during a matrix-assisted laser-induced desorption event provides high ion yields of the intact analyte, and allows the measurement of compounds with high accuracy and sub-picomole sensitivity. In MALDI analysis, the analyte is first co-crystallized with a large molar excess of a matrix compound, usually an UV-absorbing weak organic acid, after which pulsed UV laser radiation of this analyte-matrix mixture results in the vaporization of the matrix which carries the analyte with it. The matrix therefore plays a key role by strongly absorbing the laser light energy and causing, indirectly, the analyte to vaporize. The matrix also serves as a proton donor and receptor, acting to ionize the analyte in both positive and negative ionization modes, respectively. It is interesting to notice that the rediscovery of the time delayed-extraction (DE) method

has made substantial improvements to the MALDI TOFMS in the last ten years, mass resolving power more than 25000 with orthogonal extraction was reported.

Atmospheric pressure chemical ionization (APCI) [72] is widely used in the pharmaceutical industry to analyze relatively nonpolar, semi volatile samples of less than 1200 Daltons and it is an especially good ionization source for liquid chromatography. The APCI source contains a heated vaporizer which facilitates rapid desolvation/vaporization of the droplets. Vaporized sample molecules are carried through an ion-molecule reaction region at atmospheric pressure. The ionization occurs through a corona discharge, creating reagent ions from the solvent vapor. Chemical ionization of sample molecules is very efficient at atmospheric pressure due to the high collision frequency. Proton transfer (protonation MH^+ reactions) occurs in the positive mode, and either electron transfer or proton transfer (proton loss, $[M-H]^-$) in the negative mode.

It is undoubtedly that TOFMS is employed mainly in biophysics, biochemistry and biomedicine, which require analysis of large, thermally unstable molecules with masses reaching millions of Daltons. But due to some basic features, such as high transmission, relatively simple structure, high speed and its ability to record the whole mass spectrum quasi simultaneously, it is attractive to couple it to IMS to identify ions, fragments or ion clusters in IMS for a thorough understanding of an IMS measurement.

1.3. Ion mobility spectrometry / mass spectrometry

IMS use a Faraday plate as detector, that is, ions are detected as they strike the metal plate and induce a current. Faraday plate detection is simple, inexpensive and can be used for both positive and negative ions. Unfortunately, such detection does not afford qualitative information of ions other than the structure information (average collision cross-section). Because of this, coupling IMS with mass spectrometers has been tried since early in IMS development, most of the limited IMS-MS work before 1980s was performed with the commercial instrument supplied by PCP (West Palm Beach, FL, USA). The instrument consists of a ^{63}Ni IMS interfaced with a quadrupole mass spectrometer, the IMS equiped with two gates in drift tube. Mass identification of individual IMS peaks could be achieved by operating the instrument with both

gates continuously opening, in such a mode that only ions of a desired drift time could pass into the mass spectrometer. The mass spectrometer would then be tuned to a specific mass to charge ratio (m/z) [73,74], which is a tedious task and not all the ions can be detected at one time. With this kind of instrument benzene [75], isomeric dihalogenated benzene [76], p-nitrophenol [77] and dimenhydrinate [78], illicit drugs [79,80], were measured and the mass identification of the ionic species associated with the peaks in the ion mobility spectra was achieved.

In the 1990s, the coupling work continued but with self constructed instrument. Hill et al. designed and constructed an in- house electrospray IMS interfaced with a quadrupole mass spectrometer [81,82]. The instrument was used successfully for the study of chemical warefare agents [83,84], isomeric peptides [85,86] and illicit drug [87]. Recently, time-of-flight mass spectrometers coupled to IMS was developed by them and phenylthiohydantoin amino acids [88] was measured. Guevremont combined ion mobility/time-of-flight mass spectrometry and electrospray-generated proteins were investigated [89]. Later, electrospray ionization/high-field asymmetric waveform ion mobility spectrometry/mass spectrometry [90-92] was produced, ppt levels of chlorate, bromate, and iodate [93], perchlorate in water matrices and human urine [94,95], chlorinated and brominated haloacetic acids [96], microcystins [97], tryptic digest of pig hemoglobin [98], trypic peptides [99,100], amphetamine, methamphetamine, and their methylenedioxy derivatives in Urine [101] were detected. Clemmer et al. designed an IMS-MS instrument with a quadrupole mass spectrometer for characterization of oligosaccharides and proteins [46,102]. Later, they constructed an IMS-MS instrument with a time-of-flight mass spectrometer to study biomolecules [103-106], where liquid chromatograph separation was used before IMS-TOF detection of peptides [107,108]. But their IMS is operated in vacuum.

IMS-TOFMS instrument with a high-pressure matrix-assisted laser desorption ionization source was developed in Ionwerks (Houston, TX, USA), and oligonucleotide and peptide were measured [109,110]. They also designed a Fourier-transform ion cyclotron resonance mass spectrometer - ion mobility spectrometer [111].

Although so much work has been done in IMS-MS, in these instances, interests have been with electrospray sources and low pressure drift tubes with applications for

biomolecules rather than for use in general analytical IMS. Only Hill et al. [112] used a traditional ionization source (radioactive nickel (Ni-63) beta emission ionization) ion mobility spectrometer coupled with an orthogonal reflector time-of-flight mass spectrometer (IMS(tof)MS) to detect chemical warfare agent (CWA) simulants recently. Except Syagen Technology. Inc. (Tustin, CA, USA) who has developed an atmospheric pressure photoionization (APPI) quadropole ion trap time-of-flight mass spectrometer [113], till now there is little mass spectrometry technique using a photoionization source at atmospheric pressure, while there have been a lot of photoionization IMS [114-116]. Therefore coupling UV-IMS to mass spectometer is crucial to understand the complex chemistry occurring in the ionization source and drift tube and the formation of clusters leading to uncertainties in the assignment of ions traversing the drift tube. The recent development of IMS with time-of-flight (TOF) instruments has demonstrated that the time compatibility (IMS milliseconds and TOFMS microseconds) of the two techniques enables rapid two-dimensional separations to be performed, and simplicity of TOFMS instrumentation.

1.4. Objective of this work

The aim of this work is to set up an UV-IMS-TOFMS system. The most important part is the interface between high vacuum and UV-IMS at atmospheric pressure, it is a set of compromises on ion yield and vacuum performance. Studies will be proceeded using pinhole and a differentially pumped interface. The UV-IMS was made in ISAS using a 10.6 eV UV lamp. An orthogonal extraction linear time-of-flight mass spectrometer will be constructed accordingly in our laboratory. The complete construction was set up by helping of simulation with SIMION v.7 for ion trajectories from the drift tube through the interface to TOF. The ability of the mass spectrometer to identify ions and results from models and laboratory verifications will be presented in detail.

The UV-IMS-TOFMS is intended to be used to measure different organic groups which are volatile organic compounds usually detected by UV-IMS such as ketones, alcohols, aromatics, in order to thorough understand the IMS measurements. Successful interpretation of UV ion mobility spectra by using the coupling of an UV-IMS to a TOF can be accomplisched only with the accurate instrumentation of TOF and interface system. The results will be proved by simulation and experiments of

self-build TOF and interface system.

Additionally, real analyte including gasoline and fungi should be tested by the UV-IMS-TOFMS. UV-lamp in this work is 10.6 eV. There is minimal fragmentation to clutter the mass spectrum and predominant molecular ion signal for most substances. This performance feature benefits special for the analysis of mixtures and samples in complex matrices.

2. <u>Fundamental principles</u>

2.1. Ion mobility spectrometry

2.1.1. General construction of ion mobility spectrometry

The term ion mobility spectrometry refers to the method of characterizing chemical substances using gas-phase mobilities of ions in weak electric fields. A typical ion mobility spectrometer comprises an ionization source (conventionally ß-emitter sources, UV-lamp, corona discharge) associated with the ion reaction region, an ion drift region, where separation of the ions occur. The reaction and drift region are separated by a shutter grid - a Bradbury-Nielsen-shutter [117], and an ion collector - a Faraday plate to measure the ion current. A biased aperture grid is placed closed to the Faraday plate in order to increase detection efficiency and to filter out the noise caused by the pulse on the gate, thus to improve the signal-to-noise ratio. An illustration of the basic construction of an ion mobility spectrometer with reaction and drift region and main gas flow directions is presented in Fig. 2-1.
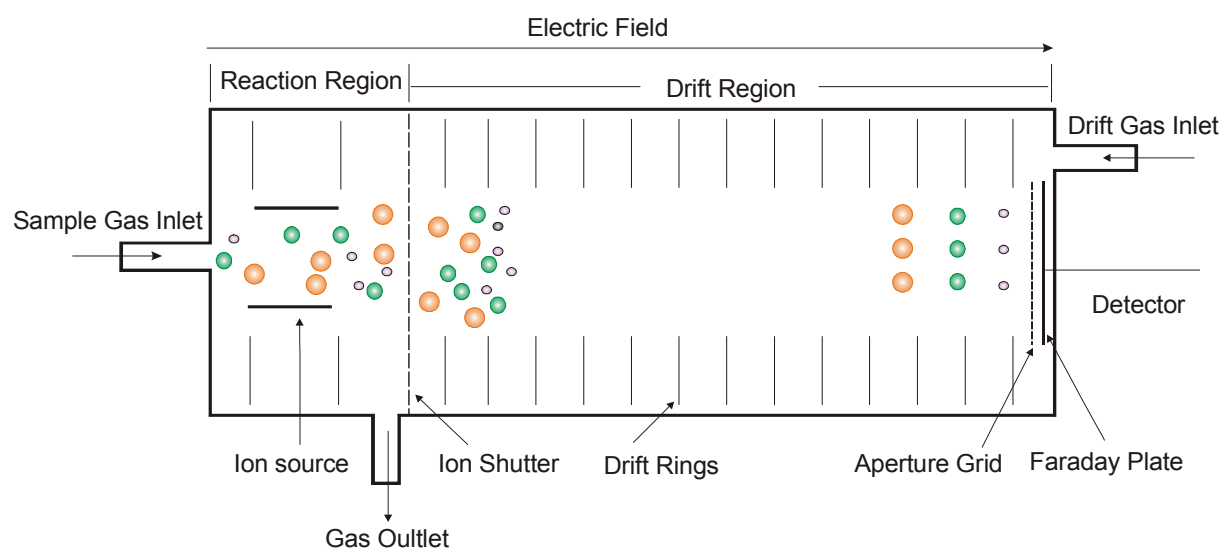
Fig. 2-1 Schematic diagram of the working principle of IMS

A flow of carrier gas, normally air or nitrogen, set at 100 to 200 mL/min, entered the cell from the front end of the reaction region while a flow of a purified drift gas, set at 200 to 300 mL/min entered the drift region from the back end of the drift tube. Both gas flows were exhausted through an exit vent in front of the ion shutter. The carrier gas served as a means transporting the sample molecules into the ionization source. Ions formed initially experience a series of ion molecular reaction in reaction region and then are injected into the drift region by means of a shutter grid pulse. In the drift

region, the ions moves through a drift gas under the influence of an external electric field E, in the range of 100 to 350 V/cm, at last reach the Faraday plate to be detected.

2.1.2. Ion mobilities in gas

Ion mobilities are characteristic of substances and can provide a means for detecting and identifying vapors. In an ion mobility spectrometer, ions strike Faraday plate and mobility spectrum or plot of detector current i (in pA or nA) vs. t_d (in ms) is produced. Consequently, the basis for selectivity in IMS is difference in drift times. For a drift region with a given length, L_d (cm), the drift time t_d of an ion is related to velocity v_d (cm/s), electric field E (V/cm) and ion mobility K (cm^2/Vs) through equations 1 and 2 [118, 119]:

$$v_d = \frac{L_d}{t_d},$$

2-1

$$K = \frac{v_d}{E} = \frac{L_d}{t_d * E}.$$

2-2

Therefore, while increasing the electric field strength will increase the average velocity of the ions. Ion mobility K is inversely proportional to the drift time t_d. In the drift tube an ion is accelerated by the field until it collides with a gas molecule and loses part, or all, of its acquired momentum, only to be accelerated once more and to collide again. So mobility is a combined property of the ion and the drift gas, this is known as the Mason-Schamp equation [118]:

$$K = \frac{3\,Ze}{16\,N} \sqrt{\frac{1}{m} + \frac{1}{M_m}} \sqrt{\frac{2\pi}{k_b T}} \frac{1+\alpha}{\Omega},$$

2-3

where Ze is the ionic charge, N is the number density of drift gas, m is the analyte ion mass and M_m the drift gas molecular mass, k_b is the Boltzmann constant, T is temperature in drift tube, α is a correction term which is less than 0.02 when m>M, and Ω is the collision cross section of the ion. This relationship holds at the low electrical field. So mobility K is unique at a fixed temperature for a given combination of an ion and a neutral gas molecule. In a given gas, the mobility of small ions is largely controlled by the reduced mass, however, mobility depends on the collision cross section (ion structure) when ions are comparatively large. This can be

exemplified for amines where mobilities increase in the trend: linear < branched, primary < secondary < tertiary, aliphatic compounds < aromatic compounds, and amines < amides [120].

Because the ion mobility is dependent upon temperature T (in Kelvin) and pressure P (in kPa), it is nomalized to reduced mobility K_0 using

$$K_0 = K\left(\frac{p}{p_0}\right)\left(\frac{T_0}{T}\right)$$

2-4

where p_0 = 101,3 kPa and T_0 = 273 K.

2.1.3. UV photoionization method

2.1.3.1. UV lamps

In low pressure gas discharge lamps, a glow discharge excites nature resonance frequency of the fill gas, producing special emission lines down to short wave cut-off of the window material. The gas discharge is confined to a capillary within the lamp. A power supply and a series resistors power the lamp. Lamp operation occur when the breakdown threshold of the fill gas is exceeded, usually on the order of -1000 to -1299 Volts DC. The series resistor limits the current of the lamp to a reasonable operating level. The spectral output of the lamp is determined by the fill gas and the transmission characteristic of window material. The gases used most frequently are xenon (8.4eV, sapphire), krypton (10 eV or 10.6 eV, MgF_2), argon (11.7 eV, LiF). the wavelength (in meter) and the eV rating are associated through Planck's constant

$L_m = 1.2395*10^{-6}$ / eV

2-5

The main advantage of photoionization sources is that by choosing the appropriate wavelength, the species of interest can be selectively ionized, there is little fragmentation, as shown in Fig. 2-2, thus simplifying the mobility spectrum and data acquisition. In this work 10.6 eV UV-lamp (116.9 nm) was chosen because the ionization energy of most volatile organic compounds are below it and the lifetime of 11.7 eV is because of the influence of the humidity on the transmission of LiF window too short.
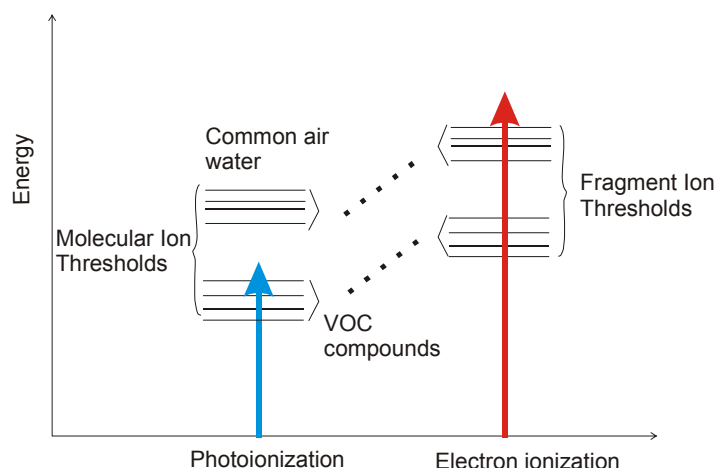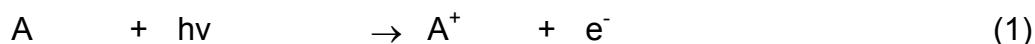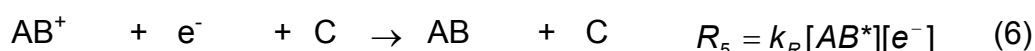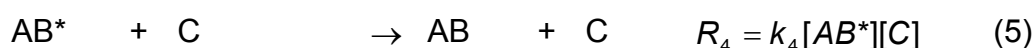
Fig. 2-2 Comparison of photoionization threshold with that of electron ionization

2.1.3.2. Photoionization process.

When the ionization energy of molecule A is under the UV lamp output energy, the molecule will absorb the photo energy and emit an electron.

$$A \quad + \quad h\nu \quad \rightarrow A^+ \quad + \quad e^- \tag{1}$$

the following process can take place too, at first the molecule AB will be excited (2), excited analytical molecule will according to equation (3) lose a electron to be ionized, dissociate to neutral fragment (4) or become quenched through collision with neutral gas molecules (5). In addition the ion can recombine with electron (6), [121, 122]:

$$AB \quad + \quad h\nu \quad \rightarrow AB^* \qquad \qquad R_1 = I^0 - I \tag{2}$$

$$AB^* \qquad \qquad \rightarrow AB^+ \quad + \quad e^- \quad R_2 = k_2[AB^*] \tag{3}$$

$$AB^* \qquad \qquad \rightarrow A \quad + \quad B \quad R_3 = k_3[AB^*] \tag{4}$$

$$AB^* \quad + \quad C \qquad \rightarrow AB \quad + \quad C \quad R_4 = k_4[AB^*][C] \tag{5}$$

$$AB^+ \quad + \quad e^- \quad + \quad C \rightarrow AB \quad + \quad C \quad R_5 = k_R[AB^*][e^-] \tag{6}$$
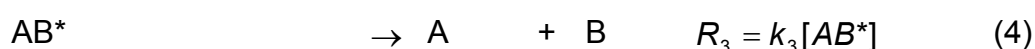
Where *AB* is analytical molecule, *AB** is excited molecule, *[AB]* the concentration of analytical molecule *AB, C* neutral gas molecule, *[C]* the concentration of *C, I⁰* and *I* are incident and transmitted photo intensity respectively, I^0-I the absorbed photo intensity, and *k* rate constant and *R* reaction rate.

The possibility for a molecule to absorb photo is dependent on the absorption cross section of molecule *AB* according to Lambert-Beer-law:

$$I = I^o \exp(-sN_0[AB]L) \tag{2-6}$$

where L_i is the length of the ionization room and N_0 is Avogadro constant.

The ionization probability is expressed by the so called photoionization efficiency η:

$$\eta = \frac{k_2}{k_2 + k_3 + k_4}$$ 2-7

It is the ratio of the number of analytical molecule ion to the whole number of excited molecules. Recombination of the ions will be impeded by the high electric field in IMS, the current i that the Faraday-plate detected in an IMS can be described:

$$i = I^0 \eta s N_0 F L_i [AB]$$ 2-8

where F is the corresponding Faraday constant. Thus the current i is proportional to ionization efficiency, Absorption cross section and to the concentration of analytical molecule AB. ηs is described as photoionization cross section, it demonstrates the probability that a molecule will absorb photo and then be ionized.

It should be noted that in the presence of water vapor or protic solvent, which is normal in IMS working conditions, the molecular ion can extract H to form MH^+. This tend to occur if M has a high proton affinity. This does not affect quantitation accuracy because the sum of M^+ and MH^+ is constant. Polar compounds are usually observed as MH^+, whereas nonpolar compounds usually form M^+.

2.2. Time-of-flight mass spectrometry

2.2.1. Principle and instrument of linear time-of-flight mass spectrometer

A linear time-of-flight mass spectrometer consists of an ion modulator, an ion accelerator, a field-free drift tube and an ion detector, as shown in Fig. 2-3.
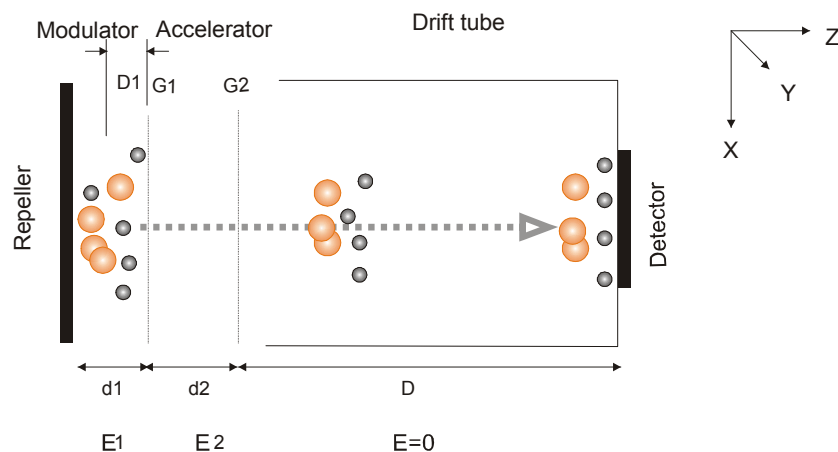

Fig. 2-3 Schematic diagram of a linear time-of-flight mass spectrometer

Ions are stored in the modulator prior to be accelated. After a voltage pulse is applied to the repeller electrode, a packet of ions moves toward the detector in Z-direction with a kinetic energy K_e, received from the extracting and accelerating fields (E_1, E_2). If an ion was rest before acceleration, the total flight time in a linear time-of-flight mass spectrometer are simply given by

$$t = t_1 + t_2 + t_D \qquad\qquad \text{2-9}$$

$$t_1 = \frac{2D_1}{\sqrt{2zD_1E_1/m}} = \sqrt{\frac{2m}{zE_1}}\sqrt{D_1} \qquad\qquad \text{2-10}$$

$$t_2 = \frac{2d_2}{\sqrt{2z(D_1E_1+d_2E_2)/m} + \sqrt{2zD_1E_1/m}} = \sqrt{\frac{2m}{z}}\frac{\sqrt{D_1E_1+d_2E_2} - \sqrt{D_1E_1}}{E_2} \qquad\qquad \text{2-11}$$

$$t_D = \frac{D}{\sqrt{2z(D_1E_1+d_2E_2)/m}} = \sqrt{\frac{m}{2z}}\frac{D}{\sqrt{D_1E_1+d_2E_2}} \qquad\qquad \text{2-12}$$

where t_1, t_2, t_D are the flight time of the ion in the modulator, the accelerator and the field-free drift tube, respectively, D_1 is the distance of the start position of the ion relative to the first grid G_1, m/z is the mass-to-charge ration of the ion, E_1 is the extracting field strength of the modulator, E_2 is the accelerating field strength, and d_1, d_2, D are the lengths of the modulator, the accelerator and the field-free drift tube respectively. In mass spectrometry it is conventional to measure resolving power by the ratio of m/Δm, in TOFMS it is convenient to work in the time domain, thus the resolving power can be measured in terms of t/Δt. Since the overall flight time t of a single-charged ion is proportional to $\sqrt{m}$, according to Eq. 2-9 to Eq. 2-12, ions of different masses $m = m_0 + \Delta m = m_0 (1 + \Delta m/ m_0)$ experience ion flight times

$$t = t_0 + \Delta t = t_0(1 + \Delta t/t_0) \propto \sqrt{m_0(1+\Delta m/ m_0)} = m_0 (1 + \Delta m/2m_0 + \ldots) \qquad\qquad \text{2-13}$$

so that in a time-of-flight mass spectrometer the mass-to-charge resolving power R_m can be expressed as:

$$R_m = \frac{m_0}{\Delta m} = \frac{t_0}{2\Delta t} \qquad\qquad \text{2-14}$$

where m_0 and t_0 are the mass and flight time for a reference ion and the finite time interval Δt is the full-width at half-maximum height of a spectral peak (FWHM). But to consider the initial conditions of the ions in a packet, Figure 2-4 illustrates the ions energy spread ΔK_e and their spatial spread Δz. In a ideal case, shown in Figure 2-4

A, the ions have no energy spread ΔK_e and start from the same position. Ions with the same mass-to-charge ratio m/z will obtain the same kinetic energy K_e, fly along the same flight path and arrive at the detector at the same time. In this case the mass resolving power of the instrument is restricted only by the data recording system. In the case of an initial spread of the Figure 2-4 B, the flight time error of the same ion due to different position can be well compensated by selecting the flight length D properly, which is called the first-order spatial focusing condition

$$D = 2zK_a^{3/2}(1 - \frac{1}{K_a + \sqrt{K_a}}\frac{d_2}{z})$$

2-15

where $K_a = (zE_1 + d_2E_2)/d_1E_1$, z is the reference start position and d_1, d_2, E_1, E_2 are the same as in Eq. 2-9 to Eq. 2-12. Considering two ions with the same initial velocity v_z, $(\Delta k_e = m\Delta v_z^2 / 2)$ however, in opposite directions, shown in Figure 2-4 C, one moves towards the repeller and is decelerated by the extraction field, E_1, until it stops. It is then re-accelerated, returning to the starting position with its original speed but in a reversed direction. Subsequently, the later motion of the ion is identical to that of the other but delayed by the "turn-around time". This "turn-around time", Δt_{turn}, can be ⌋   ⌋   ⌋ ▢ だ⌋ ⣄⌋ ⠞⣀⌋

$$\Delta t_{turn} = \frac{2\Delta v_z}{zE/m} = \frac{2m\Delta v_z}{zE}$$

2-16

where m/z is the ion mass-to-charge ratio and Δv_z is the initial velocity of the ion towards the repeller. This initial energy spread induced flight time error can not be compensated by any constant stationary electrical field. Figure 2-4 D demonstrates the common situation of ions in a modulator.
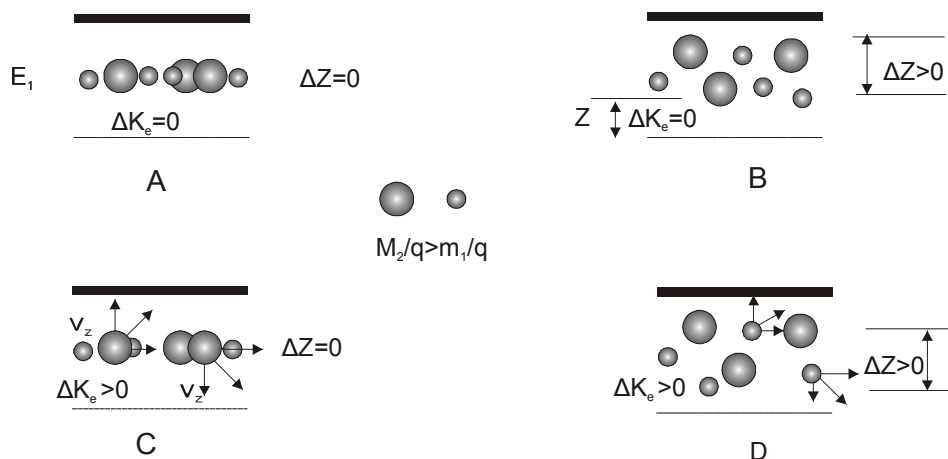

Fig. 2-4 Initial ion conditions in the ion modulator

For a linear time-of-flight mass spectrometer, the flight time error Δt is dominated by the "turn-around time", Δt_{turn}, for monoenergetic ions. To decrease this "turn-around time", the extracting field can be increased, however, the total flight time of ions will be also decreased. In order to have an adequate flight time for measuring, the length of the drift tube should be increased. As a consequence, the mass resolving power can not be increased over a few hundred with acceptable system parameters. Although several techniques were used for the design of linear time-of-flight mass spectrometers, the mass resolving powers could not be increased above ~ 3000.

2.2.2. Reflecting time-of-flight mass spectrometer

The most successful energy focusing method to date has been the "reflectron". Essentially an electrostatic ion mirror, this device creates one or more retarding fields after a drift region. These are oriented to oppose the acceleration field. Ions re-emerge from the device with their velocities reversed. More energetic ions penetrate more deeply and hence take longer to be reflected. Thus the optics can be adjusted to bring ions of different energies to a space-time focus as shown in Fig. 2-5. Usually the angle of ion entry into the mirror is adjusted slightly away from 90° so that the ions follow a different path after being turned around. The mirror has an added advantage in that it increase the drift length without increasing the size of the instrument.

For an ion which was at rest before acceleration, the total flight time in a reflecting time-of-flight mass spectrometer can be expressed by:

$$t = \sqrt{\frac{2m}{zE}}[(1-\frac{E_1}{E_2})\sqrt{D_1} + (\frac{E_1}{E_2}+2\frac{E_1}{E_3})\sqrt{D_1+\frac{d_2E_2}{E_1}} + \frac{L}{\sqrt{D_1+d_2E_2/E_1}} + 2(\frac{E_1}{E_4}-\frac{E_1}{E_3})\sqrt{D_1+\frac{d_2E_2}{E_1}-\frac{d_3E_3}{E_1}}] \qquad 2\text{-}17$$

where D_1 is the start position of the ion, m/z is the charge to mass ratio, E_1 is the extracting field strength, E_2 is the accelerating field strength, E_3 is the field strength of the first stage of the reflector, E_4 is the field strength of the second stage of the reflector, d_1, d_2, L, d_3, d_4 are the length of the ion modulator, the ion accelerator, the drift tube, the first stage of the reflector and the second part of the reflector respectively.

Fig. 2-5 Schematic view of a reflecting time-of-flight mass spectrometer
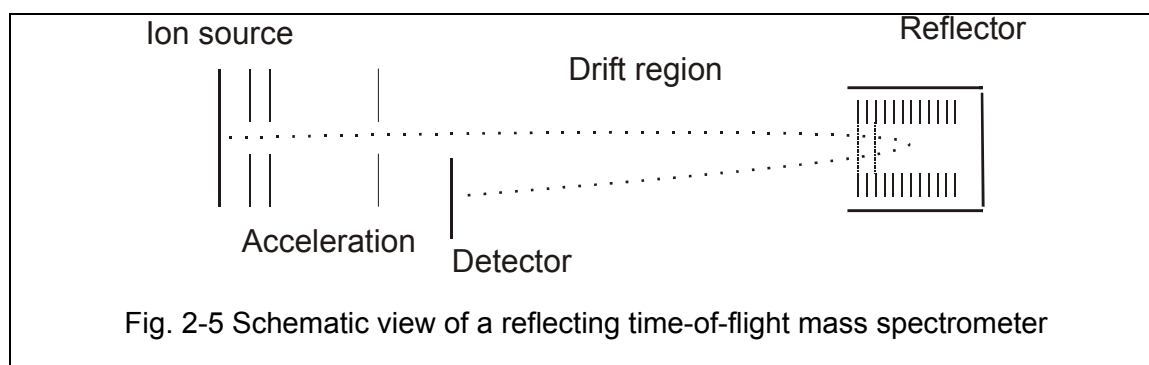
The 1970s were highlighted by a fast spread of reflectron TOF instruments, particularly after the introduction of laser-based techniques of obtaining large, thermally unstable biomolecules. Their production on an industrial scale started in 1980 with Leybold-Heraeus Co. (LAMMA-500, LAMMA-1000), Brucker Co. (TOF-1), Finnigan Mat Co. (VI-SION 2000) and others. Gridless reflectron TOF [123, 124] is preferred when in addition the transmission is taken into account, however the divergence of the ion beam in this case should be kept small. BRUCKER manufactured TOF-1 equipped with such a reflector for R= 10000 [125, 126] an obvious merit of such reflectors is not only the absence of grids but also the possibility of simultaneously focusing the reflected ions in angle, which increased the absolute sensitivity of the instrument.

2.2.3. Comparison of linear and reflector TOF

The ability of the reflector time-of-flight mass spectrometer (ReTOF) to compensate the initial energy spread of ions largely increase the resolving power of TOF instruments. But in case of metastable fragmentations, the ReTOF behaves different from the linear TOF. If fragmentation occurs between ion source and reflector, the ions were be lost by the reflector due to their change in kinetic energy. Only fragments still having kinetic energy close to that of the precursor are transmitted due to the energy tolerance of the reflector. However such ions are not detected at correct m/z , thereby giving rise to a ''tailing'' of the signal. Ion fragmenting in transit from reflector to detector are treated the same way as ions in the linear TOF. Thus above property complicate the detection of very labile analytes in the ReTOF [127].

2.2.4. Orthogonal acceleration time-of-flight mass spectrometry

The most departure of oa-TOFMS from other attempts to combine continuous ion

source with TOF is the use of a separate direction (for the TOF analysis), orthogonal to the ion beam axis of the ions source. In Fig. 2-6, the principle of an orthogonal extraction time-of-flight mass spectrometer is revealed. Initially, the repeller plate and the grid G1 are at ground potential, and the initial ion beam from an ion source outside the mass analyzer enter the ion modulator continuously in X-direction. When the modulator is filled with ions, a voltage pulse is applied to the repeller, and an ion packet is pushed into the acceleration region. This pulse should be so long that all ions in the package fly through the accelerator region and leave it. While the ion package flies through the drift tube to the ion detector, the initial DC ion beam refills the modulator. It is most important that the first stage is completely field-free in the fill-up mode. A small residual field in the fill-up region may result from penetration through G1 of the field between G1 and G2. Such fields may cause significant deflection of ion trajectories in the oa and therefore, increase the initial spatial spread of the ions. The residual field may be substantially removed by application of a relatively small positive bias potential to G1.

In an orthogonal extraction system the ion beam with finite phase space from a source can be made wide in Z-direction and thus according to Liouville's theory the ion trajectories become more parallel so that the mass resolving power is improved, on the other hand, in the orthogonal extraction system, a high efficiency can be achieved as compared to the conventional methods. In case the previous ion package is approaching the detector at the time when the initial ion beam has almost refilled the modulator, the system has the maximum transmission. Assuming that the initial ion velocity in X-direction is v_x, the length of the modulator in X-direction is b, the velocity of the ion after accelerating in Z-direction is v_z, the ion flight path is L, thus the total ion flight time

$$t = L\big/v_z \qquad\qquad\qquad 2\text{-}18$$

$$\frac{v_z}{v_x} = \sqrt{\frac{K_z}{K_x}} \qquad\qquad\qquad 2\text{-}19$$

where K_x is the initial ion energy and K_z is the ion energy after orthogonal acceleration. Also the mass spectrum repetition rate should be low enough to enable the heaviest ions of the mass M_m to fill the modulator:

$$f < v_x / b \qquad\qquad\qquad\qquad 2\text{-}20$$

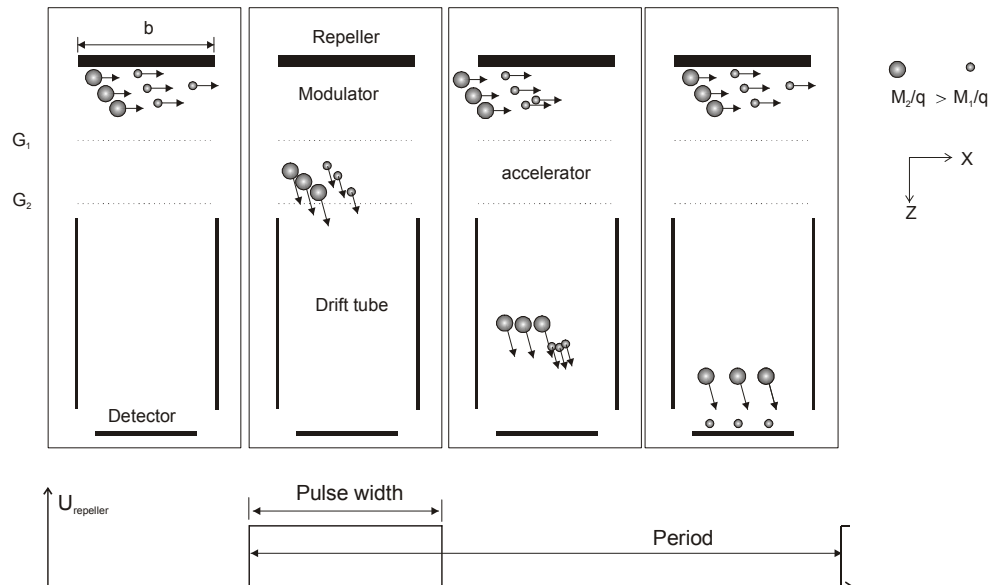where b is the length of the modulator in X-direction.

Fig. 2-6 Principle of an orthogonal extraction for time-of-flight mass spectrometer

2.2.5. Microchannel plate and the time-to-digital converter

The cascade of secondary electrons can be produced in a continuous tube, such detectors, known as channeltron is one of the most common means of detecting ions, achieving high sensitivity, which can be arranged to give gains in the range $10^5 - 10^7$. In order to increase the sensitivity and time resolution of the ion registration, detectors with large active area are used. To meet the requirements of low weight, large active area and the high timing accuracy, the microchannel plate (MCP) [128] is the best choice for particle detection at this time [129, 130]. Microchannel plate is a channel electron multiplier array that one channel is some micrometers in diameter. To avoid that the ions enter the microchannels parallel to their axis, these are inclined by some degrees from the perpendicular to the plate's surface. The gain of a MCP is 10^3 to 10^4, i. e., much more lower than that of channeltron. But in stead of a single MCP, two MCPs are often sandwiched together in such a way that the small angles oppose each other (Chevron Plate) to obtain gains of 10^6 to 10^7. Occasionally, even three MCPs are stacked analogously (z-stack, gain up to 10^8).

Ion counting devices are usually base on a multistop time-to-digital converter (TDC). These devices sense the onset of pulses (start and stop events) and store the times

or intervals between these events. Compared to the analog based method - intergrating transient recorder (ITR), it does not require a good signal peak form for a single ion, which is a great benefit for achieving high mass resolving powers. At present channel width of the TDCs were reduced to 600 ns and even 277 ps, so that the usual obtained MCP signals of widths of less than 1 ns could be registered. However, since it is difficult to extract a precise intensity information from a TDC, the slower ITR with 1 ns or 2 ns channels have their place in the TOF area.

In this work, the Chevron Plate MCP was used to obtain enough signal intensity, while compared to normal ionization source the UV-lamp is relatively weak. A 5 ns channel multiscaler was good enough for small signal acquisition and a 10 ns resolution analog to digital card was applied for high signal acquisition.

3. <u>Instrumentation</u>

3.1. Instrumental layout

An overview of the oa-TOFMS with UV ionisation source and three stage pinhole interface setup in this work is illustrated in Fig. 3-1. It consists of three parts, firstly UV-ionization room, which was made in ISAS; secondly the self-built interface system, it is composed of three pinhole system; and thirdly the self-made linear TOF mass analyser. the complete TOF mass analyser is mounted horizontally on a flange of the main vacuum vessel. The interface system and UV ionisation source are stacked above a gate valve, such a construction provides for a precise mechanical assembly and allows to remove the complete mass analyser and interface in one piece from the vacuum chamber for modification.
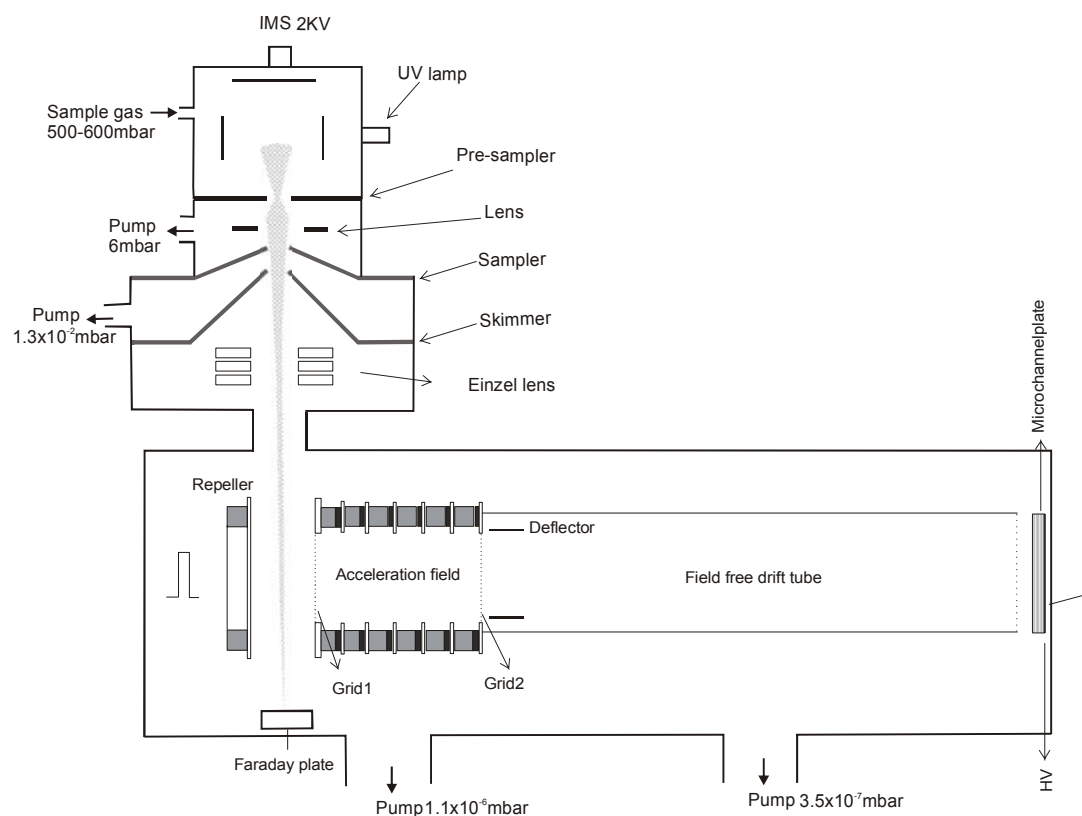
Fig. 3-1 Schematic view of the home made orthogonal extraction time-of-flight mass spectrometer with UV- ionization source and interface

For the purpose of increasing the strength of the ions and simplifying the construction, firstly only ionisation region of an UV-IMS was coupled to TOF. In order to operate later as a complete IMS, it was located directly at the end of the ionisation room a flat metal plate with a pinhole diameter 0.5 mm intended to be a Faraday

plate. It acts as the first step of vacuum system, too. The photo of the whole system is shown in Fig. 3-2.

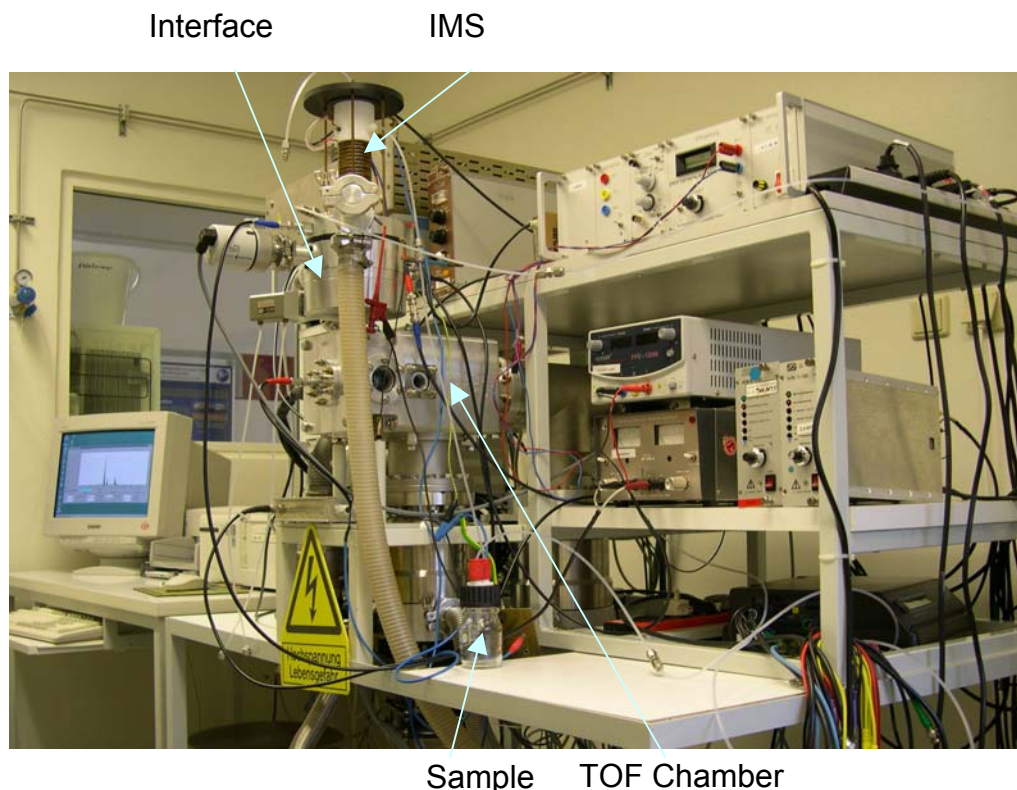Interface   IMS

Sample   TOF Chamber

Fig. 3-2 Photo of self-made UV-IMS-TOFMS

3.1.1. The principle of operation.

The sample gas is introduced into UV-IMS through a carrier gas flow of 1 L/min. The ions are produced by an 10.6 eV UV lamp which is operated at one atmosphere pressure as normal UV-IMS, then pass through a pinhole into the first vacuum stage, where the ions are focused with a lens and go through sampler and skimmer. The ions fly through a Einzel lens to become parallel into the ion modulator of oa-TOF mass analyser.

In the mass analyser, ions enter the ion modulator in X- direction. There is a Faraday plate at the opposite end of the ion modulator to monitor the ion current. When the modulator is filled with ions, the push out voltage pulses are applied to the repeller, while the grid 1 is always kept at ground potential. A package of ions is then extracted from the modulator to the accelerator. After being accelerated to an energy of 2000 eV between grid 1 and grid 2, the package of ions will fly through the field free drift tube. In order to adjust the ion trajectory two piece of deflecting plates were mounted on the entrance of the drift tube. A Chevron micro channel plate [128] is

used for the ion detection.

The main working parameters of the instrument are shown in Table 3-1.

Table 3-1 System parameters for instrumentation

| UV ionisation source	Value / Unit
UV-Lamp	10.6 eV
Voltage of ionisation region	2 kV
Carrier gas flow	1 L/min
Interface system	
Pre-sampler	30 V
Lens	150 V
Sampler	104-120 V
Skimmer	0 V
Einzel lens	30 V
TOFMS	
Repeller	350 V
Repeller offset	50.6 V
Pulse width	1 µs
Frequency	20 kHz
Deflector up and down	280 / -320 V
Grid 1	0 V
Acceleration voltage	-2 kV
Microchannel plate	-1.75 kV
Geometry parameters	
Pre-sampler	Φ 0.5 mm
Sampler	Φ 0.25 mm
Skimmer	Φ 0.4 mm
Repeller	Φ 90 mm
Average ion start position from grid 1	3 mm
Acceleration length	32 mm
Free length	480 mm
Vacuum parameter	
In IMS	960 mbar
First stage	~ 6 mbar
Second stage	1.4×10^{-2} mbar
Third stage	4.0×10^{-7} mbar

3.1.2. Vacuum system
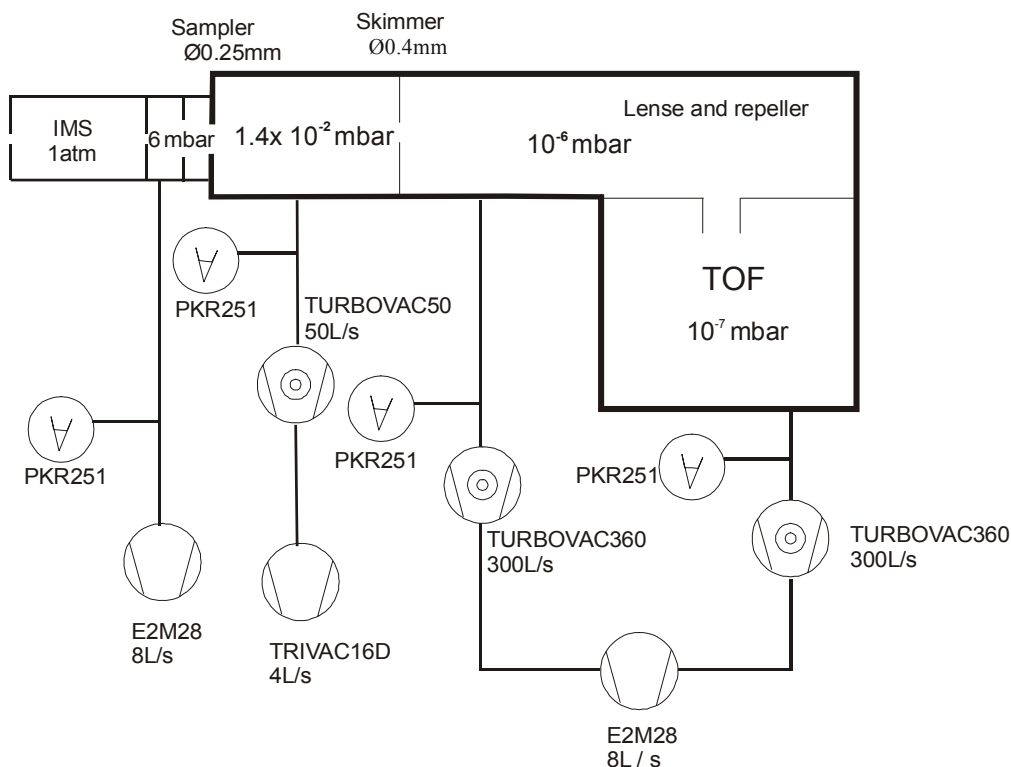
Fig. 3-3 The vacuum system of home made TOF

The three-staged vacuum chamber is evacuated by a differential pumping system, shown in Fig. 3-3. The first vacuum stage is between Φ 0.5 mm pinhole (open to IMS) and Φ 0.25 mm sampler (open to the second vacuum stage), where a pressure of ~6 mbar is retained by a rotary pump (E2M28 Edwards, 8L/s). The second vacuum stage is between the sampler and a Φ 0.4 mm skimmer. The third stage is the main vacuum chamber, which contains the TOF mass analyzer. To keep an oil-free vacuum for the sake of measurement, the second and the third vacuum stages are evacuated by a 50 L/s (Turbovac 50, Leybold-Heraeus GmbH) and two 300 L/s (Turbovac 360, Leybold-Heraeus GmbH) oil-free turbo molecular pump, respectively. The tubo molecular pumps are backed by 4 L/s Trivac 16D (Leybold-Heraeus GmbH) and 8 L/s E2M28 Edwards pre-vacuum pump respectively.

For the first step of pumping, both the pre-vacuum pumps (E2M28 Edwards and Trivac 16D (Leybold-Heraeus) are switched on, and all the three vacuum stages are evacuated by the vane rotary pump. Once the pressure measured in second stage is lower than 0.1 mbar, the Turbovac 50 should be switched on. Till the vacuum reach to 0.01 mbar, the gate valve to mass analyzer can be opened. In mass analyzer when the measured pressure is lower than 0.01 mbar, the two turbo molecular

pumps Turbovac 360 are switched on. The vacuum will quickly evacuated to 10^{-5} mbar. This process takes about 5 minutes. All the pressure are measured with compact full range gauge PKR 251 (Pfeiffer Vacuum GmbH, 1000 mbar to 5×10^{-9} mbar). The high vacuum in TOF mass analyzer is kept all the time and the vacuum in first and second stage are pumped only during measuring time.

3.2. ISAS made UV-IMS

The ISAS made UV-IMS is illustrated in Fig. 3-4. The ionization source is a 10.6 eV krypton discharge lamp (1). The drift tube (3) is a 12 cm long Teflon cylinder with an inner diameter of 15 mm, there are guard rings inserted to maintain a uniform electric-field gradient of 324 V/cm. Between the ionization region and drift tube there is a Bradbury-Nielsen [117] type shutter grid (2), where a potential difference is placed between two sets of thin wires positioned in parallel and very close to one another, thus creating a strong electric field (of about 650 V/cm) perpendicular to the axis of the field gradient across the drift tube. At the end there is a Faraday plate (4) to detect the ion current and this current will be amplified by a amplifier (6), the signal will then be acquired and processed with a computer. A biased aperture grid (5, not visible, it is inside drift tube) is placed close to the Faraday plate (about 0.5 mm). The bias on this aperture grid prevents the buildup of an ion charge on the collector plate, impart energy to the ions to increase the detection efficiency and to filter out the noise caused by the pulse on the gate, thus improving the signal-to-noise ratio.

1 UV-lamp
2 Shutter grid
3 Drift tube
4 Faraday plate
5 Aperture grid
6 Amplifier
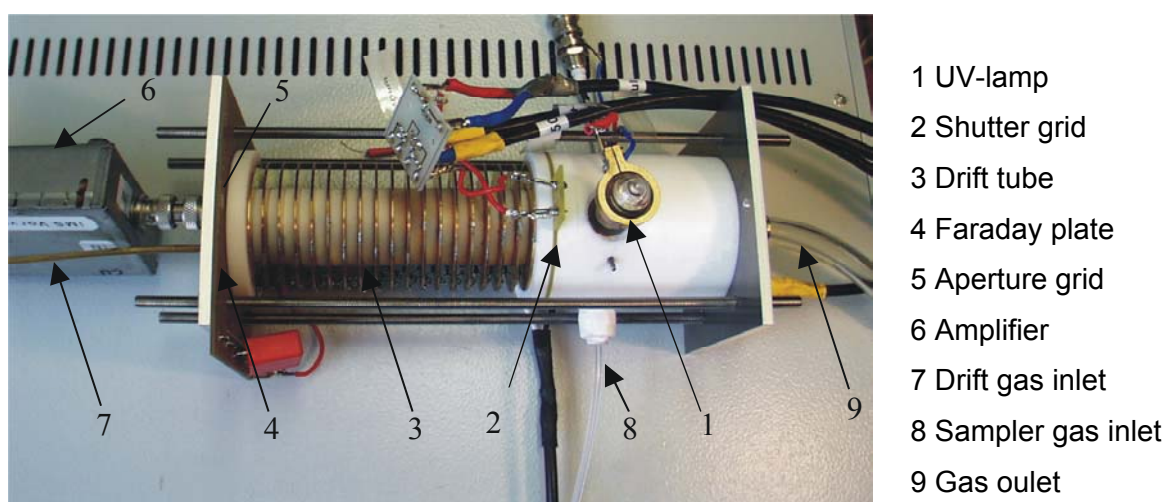7 Drift gas inlet
8 Sampler gas inlet
9 Gas oulet

Fig. 3-4 Photo of the ISAS made UV-IMS

A flow of carrier gas, set to 100 to 300 mL/min enter the IMS at the side of ionization and reaction region (8) through a 1/8" Teflon tube, while a flow of a drift gas, set to

300 to 700 mL/min, enter the IMS from the back end of the drift tube (7). Both gas flows are exhausted through a exit vent (9) just in front of ionization room. The carrier gas served as a means of transporting the sample molecules into the ionization source, and after initial ionization, subsequent ion-molecule reactions took place in the reaction region.

The power supply and controls of IMS were in ISAS developed and built [131]. The drift voltage can be adjusted through a high voltage module from 0 to 5 kV, normally 4 kV drift voltage was used by measurement. The shutter grid pulse period is 20 or 100 ms while the shutter grid open time can be selected between 100 µs and 1 ms. Normally using a ^{63}Ni β-radiation ionization source positive as well as negative ions can be produced, so the polarity of drift voltage between positive and negative could be changed. But, in the case of UV ionization only positive ions are produced. Therefore only positive drift voltage is needed to operate an UV-IMS. All of the parameters for UV-IMS are listed in Table 3-2.

Table 3-2 Parameters of ISAS made UV-IMS

Parameters	UV-IMS
Ionization source	10.6eV
Electric field	324 V/cm
Diameter of drift tube	15 mm
Length of ionization room	25 mm
Length of drift tube	12 cm
Open time of shutter grid	100 - 1000 µs
Pulse period of shutter grid	20 ms / 100 ms
Samplegas / Driftgas	Nitrogen 5.0 (99.999%)
Samplegas flow rate	100-300 mL/min
Driftgas flow rate	300-700 mL/min
Temperature	24 °C
Pressure	101 kPa

3.3. Interface system

The interface between high vacuum and the source of ions at atmospheric pressure is a set of compromises on ion yield and the vacuum performance. At first, two skimmers system was investigated. The signal was high enough to be detected in TOF, but the vacuum can not reach the requirement of micro channel plate working conditions. So, the three pinhole system was studied in addition and finally adopted

to couple UV-IMS to TOFMS.

3.3.1. Two stage interface

The schematic diagram of the UV-ionization chamber with an interface comprised of two skimmer cones is shown in Fig. 3-5. In the current work, acetone was chosen as the sample gas and flow rate was set to about 200 mL/min, the signal was taken with a Faraday cup which was placed directly under the second skimmer and was amplified using a R8240 Digital Electrometer (Advantest, Japan). The vacuum chamber was evacuated using one E2M28 (8 L/s) rotary vacuum pump and two Pfeiffer turbomolecular pump TPU 240 (230 L/s) and TPH 330 (300 L/s). For the whole system, the pre-vacuum was 0.7- 2 mbar, the vacuum inside TOF was 10^{-3}-10^{-4} mbar depending on the distance between two skimmers and the dimension of the skimmer.
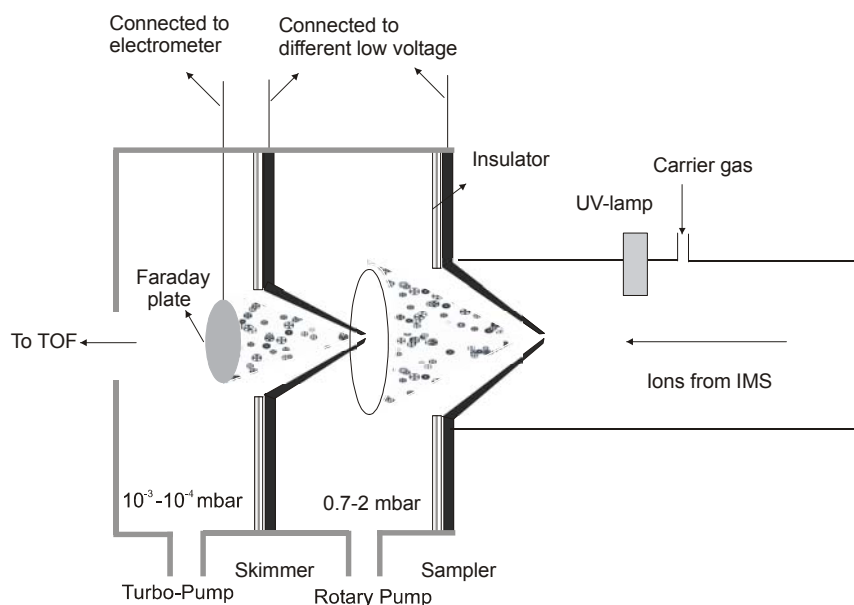

Fig. 3-5 Schematic diagram of interface region

3.3.1.1. Influence of sampler orifice diameter and voltages.

The diameter of the second skimmer is set to 0.7 mm. When the sampler (front skimmer) orifice is 0.35 mm, the intensities of signal increases as the distances between two skimmers is changed from 8 to 4 mm as shown in Fig. 3-6. In each instance, the signals increase linearly with voltage on sampler increases from 0 to 300 V and the voltage on the skimmer was kept at 0 V (left frame). However, the signal decreased when the voltages on skimmer were changed from 0 V to 50 V

while the voltages on sampler was kept at 200 V (right frame), except when the distance between two skimmers was 4 mm, the signal increases significantly when the voltage on skimmer is increased from 0 to 2 V.

The vacuum can be kept up in the range of 10^{-4} mbar when the distances between two skimmers between 5 to 8 mm; however, the vacuum goes to $1.2*10^{-3}$ mbar when the distance is optimized for signal, i.e. 4 mm.
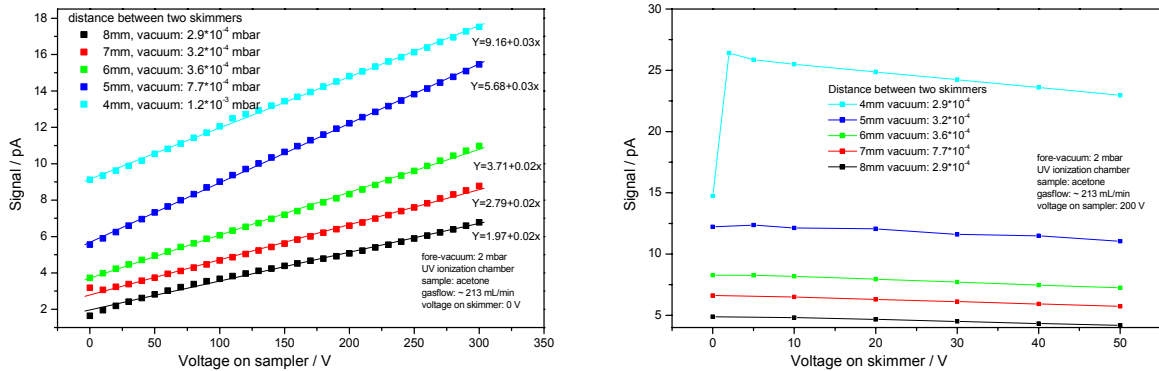

Fig. 3-6 Relationship of intensities of signal to voltages applied on sampler and skimmer with different distances between two skimmers and sampler orifice 0.35 mm

Consequently, the signal is highest with the voltage of 300 V on the sampler and about 2 V on the skimmer. In consideration of the vacuum and the intensity of signal, the best distance was empirically determined as 5 mm.
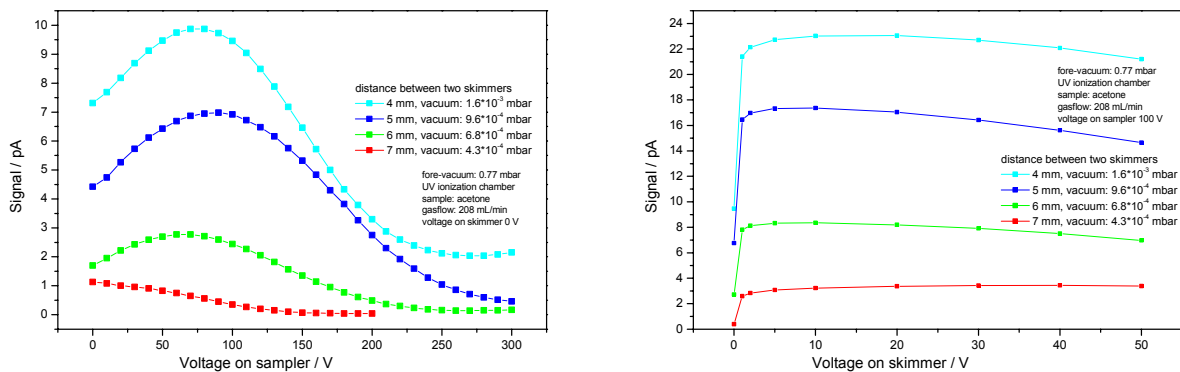

Fig. 3-7 Relationship of intensities of signal to voltages applied on sampler and with different distances between two skimmers and sampler orifice of 0.25 mm

In the case, that the sampler orifice is 0.25 mm, the dependence of the intensities of signal on the voltages on skimmers is unlike prior results (see Fig. 3-7). The signals reached the highest when the voltage on sampler is about 80 V and on skimmer is about 2 to 5 V for the distances between two skimmers of 4 to 6 mm. For a distance

of 7 mm, the signal was too low, regardless of the voltages on skimmer cones.

In summary, with consideration to the ion yield and vacuum performance, the best alternative is 5 mm between the two skimmers. These results demonstrated that simple measurements of ion yields were possible within the interface region and that the results were a complex mixture of geometry, vacuum and ion yield. The use of ion optical bench software was deemed a reasonable approach to designs for geometry and ion yield.

3.3.1.2. Sampler made from aluminium foil as interface inlet

In order to improve the vacuum and a orifice small as 0.25 mm is difficult to be produced with normal mechanical method. Instead of a skimmer cone as sampler a blank foil with a slit cut carefully by a razor blade as new vacuum interface inlet was made (Fig. 3-8). When the foil without slit using same pump system mentioned above after pumping overnight, the vacuum reached 6.2×10^{-7} mbar, with a slit on aluminium foil, the vacuum was 5.2×10^{-5} mbar.
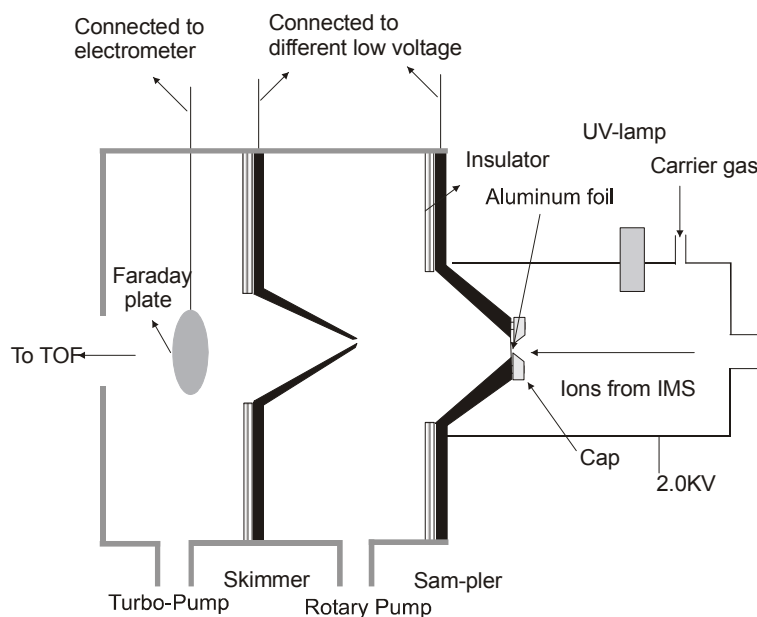

Fig. 3-8 Schematic diagram of interface system for IMS-TOF with aluminum foil as inlet

Acetone test gas was introduced into the IMS and the signal received was recorded at different voltages applied on the aluminium foil and the second skimmer, the signal was not stable compared with skimmer cone, the signal dependence on voltages are shown in Fig. 3-9, the signals increase with the voltages, but when the voltage on second skimmer increased from 0 V to 5 V, the signal varied not much. And the higher the voltage, the unstabler the signal.
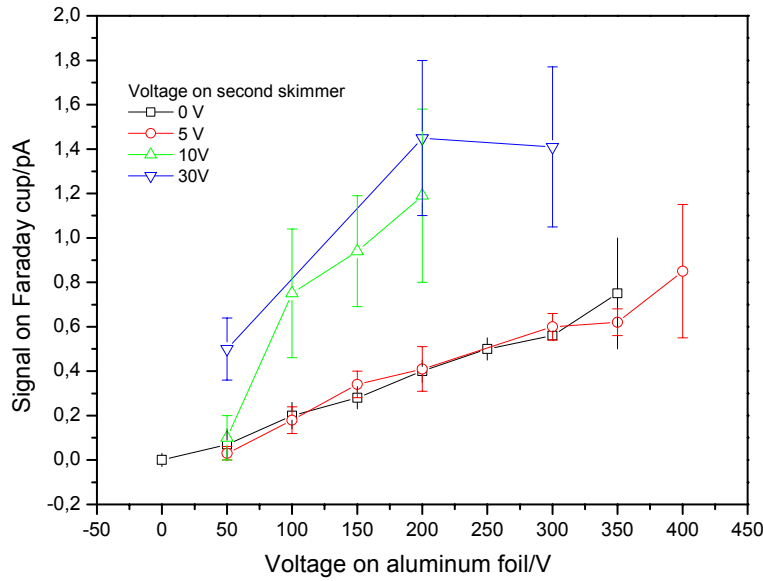
Fig. 3-9 Signal dependence on voltages on the aluminum foil and the second skimmer

3.3.1.3. Influence of skimmer orifice diameter and voltages

The pumps for TOF were strengthened, two TRIVAC-B / D16B Rotary vane pump are used as fore vacuum pumps and two TURBOVAC 360 Turbomolecular pumps are pumping now. All the pumps are working well, but with Φ 0.25 mm orifice inlet of the sampler, the vacuum in TOF can only minimum reach 2.1×10^{-4} mbar, so a small orifice of skimmer is needed. A smaller second skimmer cone of Φ 0.4 mm was used and different distances between the sampler and skimmer were tested to obtain better vacuum. The signal was detected by Faraday plate at the end of modulator with the orthogonal extraction parts inside TOF.

The distance between the sampler and skimmer were varied with the dimension of sampler of Φ 0.25 mm and skimmer of Φ 0.4 mm respectively. The vacuum and signal intensity were tested. As shown in Table 3-3, when the distance between the sampler and skimmer set to 5 mm, vacuum can be improved to 4.3×10^{-5} mbar instead of 2.1×10^{-4} mbar with the second skimmer diameter of Φ 0.7 mm mentioned before. compared to 5 mm and 6 mm interval, the signal is nearly the same and the vacuum is better with 6 mm. When the distance set to 7 mm, the signal intensity decreases to 1/3 of that with 6 mm. With consideration of vacuum performance and ion yield, 6 mm distance between sampler and skimmer was preferred.

Table 3-3 Vacuum and signal intensity with different distance between sampler (Φ 0.25 mm) and skimmer (Φ 0.4 mm)

Distance between sampler and skimmer / mm	*Signal /pA	Vacuum in TOF / mbar
5	1.9	4.3×10^{-5}
6	1.8	2.5×10^{-5}
7	0.6	1.6×10^{-5}

* no connection from sampler and skimmer to power supply, stand-by.

The influence of voltages on sampler and skimmer on the intensity of signal were also investigated. The magnitude of signal increases with the voltage on the sampler going up and it reaches highest when the voltage on the skimmer set to 60-70 V, as demonstrated in Fig. 3-10.
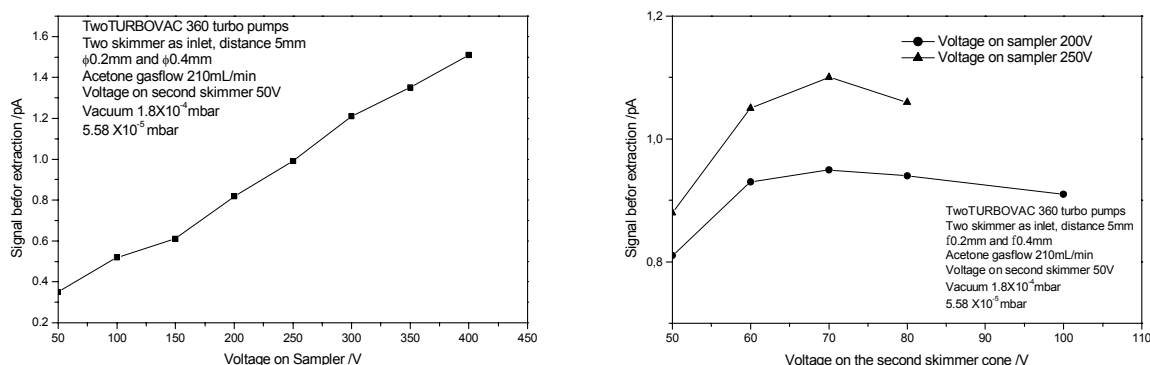

Fig. 3-10 Influence of the voltages on the sampler and skimmer to the intensity of signal, sampler diameter of Φ 0.25 mm and skimmer of Φ 0.4 mm.

In order to get vacuum in 10^{-6} range, a test were done with the distance between sampler and skimmer set to 6 mm. With the dimension of sampler of Φ 0.25 mm and skimmer of Φ 0.3 mm, respectively, vacuum can reach 8.2×10^{-6} mbar. The results are compared with those before, shown in Table 3-4.

Table 3-4 Vacuum and signal with different dimension of the skimmer.

Diameter of sampler / mm	Diameter of skimmer / mm	*Signal / pA	Vacuum in TOF / mbar
0.25	0.4	1.8	2.5×10^{-5}
0.25	0.3	0.55	8.2×10^{-6}

* no connection from skimmers to power supply, stand-by.

Thus in general, the vacuum can only reach 10^{-6} range with diameter of sampler in Φ 0.25 mm and diameter of skimmer in Φ 0.3 mm, respectively. The distance between sampler and skimmer should minimal set to 6 mm. But in this case the vacuum is still not desirable for TOF. With these dimensions of sampler and skimmer, if the distance extended to 7 mm, regardless of the voltage applied on it, no signal was detected. So another design with three stage was investigated.

3.3.2. Three stage interface.

Another chamber with a pinhole (pre-sampler) was designed and finished to stack on the sampler of TOF, so that there are three stage pumping system and the vacuum inside TOF can drop dramatically (Fig. 3-11). The first stage vacuum was several mbar to 100 mbar depending on the dimension of the pinhole, the ions produced by UV-lamp can be measured with this construction. Signal was detected with a Faraday plate set in the middle of TOF. Different sizes of the first pinhole, sampler and skimmer, and different distances between the sampler and skimmer were investigated.
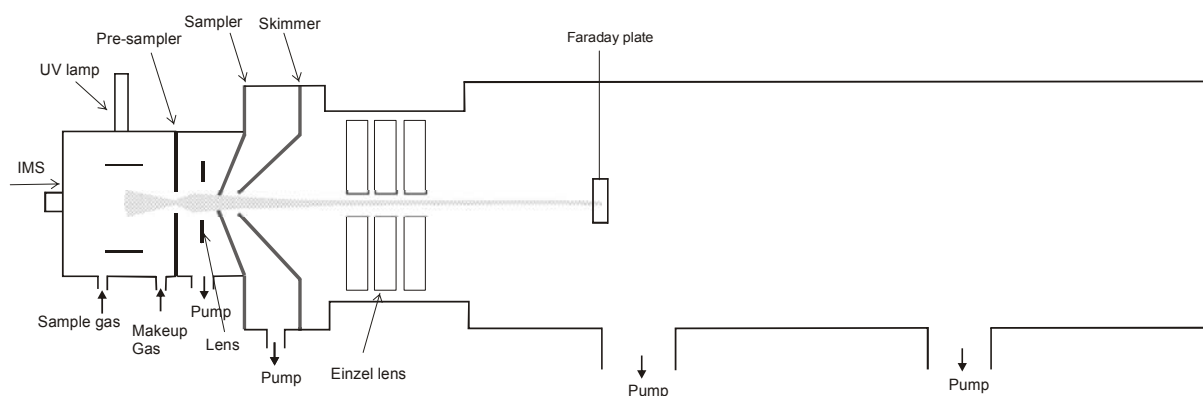

Fig. 3-11 Measurement set-up with 3 pinhole interface system

At first before the metal piece with Φ 1.3 mm pinhole was selected. With this configuration, different distances between sampler and skimmer were investigated and the intensity of the signal and the vacuum were measured. Dimension of the sampler and skimmer was Φ 0.25 mm and Φ 0.3 mm, respectively. Results are shown in table 2. A extra gas was needed to compensate the gas pumped to TOF as shown in Fig. 3-11 the makeup gas.

As illustrated in Table 3-5, the vacuum is two times better and the signal is nearly the same with the distance between sampler and skimmer set to 5 mm and 4 mm, and

the signals are much more stable than those with 6 mm. With this configuration, the voltages on the sampler and skimmer have no effect on the intensity of the signal on the Faraday plate.

Table 3-5 Vacuum and signal intensity with different distances between the sampler and the skimmer

Distance /mm	Signal on /pA			Vacuum 1 /mbar	Vacuum 2 /mbar	Vacuum 3 /mbar
	sampler	skimmer	Faraday Plate			
6	2×10^3	7	0.08 – 0.18	40	0.12	1.4×10^{-6}
5	2×10^3	9	0.23	40	0,16	2.3×10^{-6}
4	2×10^3	7	0.26	40	0,16	5.0×10^{-6}

Different dimensions of pinhole on pre-sampler were measured too, with the distance between sampler and skimmer set to 5 mm, dimension of the sampler and skimmer was 0.25 mm and 0.35 mm respectively, results are shown in Table 3-6.

Table 3-6 Vacuum and signal intensity with different diameters of the pinhole on metal piece

Pinhole /mm	Signal /pA			Vacuum 1 /mbar	Vacuum 2 /mbar	Vacuum 3 /mbar
	sampler	skimmer	Faraday Plate			
2.0	300	13	0.22	100	0.27	4.0×10^{-6}
1.3	2×10^3	9	0.23	40	0,16	2.3×10^{-6}
0.8	1.9×10^3	4.5	0.5	15	0.065	1.1×10^{-6}
0.5	395	1.1	0.4	6	0,031	5.3×10^{-7}
0.3	-	-	-	4	0.01	2.8×10^{-7}

The influence of voltages on the sampler and skimmer were studied. It depends on the size of the pinhole on pre-sampler. The bigger is the pinhole, the higher voltage is needed to reach the highest signal, as for the Φ 0.8 mm and Φ 0.5 mm pinhole on pre-sampler, the signal increased with the voltage on the sampler. Seen in Fig. 3-12 left. The voltage on the skimmer has not great influence, the signal decreased a little bit when the voltage increased. For example, the signal went from 0.24 pA to 0.14 pA when the voltage on the skimmer were 10 V and 50 V respectively. The voltage on the metal piece has the same affect as that on the skimmer.
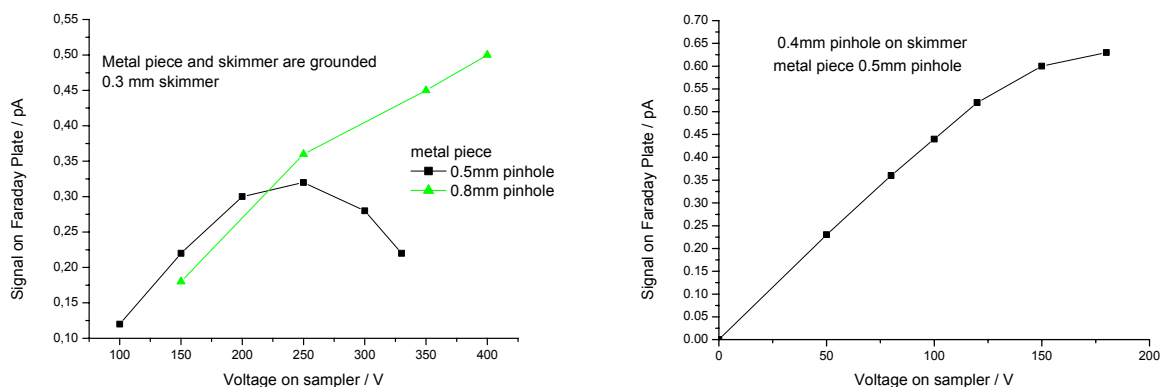
Fig. 3-12 Influence of the voltage on the sampler to the intensity of signal with sampler diameter in Φ 0.25mm. (left) different diameter of pre-sampler, and Φ 0.3mm skimmer; (right) Φ 0.5 mm pre-sampler and Φ 0.4mm skimmer

The skimmer diameter of 0.4 mm were investigated. with the distance between sampler and skimmer set to 5 mm and Φ 0.2 mm pinhole on the sampler, Φ 0.5 mm pinhole on the pre-sampler. The vacuum can reach 6 mbar, 0.031 mbar and 1.1×10^{-6} mbar respectively, but the signal can reach maximum 0.67 pA on Faraday plate when the other connections are open. with lower voltage the signal can reach highest compared with the measurement with Φ 0.3 mm pinhole on skimmer, shown in Fig. 3-12 right.

Instead of the Φ 0.25 mm pinhole on sampler, Φ 0.35 mm pinhole on sampler was studied too, The signal with Φ 0.35 mm pinhole sampler is not better than that with Φ 0.25 mm pinhole, it is 0.45 pA. The intensity of the signal depends on the alignment of the IMS and the skimmers system, so the results mentioned before may deviate but in this range.

According to the results mentioned above, with the construction of 3 pinhole system, the vacuum can reach 10^{-6} mbar and signal can also be detected with different dimensions of pinhole, the best is with Φ 0.5 mm pinhole on metal piece, Φ 0.2 mm pinhole on sampler, Φ 0.4 mm pinhole on skimmer and the distance between the sampler and skimmer set to 5 mm.

The whole interface system was then put orthogonal to TOF, another Faraday plate was set and signal of 0.17 pA can be detected with the following parameters listed below in Table 3-7.

Table 3-7 optimized parameters for the interface

Vacuum (3 step)	6 mbar, 1.5×10^{-2} mbar, 4.6×10^{-7} mbar
UV ionization source	2 kV
Voltage on metal plate	114 V
Voltage on lens	190 V
Voltage on Sampler	130 V
Skimmer	0 V
Voltage on Einzel Lens	45 V
Signal detected on Faraday Plate	0.17 pA
Sample gas flow	1-1.2 L/min

3.3.3. Einzel lens

The Einzel lens consists of a tubular electrode that is sandwiched between two other tubular electrodes. The assembly was drawn based the modelling studies with Simion 7.0. Dimensions were: diameter, 10 mm; lens length, 12 mm for each; and distance between each lens, 1-2 mm. Wall thickness is 1 mm. The lens was assembled using three thread rod support and will be isolated by several ceramic sleeves. A sketch of this is shown in Fig. 3-13.
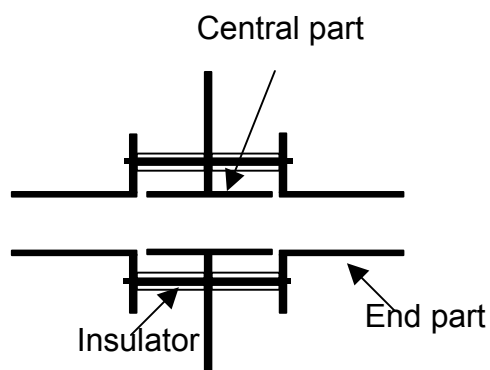

Fig. 3-13 Einzel lens assemble for the IMS/TOF MS. The lens assembly will attach to the vacuum flange on the extended arms of the center lens. Ceramic insulators are shown as clear boxes.

In all the case, the first and the last electrode are at the same potential (tied together) while the central lens was set to another potential. the overall effect of the Einzel lens is focusing [132].

A retarding Einzel lens for positive ions is shown in Fig. 3-14 (end tubular electrodes

are grounded and the middlel one set to positive potential). The main effect is that the ion velocity is drastically decreased in the first half of the lens and then drastically increased again in the second half. The decelerating and accelerating forces are indicated by small black arrows which indicate the direction of the forces on positively charged ions. These forces have small components perpendicular to the optical axis. In the first and last part of the Einzel lens, these forces are defocusing and drive the ions away from the optical axis, the z-axis, while in the middle region they are focusing and drive the ions towards the optical axis. The overall effect of these forces is illustrated by the hollow arrows. Since these forces away and toward the axis are of comparable magnitude, they are most effective in the middle region where the ions are slow and consequently spend most of their time. For this reason the lens shown overall is focusing.
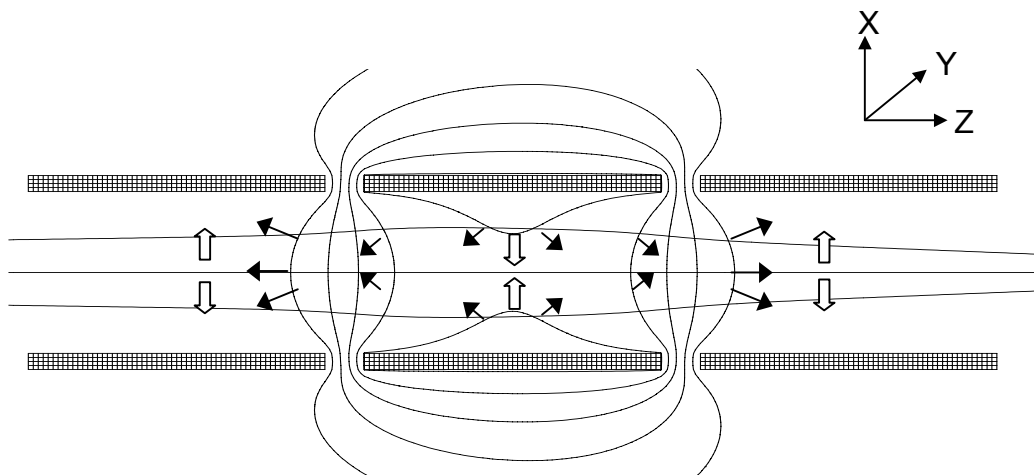

Fig. 3-14 Principle of Einzel lens illustrated by Simion plot of the electric field, the middle tubular electrode is set to positive potential and the end electrode grounded.

At this point it should be mentioned also that the potential on the first and last electrode can also be at positive potential and the middle electrode be grounded. In this case it acts as two of the above mentioned lens.

If the middle electrode is negatively charged, it will be an 'accelerating Einzel lens' for positively charged ions. In this case all arrows in Fig. 3-14 will be reversed. Thus the focusing forces act in the side region and defocusing forces ac in the middle region. Since in this case the ions move slower in the side regions, the focusing forces are more effective than the defocusing forces and the 'accelerating Einzel lens' is overall focusing as well.

Experiments were carried out using Einzel lens in TOF with alluminum foil interface. The signal was firstly collected by a Faraday plate direct behind the Einzel lens, the

focusing effect is not so apparent, signal can maximal improved by 10%. then the Faraday plate was placed at the end of ion trajectory in TOF chamber before it was orthogonal extracted, in this case the signal was improved by 52%. So the Einzel lens is proved to be effective.

3.4. Self-built TOF set-up

3.4.1. Orthogonal extraction and acceleration

The orthogonal accelerator is a high efficient device for sampling ions from an ion beam into a TOF mass analyzer. The ion beam enters oa at right angles to the TOF direction. It consists of two stages of acceleration (different electric field) which are defined by conducting electrode and grids. The first one is between repeller and grid 1, while the second one is between grid 1 and grid 2, as illustrated in Fig. 3-15. All the acceleration rings are mechanically separated and insulated by PEEk pieces and electrically connected by a resistor chain. To prevent electrical field penetration, both sides are shielded by grids.

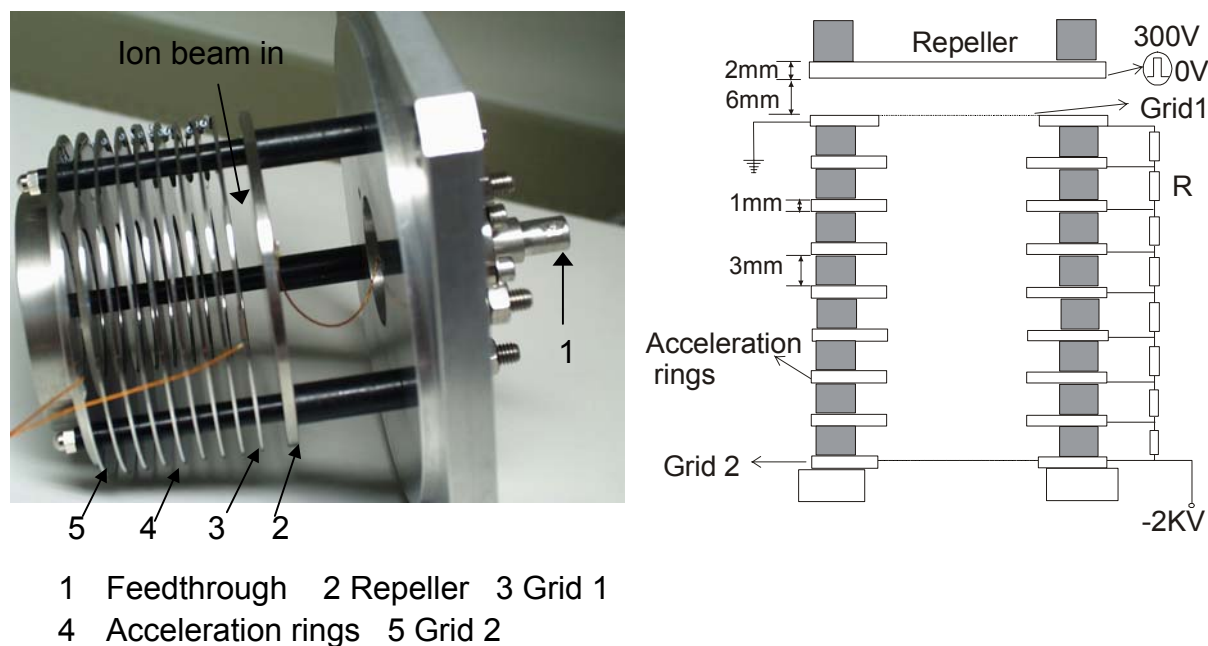1 Feedthrough   2 Repeller   3 Grid 1
4 Acceleration rings   5 Grid 2

Fig. 3-15 The constructure of orthogonal extraction and acceleration system

It is necessary to note that the inner diameter of the rings with grid is 5 cm slightly larger than the others 4 cm. Because the ions that pass near the edges of the oa should not be allowed to enter the drift region as the fringing fields there may cause deflections that affect the time-of-flight. This design reduced the chance of ions passing near the fringing fields within the oa on the beam entry side.

The choice of grid material and geometry is important. Close spaced wires create better separation of regions of different field strength but decrease transmission, particularly as the angle of incident ions on the mesh deviated from 90° as is the case for gride 1. The mesh is made by Buckbee-Mears St. Paul, there are 117.6 wires per inch. The wire width is 13 µm and the hole size is 203 µm, the maximum transmission 88.6%.

Once the ion beam is filled up between the repeller and the grounded grid G1, a push out pulse is applied to the repeller which is also used to start the timing electronics. The ions are then orthogonally accelerated and they are thus raised to a much higher kinetic energy. It was shown in Fig. 3-16.
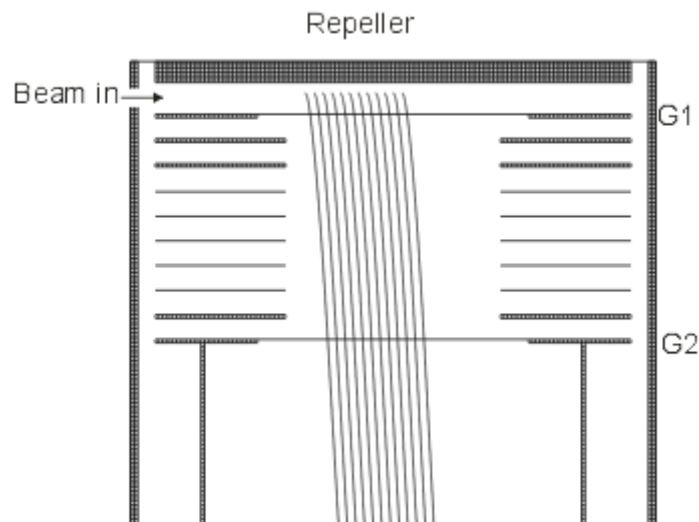

Fig. 3-16 the simulated trajectories of ions entering (left) orthogonal accelerator and sampled for TOFMS (downwards)

The push-out pulse needs to be fast enough that all the ions experience acceleration at essentially the same time. Fig. 3-17 shows the push out pulse for the orthogonal acceleration TOF constructed in ISAS. The rise time is 30 ns by a 300 V pulse. It is most important that the first stage is completely field-free in the fill up mode. A small residual field in the fill up region may result from the baseline of pulse is not really 0 V. Such fields may cause significant deflection of ion trajectories in the oa-TOF and therefore, increase the initial spatial spread of the ions. The residual field may be substantially removed by application of another relatively small positive voltage, shown in Fig. 3-18.
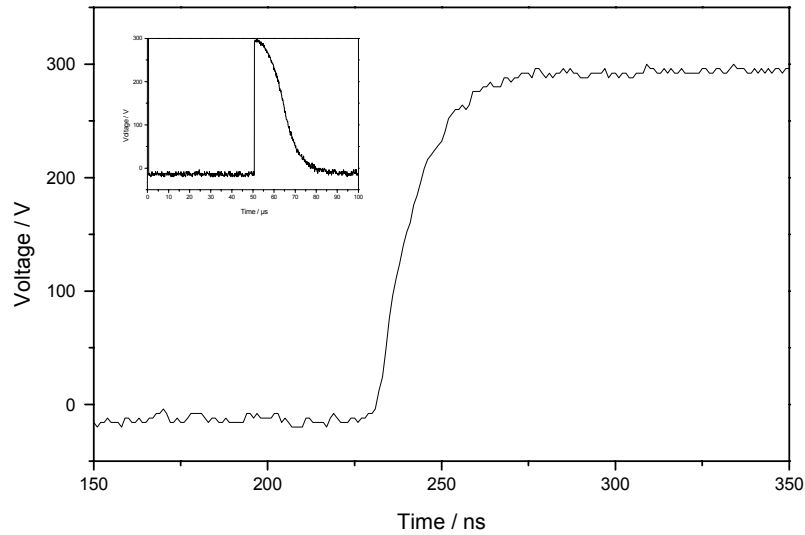
Fig. 3-17 The rise time of a 300 V 10 kHz pulse for the orthogonal accelerator. The insert is the entire pulse.
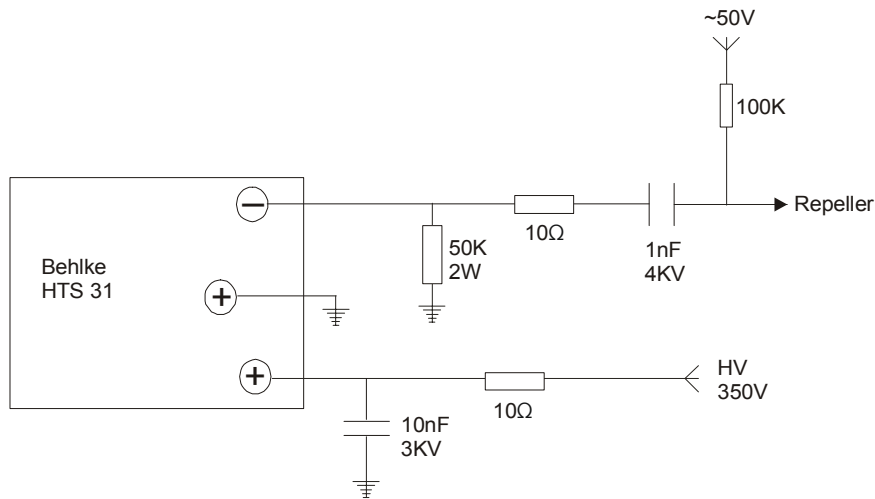

Fig. 3-18 Circuit of pulse switch mode on repeller

3.4.2. Deflector

As shown in Fig. 3-1, there are two parallel ion steering plates located just after the orthogonal accelerator. They are the so called deflector which is used to steer the ion packets into a transverse trajectory [133]. This allows the tube containing the drift region to be at right angle to the ion source axis. It does so at the expense of resolving power. This is attributed to the combination of ion packet rotation and folding that results from the inherent inhomogeneneity of these deflection field [134]. A better approach is to reduce the initial energy of the ions from ion source, that is to use a collisional cooling device such as RF only quadrupole or octopole.

3.4.3. MCP and data acquisition system.

To achieve a high mass analyser efficiency, it is desirable to make the detector at least as wide as the length of the ions beam that is accelerated into the drift region. The microchannel plate was produced in BURLE and constructed together by BRUKER, (Fig. 3-19 left). Two microplates are sandwiched together in such a way that the bias angles aligned 180° opposite to obtain a gain of 10^6 to 10^8, as shown in Fig. 3-19 (right), it is the so called Chevron style. The MCPs are 40 mm in diameter and have 6 μm diameter channels biased at a angle of 8° to the MCP input surface. The voltages are applied to each MCP through a resistor divider. The output signal is derived from a 50 Ω conical anode, connected directly to computer. The anode is held at ground potential.
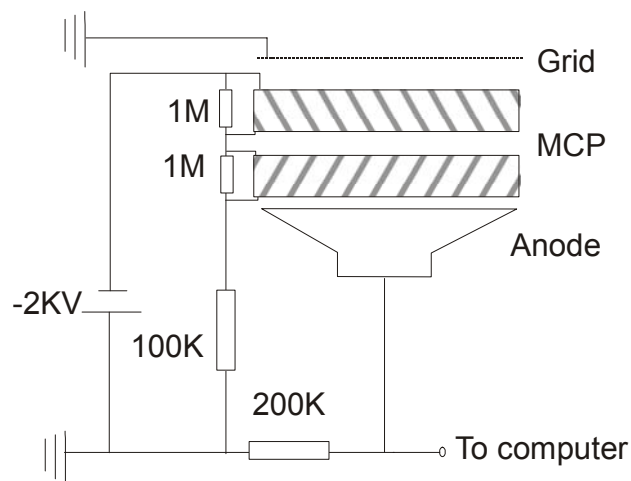

Fig. 3-19 Microchannel plate detector mounted on a flange, and circuit of it.

For data acquisition, three cards ADA-100, DDG-100, MSA-200 are used. They are produced by Becker & Hickl GmbH. DDG-100 is a digital pulse/delay generator (pulse width 10 ns to 655.35 μs, pulse period 40 ns to 655.35 μs) . ADA-100 is a 10 ns ADC module and MSA-200 is a 5 ns multiscaler. As shown in Fig. 3-20, the signal from MCP is pre-amplified by a 1.8 GHz wide band amplifier (ACA-2, Becker & Hickl GmbH), then the signal is divided by a power divider (50 Ω, 6dB, 12.4 GHz, Suhner) connected to MSA and ADA card. The start time is triggered from DDG-100 digtital pulse / delay generator.
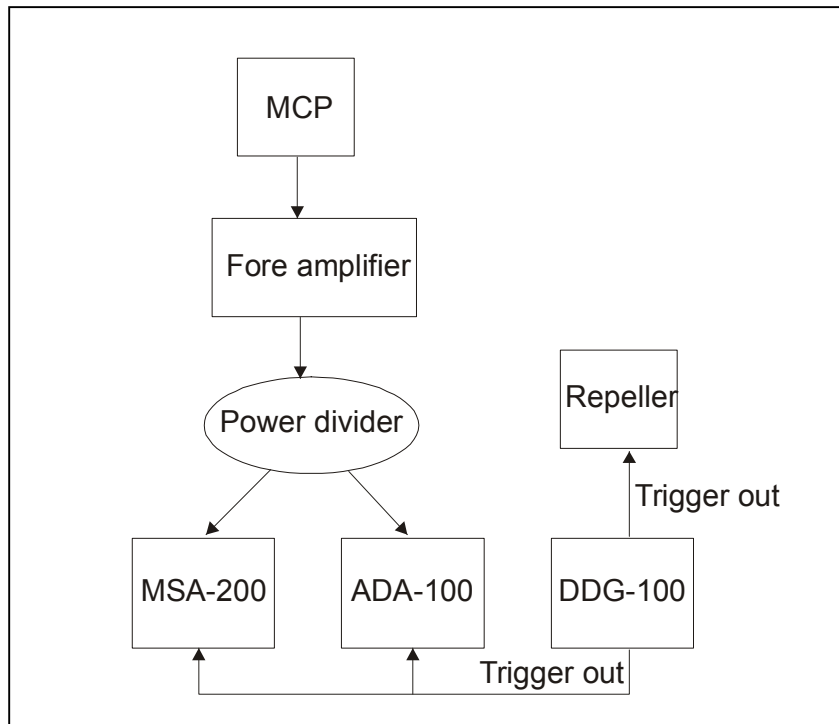
Fig. 3-20 Block diagram of data acquisition of TOF

A data acquisition program has been written by Mr. Skole in ISAS Berlin, which was run under windows 98 operating system by a pentium IV computer.

4. <u>SIMION simulation of UV-IMS-TOF</u>

The ion simulation software SIMION v. 7.0 is used to model ion trajectory in interfacing UV-IMS to TOFMS. The purpose of this study is to design a interface and TOFMS to detect ions produced in UV-IMS. The device was modelled before building the prototype. SIMION is a ion optics software program originally developed by David Dahl at the Idaho National Laboratory, USA. The latest version allows for great expanded simulation capabilities. These include larger array size (50 million points) and three dimensional modelling. Dynamic parameter variation and time varying potentials are now also possible.

4.1. Simulation of interface

The pinhole interface to an ion mobility spectrometer/mass spectrometer (IMS/MS) is simulated by SIMION 7.0. IMS is working under ambient pressure, so the commercial SIMION software can not directly applied to it for ion trajectory, but the electric field can be simulated.
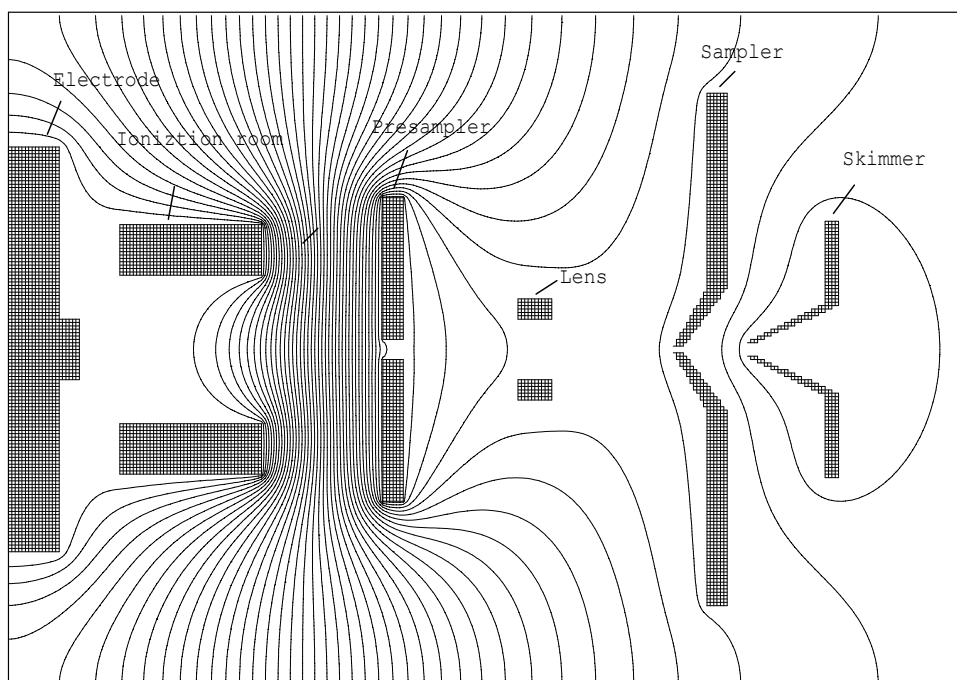

Fig. 4-1 SIMION plot of electric field of self-made UV-IMS ionisation region and the pinhole system. The IMS ionisation room and the electrode is 2 kV, fore-sampler set to 30 V and lens 150 V, sampler 120 V, skimmer 0 V.

At first the dimensions, angles and distances of all the components are exact proportional defined in SIMION. The IMS is under atmospheric pressure, the region

between pre-sampler and sampler is about 6 mbar, between sampler and skimmer is 1.4 x 10^{-2} mbar. In addition to gas flow, the ions are brought into TOFMS through all the pinholes by electric field, as shown in Fig. 4-1 the contour draw of interface, the ions created by UV-lamp are pushed and focused to go through the 0.5 mm orifice on pre-sampler by the electrical field in ionisation room. Behind the pre-sampler there is a lens set to 150 V, this lens act as an Einzel lens (central electrode) and the pre-sampler and sampler as end electrode which have different potential, it directs and focuses the flow of ions toward sampler. Between sampler and skimmer the field strength increases from 2 V/mm (immediately behind sampler) to 50 V/mm (before skimmer) and brings the ions into TOFMS. According to the simulation, the potential of lens is critical for ion transmission, because the entrance aperture of sampler is only 0.25 mm in diameter. It is in accordance with the experiment results.

Experiments with this configuration has been performed too, the distance between the fore-sampler and sampler are 12 mm, distance between the UV ionization room and fore-sampler was set to 7 mm, the ions signal can reach 0.52 pA maximum. When the distance between the fore-sampler and sampler were prolonged to 43 mm maximum signal can reach 0.29 pA. When the voltage on sampler set to a certain amount, the voltage on skimmer affect the signal not so much. The voltage difference between the sampler and skimmer can not more than 400 V, otherwise there is discharge between.

4.2. Effects of Einzel lens in TOFMS

In an actual design, the ion beam should have a narrow and parallel shape in the region of the TOFMS extraction region before it is orthogonal extracted and accelerated.

At first step, only Einzel lens was used to bundle the ions together after they entered TOFMS through orifice cones. In Fig. 4-2, an ion beam is shown where ions are reached at the end of orthogonal extraction of the TOFMS, in this case 240 mm from the sampler cone.
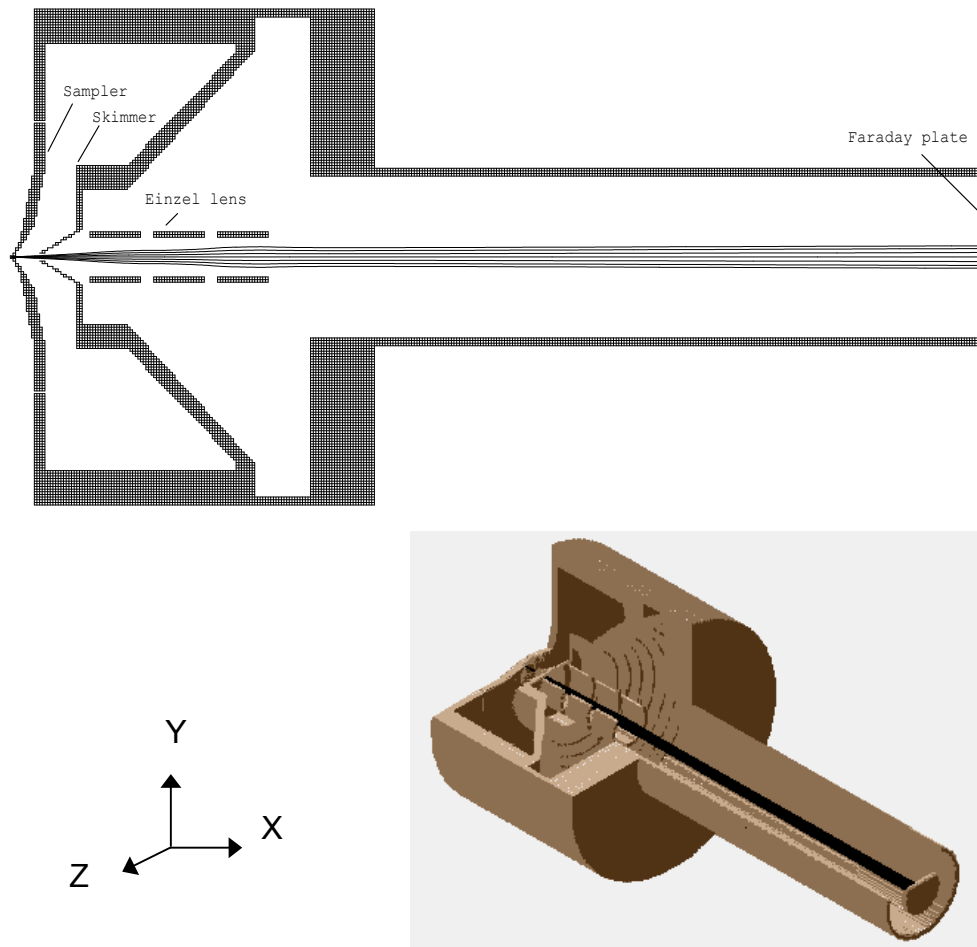
Fig. 4-2 Ion trajectory through Einzel lens, for 3D diagram a section is cut away to show the passage of ions

Some effort was given to modelling the geometry and potentials of Einzel lens as demonstrated in Fig. 4-2 where Einzel lens had a length of 12 mm, 10 mm in diameter. Voltage on sampler cone are 120 V, skimmer cone are 0 V. In all instances, the voltage on the first and third lens were tied together while the central lens was fixed at 0 V.
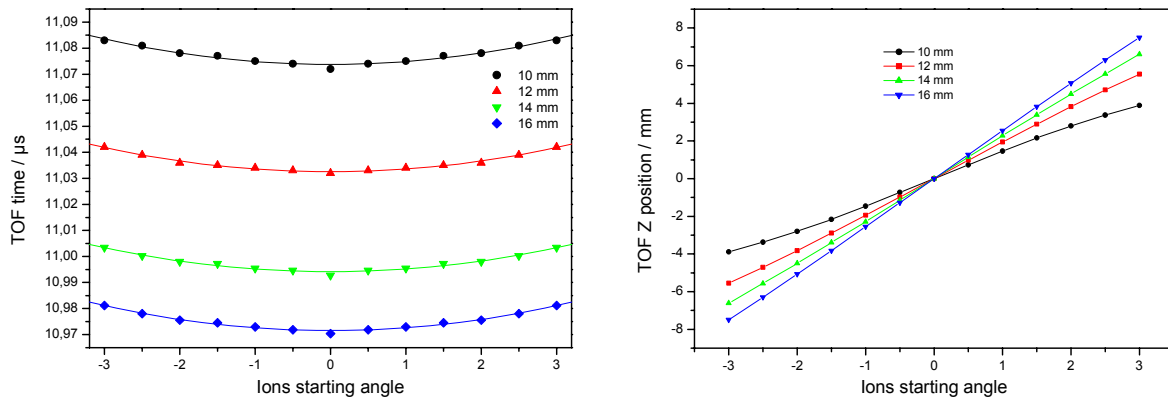
Fig. 4-3 Influence of Einzel lens with different diameters to ions trajectory

The results obtained when ions originated from a point are shown in Fig. 4-3, the ion's definition are as follows: Ion mass: 100 amu, charge: 1.00+, First Az angle: +3 degrees, Delta Az: -0.5 degrees, First El Angle: 0 degrees, Delta El 0 degrees, Ion kinetic energy: 100 eV, and Grouped, Coul Repl 1.0×10^{-7}. For same potential 60V on the lens, the larger the diameter of the Einzel lens, the less time for the ions to hit the Faraday plate and the larger space distribution have the ions. Regardless of the dimension of the lens, the difference in flight time ranges were 10 ns compared the ions start with 0 degree and 3 degrees (Fig. 4-3 left), for example, for 10 mm diameter the ions reached the Faraday plate in 11.072 ns and 11.082 ns, for 16 mm in 11.032 ns and 11.042 ns respectively. The parabolic shape is due to the decelerating effects of the Einzel lens. Those ions that pass closest to the electrode surface are most strongly affected. The space distributions were even more pronounced, it was from ±3.9 mm to ±7.5 mm for 10 mm diameter lens to 16 mm diameter (Fig. 4-3 right). The larger the diameter of the Einzel lens, the greater the space distribution. So in this sense, the possible smaller diameter should be adopted, therefore, 10 mm inner diameter was chosen for our TOF instrument.

As for 10 mm Einzel lens, different voltages were applied, as shown in Fig. 4-4. for 60 V, 65 V, 70 V and 75 V on the lens, the ions flight time increased with the increasing of voltage, despite the potential on Einzel lens, ions flight time ranges were 10 ns compared the ions start with 0 degree and 3 degrees. The ions expand in z-direction were only ±0.54 mm and ±1.1mm when the voltage on lens were 75 V and 70 V respectively. These values clearly show the importance of selecting the correct voltage.

the ion trajectory can be controlled by the voltage of the central part of the Einzel lens too, according to the simulation, the ions distribution in z-direction can be

reduced when negative voltage applied on the central electrode, but negative potential on the lens will accelerate the ions pass through it, it is not desirable for oa extraction and acceleration in z-direction.

The results presented above demonstrate the advantage of using SIMION to examine ion optics in TOFMS, it is helpful for design and optimise the system.
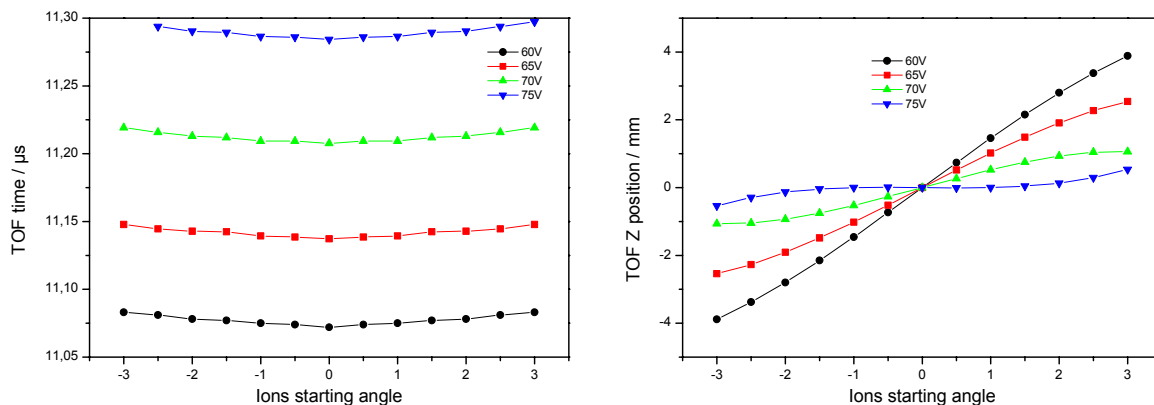

Fig. 4-4 The influences of different voltages on Einzel lens of 10 mm in diameter to ions trajectory

4.3. Influence of grids and grid geometry on ion trajectory

Grids are used in oa-TOFMS to divide regions of ion modulator and ion extraction and acceleration region. A grid consists of evenly spaced metal wires running at right angles to each other. There are a wide variety of wire densities and transmissions which provides a wide choice of specifications of grids.
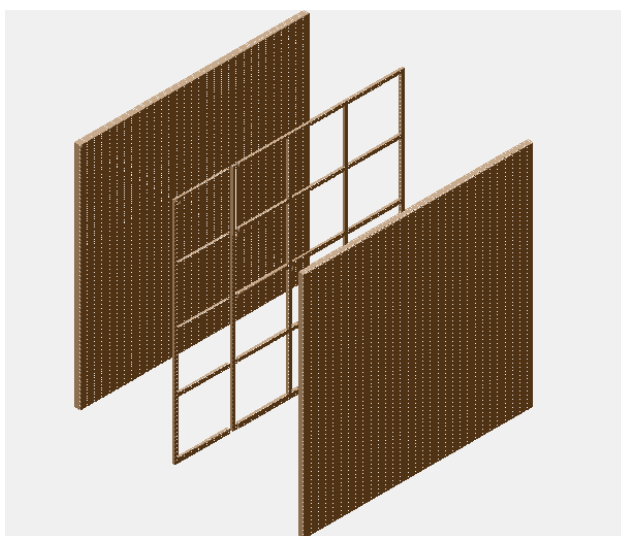

Fig. 4-5 Simulated section of grid of evenly spaced metal wires running at right angles to each other

Fig. 4-5 shows the SIMION 3D simulation of grid. It includes 16 grid holes with wire density of 117.6 lines per inch (13 µm wires, hole 203 µm) and two solid electrodes in a distance of 0.4 mm to grid to establish the fields in either direction.

When different electric fields are placed on each side of a grid, a small electrostatic lens is produced at each opening. The simulated potential function for such a boundary is illustrated Fig. 4-6, the grid separate fields having a fivefold difference in strength.
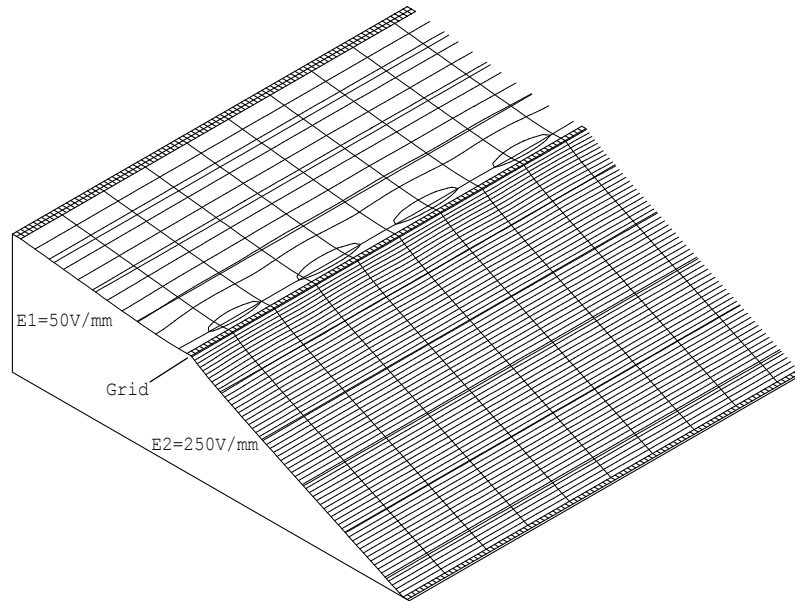

Fig. 4-6 Representation of potential contours at the boundary of two electrical fields separated by a grid

When ions flight through the grid, it will be deflected and the deflection depends on the ion energy and the electrical field difference between the two sides of the grid, Fig. 4-7 shows the ion trajectory through one cell of the grid from E_1 to E_2. The ions are focused. The focal length can be determined by

$$f_0 = \frac{2K_e}{E_2 - E_1}$$
4-1

where K_e is the energy of the ion crossing the grid cell, E_1 and E_2 are the electrical field strengths at each side of the grid. The total ion energy K_e can be described as the sum of three velocity components $K_e = \frac{1}{2}m\sqrt{v_x^2 + v_y^2 + v_z^2}$, where v_x is the ions' initial velocity component in X-direction, which is conserved during the flight time, v_y is the velocity component in y-direction, which is perpendicular to the extraction direction and v_z is the velocity component in the orthogonal acceleration and flight

direction.

The velocity components v_y and v_z will change after the ions passing the grid and deflected according to their position in the gap between the wires of the grid. Ions are accelerated in the z-direction and simultaneously decelerated in the y-direction so that total kinetic energy is conserved. The variation of v_z causes a flight time error and the variation of v_y results in an arrival spread in y-direction from the center of the MCP.
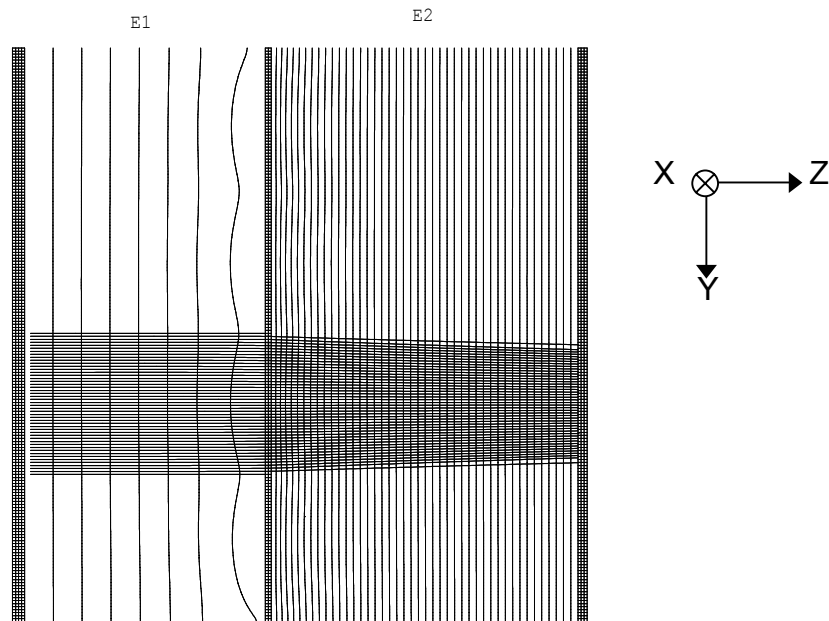

Fig. 4-7 Ion trajectory through the grid from E_1 to E_2

The grid material most commonly used is produced by Buckbee Mears of St. Paul, MN, USA. Their products include a wide variety of wire densities and transmissions. The most popular meshes have wire densities of 70, 117.6 and 333 lines per inch (lpi). These have transmissions of 90%, 88.6% and 70% respectively. Fig. 4-8 shows the flight velocity spread through grid with wire densities of 70, 117.6 and 333 lpi respectively. The values are given in one quadrant of a hole. Real operating conditions are taken into account. The electrical fields in front of and behind grid are 50 V/mm and –250 V/mm respectively. The difference in ion velocity increases with the wire density decreases, for 70 lpi the difference is nearly 14 fold higher than that of 333 lpi.
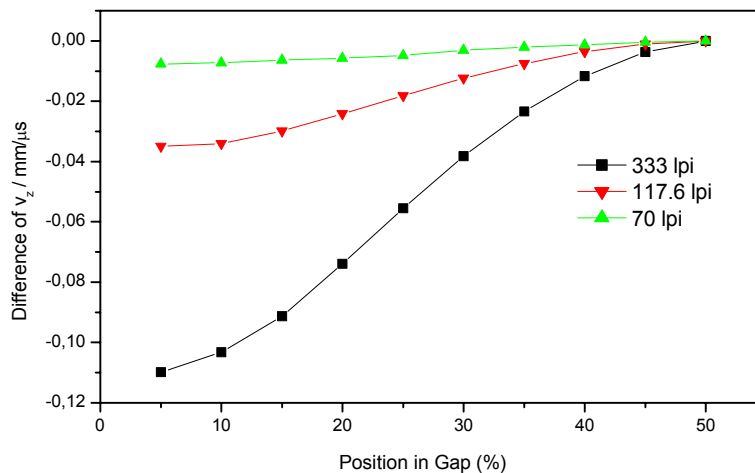
Fig. 4-8 The effect of grid density on the magnitude of the velocity spread

Take into account the y-displacement caused by grid. Shown in Fig. 4-9, the lower the wire density is, the worse the y-displacement is required.
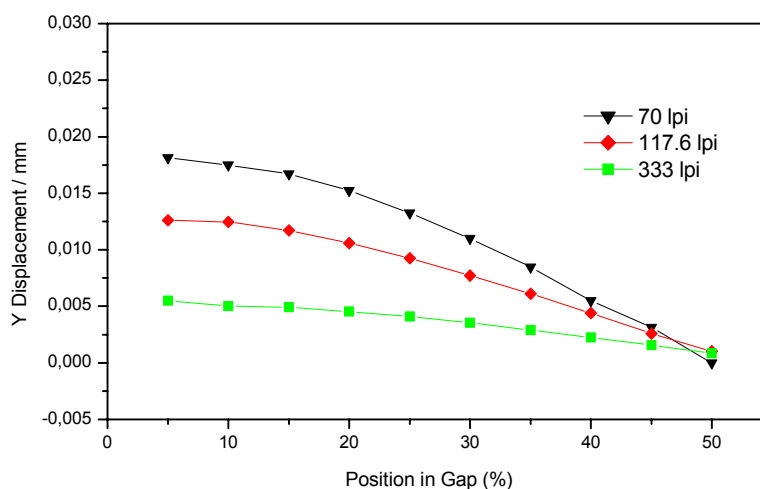
Fig. 4-9 Ions' y- displacement at 0.4 mm behind grid with wire densities of 70, 117.6 and 333 lines per inch

Although they are quite small. but with regard to the linear TOFMS with a acceleration stage followed by a drift region and detector. With the 70 lpi grid, a 20 mm radius detector at 48 cm from the source would be demanded. Although 333 lpi wire density provides a higher mass resolving power limit and less y-displacement, it will reduce the ion transmission. It seems that 117.6 lpi wire density is a good compromise.

In oa-TOFMS, the angle deviates from 90° for the grid in an orthogonal accelerator where ions have far less than their final velocities in the TOF direction. The effect of angle of incidence is shown in Fig. 4-10. the effect is significant when the field

strength on either side of the grid are 50 V/mm and 500 V/mm respectively.

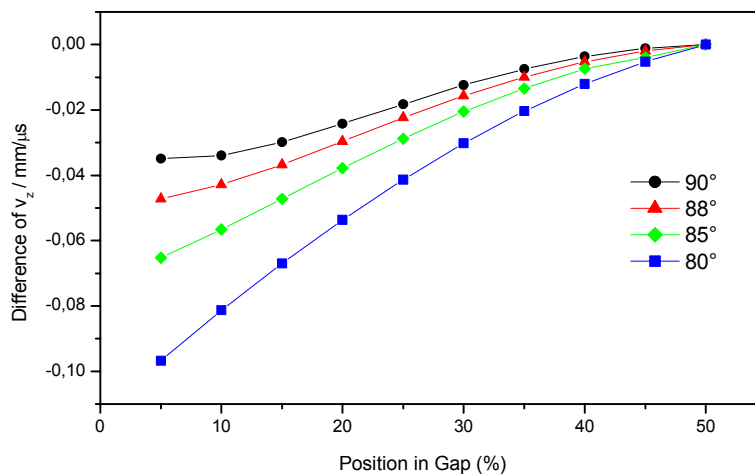Fig. 4-10 Simulated ions velocity spread passing through 117.6 lpi grid boundary in an oa-
TOFMS when ions approaching the grid at an angle not equal to 90°

4.4. Simulation of oa-extration and acceleration.

The parameters for the simulation are shown in Table 4-1.

Table 4-1 parameters for oa-extraction and acceleration simulation

Microchannelplate	Ø 26 mm
Length acceleration	47 mm
Drift region	480 mm
Grid /out/inner	Ø 90 mm / Ø 20 mm
Repeller	Ø 90 mm
Distance between the repeller and Grid 1	6 mm
Thickness of field gard plates	1 mm
Distance between two field guard plates	5 mm

Different numbers of field guide rings, interval between the rings and different voltages for the extraction and acceleration were investigated. For the ion mass of 100 amu, when the initial K_e is 10 eV, the y position when it hit the MCP (starting from Y=0) are shown in Table 4-2. The voltage on repeller and the acceleration voltage affect the ion trajectory very much compared to the interval between each ring for the acceleration rings. For example, for 7 rings, with the interval between each ring varied from 3 mm, 4 mm and 5 mm the y position of ion (100 amu) at the end of TOF was 30.36 mm, 30.35 mm and 30.78 mm respectively when the voltage

on repeller was 0.35 kV and acceleration voltage was set to –2 kV. For 7 rings system and interval between each ring set to 4 mm, The y position change from 30.36 mm to 35.17 mm only the acceleration voltage go from –2 kV to –1 kV. And the voltage on repeller increases from 0.35 kV to 2 kV, the Y position change from 30.36 mm to 25.90 mm.

When the other conditions are same, only the number of field guard rings increase from 7 to 8 and 9, the Y position changed from 30.36 mm to 30.73 and 30.74. it affects the ion trajectory not so much either.
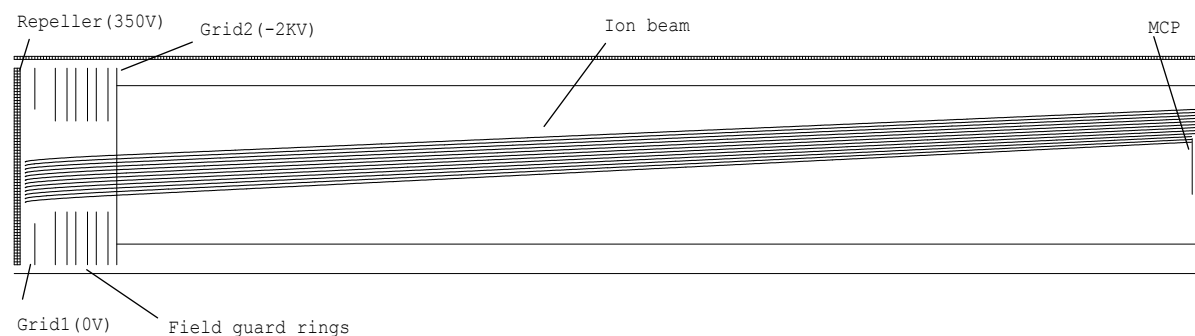
Fig. 4-11 1 Ion trajectory by orthogonal extraction and acceleration system with 7 field guard rings and the interval between rings 4 mm. repeller voltage 350 V, acceleration voltage –2 kV, MCP –2 kV. The initial ion's K_e is 10 eV.

The initial energy of ions is very important for oa-extraction, when the ion's initial K_e increase to 50 eV, the ions flight angle are too big that for the above mentioned voltage it is impossible to reach MCP. Taken into account of the diameter of the microchannelplate, a deflector is indispensable when the ions' initial energy perpendicular to extraction are high.

Fig. 4-12 The ions trajectory with deflector after the orthogonal extraction. The acceleration voltage is –2 kV, repeller Pulse voltage 0.35 kV, deflector voltage 170 V and –170 V respectively.

The deflector was simulated with SIMION 7.0, shown in Fig. 4-12, they are two parallel plates each 40 mm in length and 30 mm in width, the ions (max 100 amu,

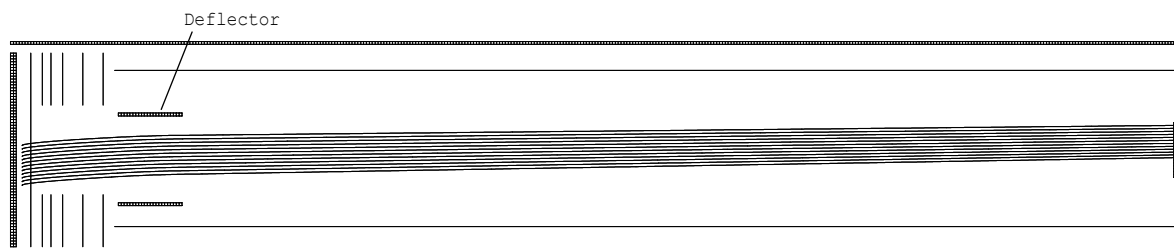initial energy 10 eV) can reach the detector when the voltage on deflector was set to 170 V and –170 V respectively. The experiments were consistent with simulation. When no deflection voltage was applied, no signal was observed by MCP.

Table 4-2 Ion position at the end of TOF with different configurations and different extraction and acceleration voltages

Number of Field guard rings	Interval between each ring/mm	Voltage on repeller/kV	Acceleration voltage/kV	Y position of ion at the end of TOF/ mm
7	4	0.35	-2	30.36
		1		27.81
		2		25.90
		0.35	-1	35.17
		1		31.39
		2		28.71
		0.35	-4	23.12
		1		21.88
		2		20.90
	3	0.35	-2	30.35
		1		27.75
		2		25.82
	5	0.35	-2	30.78
		1		28.03
		2		26.02
		1	-4	23.59
		2		22.20
		3		21.14
8	4	0.35	-2	30.73
		1		28.07
		2		26.10
9	4	0.35	-2	30.74
		1		28.07
		2		26.11

5. <u>Characterization of the pinhole interface for IMS-TOF</u>

The ions formed in IMS have been characterized using mass spectrometry, unfortunately the ability of mass spectrometer to identify ions has been questioned. The concern is that the ions are molecular or clusters and that the distribution of the cluster ions changes as the stagnant drift gas expands into the vacuum system of the mass spectrometer.

The ability of ions to attract and attach neutral molecules is a subject with a long history. A free jet expansion can be viewed as a fast flow reactor. This has been the case, any ions in the expanding buffer gas can change composition. When the buffer gas is helium or hydrogen heated to 125°C - 250°C, the sampling errors are reduced so that relative ion intensities are essentially identical to those theoretically anticipated in the stagnant gas. Because nitrogen and air are commonly used gases for IMS, so in this work nitrogen was used to make the studies.

5.1. Effusion into the vacuum system

The pinhole interface between IMS and TOFMS can be viewed as a fast flow reactor. Once in the vacuum, the gas expands adiabatically and forms a free jet [135, 136]. Gasflow rate G_0 through the first orifice is

$$G_0 = 0.445 \, n_0 \, a_0 \, D_0^2, \qquad\qquad 5\text{-}1$$

Where n_0 is source number density,

$$n_0 = P_0/(T_0 \, k_b), \qquad\qquad 5\text{-}2$$

P_0 and T_0 are pressure and temperature respectively, k_b is Boltzmann constant. a_0 is speed of sound in the source,

$$a_0 = (\delta R_g T_0)^{1/2}, \qquad\qquad 5\text{-}3$$

where δ is the specific heat ratio, R_g is the individual gas constant, for nitrogen R_g is 297 J/kg*K, and D_o is the diameter of the orifice. As for D_o = 0.5 mm, G_0 is 35 ml/s. Mach disc at x_m downstream from the orifice is 4 - 6 mm, according to following equation [137].

$$\frac{x_m}{D_o} = 0.67 \left(\frac{P_0}{P_1} \right)^{1/2}, \qquad\qquad 5\text{-}4$$

where P_0 the pressure in IMS (here is 815 mbar) and P_1 is the background pressure

for the expansion within the chamber (here is fore-vacuum 3-6 mbar), D_o is the diameter of the orifice.

So the Mach disc locates before the ions enter the sampler of TOF. The ions may react with water or neutral molecules to form adducts and clusters downstream the Mach disc. When such ions are analysed in mass spectrometer, the weak bonds associated with the ion adduct and clusters leading to false information about the relative concentration of the ions exist in IMS. Therefore care must be taken in applying the TOFMS results to IMS.

For example, normal UV-IMS spectrum of acetone shown in Fig. 5-1. There is only one peak at K_0=1.80 cm^{2}V^{-1}s^{-1}. But the acetone mass spectra shown in Fig. 5-2 are different with different voltages applied on sampler.
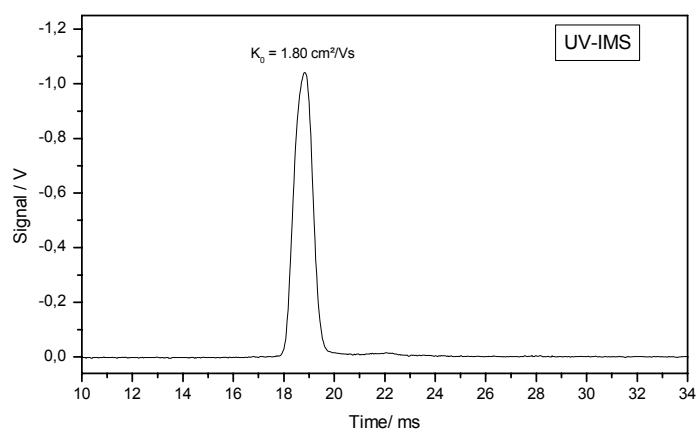

Fig. 5-1 UV-IMS spectrum of 26 µg/L acetone

The water content of the sample gas was 0.197 ppm (measured with Panametrics moisture monitor series 35). The major ions are $(CH_3COCH_3)_n(H_2O)_mH^+$ with m/z ratios of 59, 77,116, 134, 174, 192. When thevoltage on the sampler is 50 V, the most abundant ion is $(CH_3COCH_3)_2^+$, which has an amplitude 6.7 times that for $(CH_3COCH_3)^+$ and 5.5 times that for $(CH_3COCH_3)_3(H_2O)^+$. When the voltage on sample increases to 80 V, the most abundant ion is still $(CH_3COCH_3)_2^+$, but the ratio decreased, it has an amplitude 1.7 times that for $(CH_3COCH_3)^+$, the trimer and trimer water adduct ions disappear. If the voltage on sampler goes up to 110V, the major ion change to $(CH_3COCH_3)H^+$, which has an amplitude 4.0 times that for $(CH_3COCH_3)H_3O^+$ and 35.5 times that for $(CH_3COCH_3)_2^+$. When the voltage increases to 130 V, the spectra is nearly the same as that of 110 V, but if the voltage on the sampler is below 40 V, there is no signal which can be detected in mass spectrometer. Other ketones display the same feature, for example, 2-hexanone has

the most abundant dimer ion, which is 5.2 times amplitude that for monomer ion when the voltage on the sampler is 50 V. When the voltage increases to 110 V, there is nearly no dimer ion.
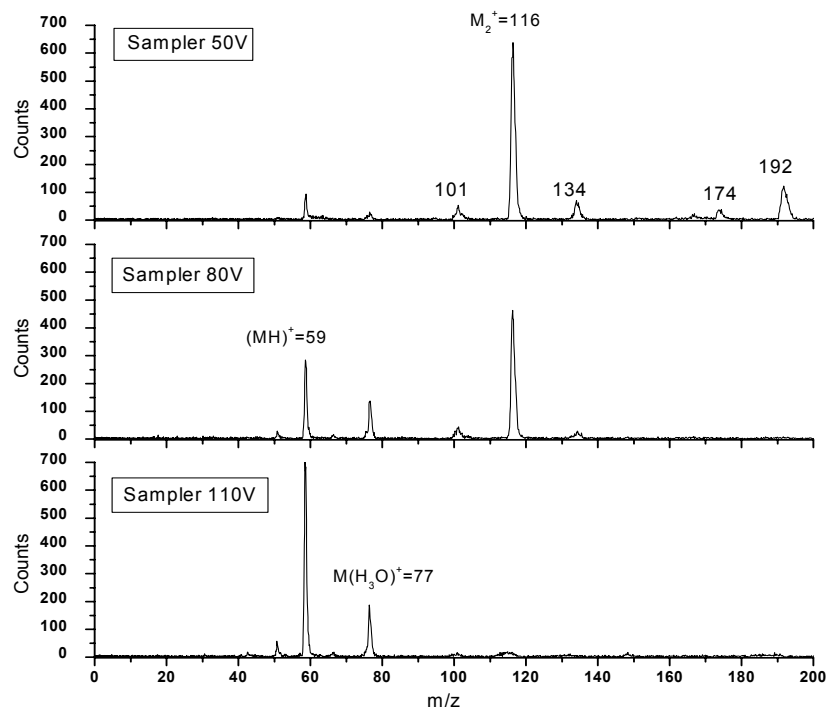

Fig. 5-2 IMS^{PID} TOFMS spectra of acetone with different voltages applied on the sampler

So the electric field in the first stage vacuum can dissociate the ions as they gain energy from the field and collide with neutral gas molecules during the expansion. Collisional dissociation of larger cluster ions is favored over smaller cluster ions because the larger ions are more weakly bounded to their adducts. This may occur just beyond the Mach disc. Because changes of the voltage on the pre-sampler and the lens can only vary the total intensity of signal, and the relative magnitude of the peaks doesn't change.

5.2. Comparison with Finnigan LCQ™ mass analyzer

In order to determine what kind of ions are the major one in IMS, UV-IMS was coupled to a Finnigan LCQ^{TM} MS detector. This system was originally equipped with an APCI interface and coupled with liquid chromatographic columns. As shown in Fig. 5-3, instead of the pinhole a heated capillary is used as sample ions inlet, so the ions should have totally different conditions.
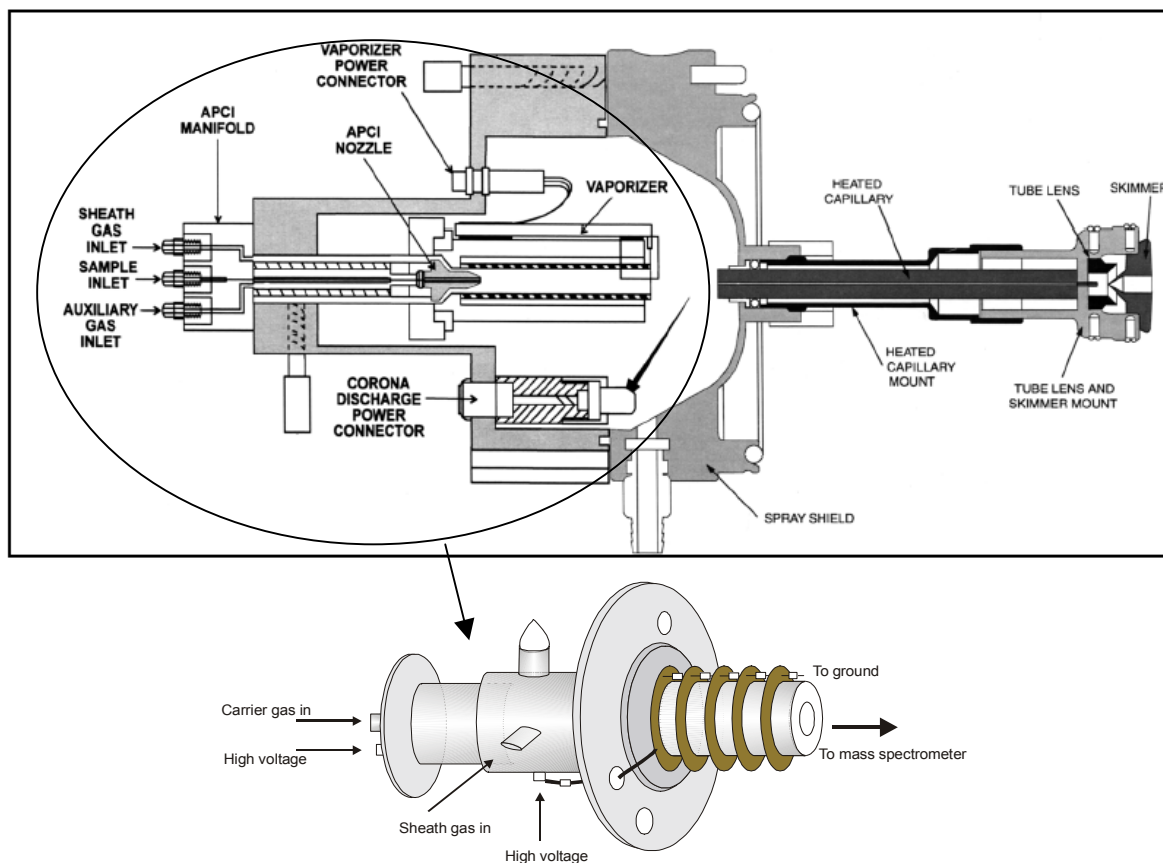
Fig. 5-3 . Schematic diagram of APCI ionisation source of Finnigan LCQ (above), from Finnigan LCQ hardware mannual 1996. Instead of APCI source, the UV-IMS without shutter grid (bottom) was used as ionisation source coupled to MS detector

With this equipment acetone was measured and all the data were collected at normal operating conditions for Finnigan LCQ™. the shutter grid of the UV-IMS was removed and the IMS was driven as a IMS[PID]. Fig. 5-4 shows the spectra of the UV-IMS coupled to the Finnigan LCQ™ MS detector, the major peak is at m/z 59, which is corresponding to protonated acetone molecular ion. This result is the same as that of IMS TOF spectrum with sampler voltage of 110 V.
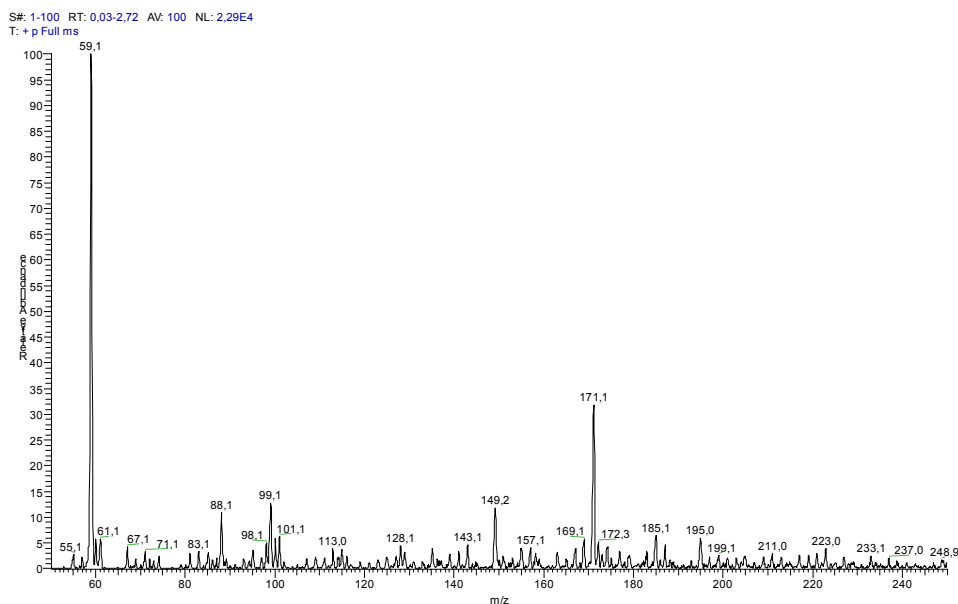
Fig. 5-4 IMS [PID]-mass Finnigan LCQ[TM] MS spectrum of acetone

Toluene was measured with both system. Fig. 5-5 shows the IMS [PID]-mass spectrum of toluene, there are mainly four peak groups at m/z 81, 92, 107, and 220. The first one may be due to contaminations from the IMS cell, because the cell was used after short activation. 92 is the monomer peak M^+, 107 and 220 should be clusters.
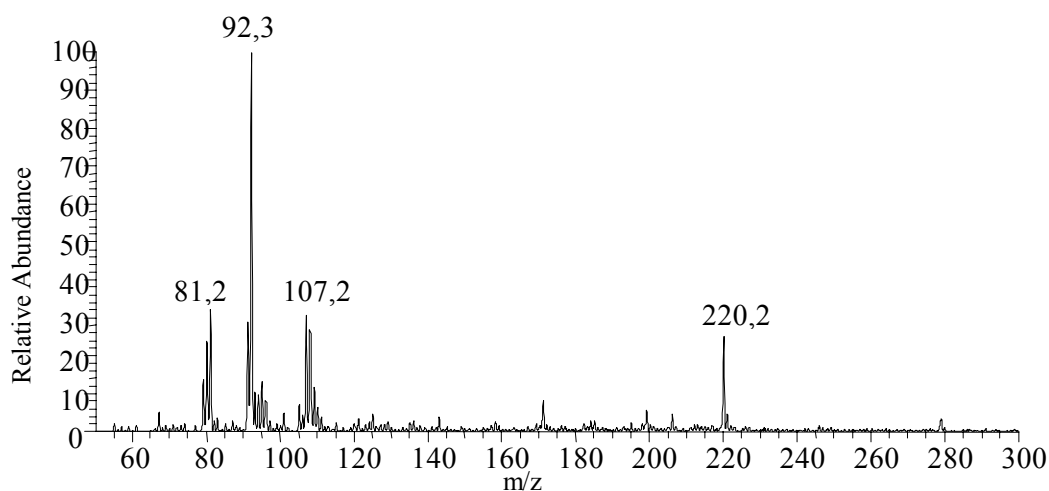
Fig. 5-5 IMS [PID]- Finnigan LCQ[TM] MS mass spectrum of toluene

The IMS-TOF spectrum of toluene is shown in Fig. 5-6, compared with that of the Finnigan LCQ[TM] MS spectrum, the major ion has m/z ratio of 92, which corresponds to the molecular ion, and a peak at m/z 78 and 107 which corresponds to benzene and xylene ions, respectively.
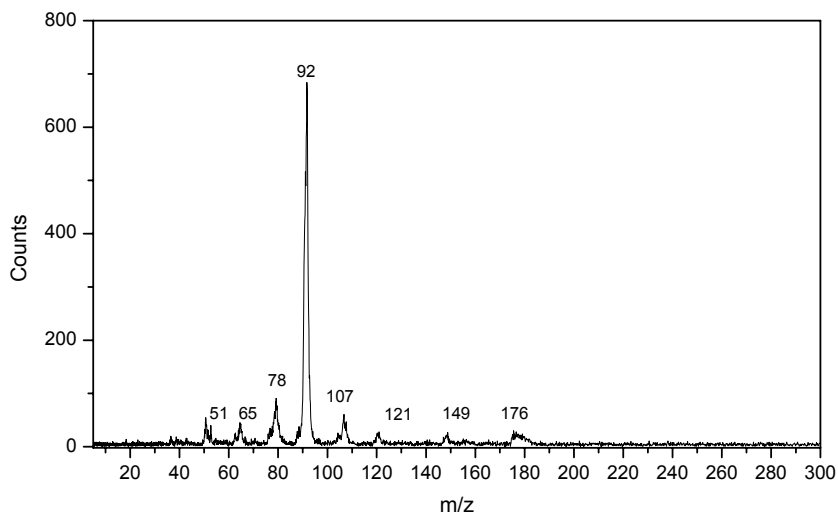
Fig. 5-6 Spectrum of toluene using IMS -TOF

Fig. 5-7 shows the IMS[PID]- Finnigan LCQ^{TM} mass spectrum of methyl t-butyl ether (MTBE). The highest peak is at 57 m/z. Obviously it results from $[CH_3]_3C^+$, The peaks at m/z 88 and m/z 177 are MTBE monomer and protonated dimer respectively, which have amplitude of 60% and 35% that of $[CH_3]_3C^+$. Fig. 5-8 shows the spectrum of MTBE using IMS –TOF with the sampler voltage on 110V, the most abundant ion is at m/z 107, it corresponds to $(C_5H_{12}O^.H_3O)^+$. The MTBE molecular ion and the fragment of $[CH_3]_3C^+$ have the amplitude of 88% and 51% that for major peak respectively. The obvious difference between TOF and Finnigan LCQ^{TM} MS is that the protonated molecular ion is much greater in TOF. Especially, for substances with high proton affinities like MTBE, which has a proton affinity of 841.6 kJ/mol.
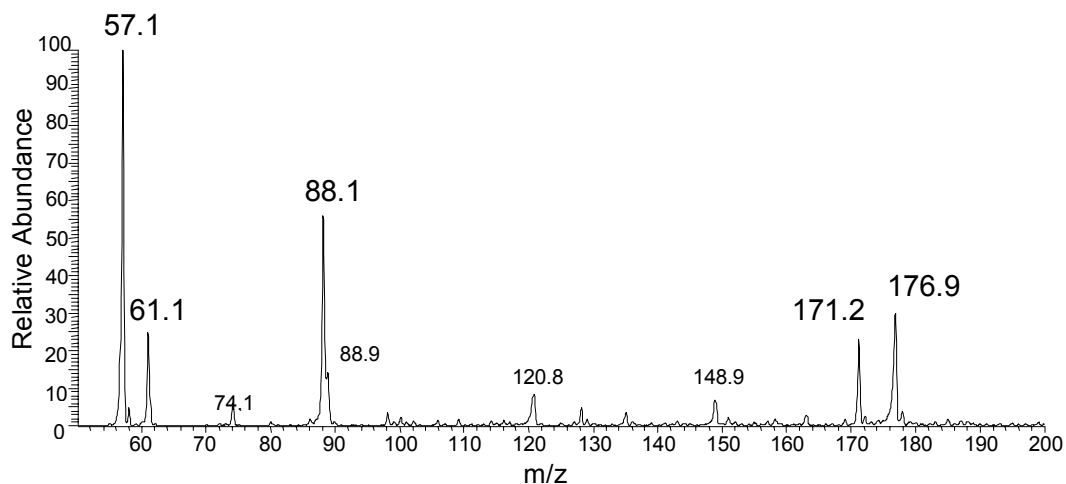
Fig. 5-7 IMS[PID]- Finnigan LCQ[TM] mass spectrum of MTBE

Fig. 5-8 Spectrum of MTBE using IMS -TOF

Selected other substances have also been measured, shown in Table 5-1. According to these results, for most volatile organic compounds the major ions corresponding to monomer ions and the normally used UV lamp can lead to cleavage of bonds for some compounds the fragments are very stable, but for some other substances such as isoprene, it is easy to form clusters.
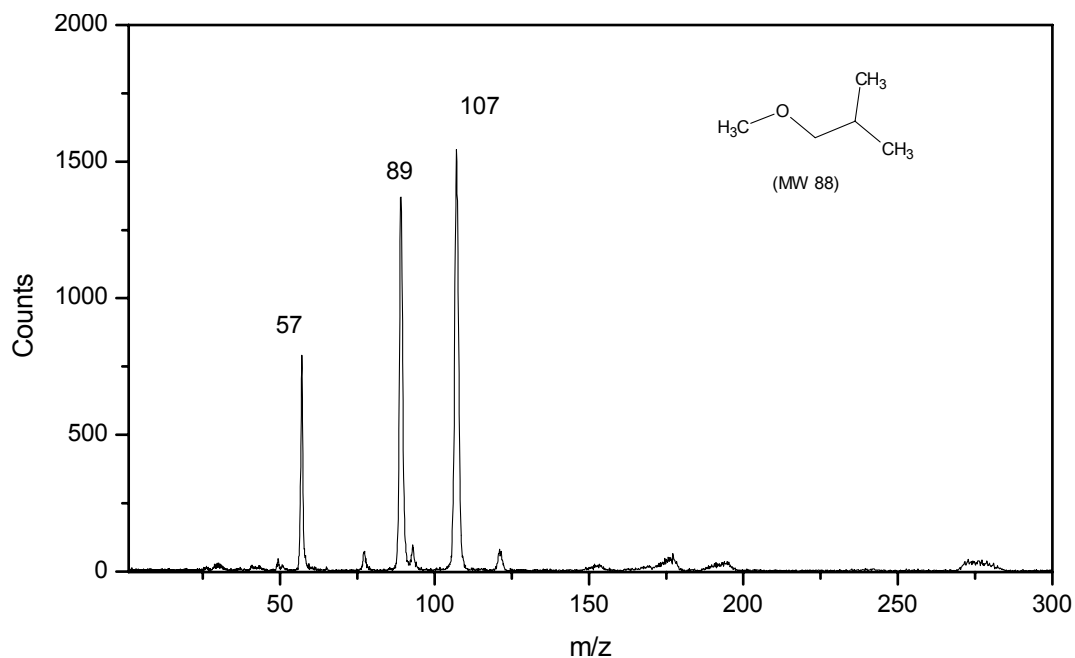
Table 5-1 Substances and their mass signals measured using Finnigan LCQ mass spectrometer

Substance	Molecular weight	Peaks			
		Fragment	monomer	Dimer	Cluster
acetone	58		59[MH+]*		
butanone	72		73[MH+]*		
benzene	78		78*		
toluene	92		91,92*		107,220
o-xylene	106	80, 91	106*		
mesitylene	120	93, 105	120*		136
m-dichlorobenzene	147	92	146*, 148		
tetrachloroethylene	166	92	166,*164,168		
trichloroethylene	131	59,61			
MTBE	88	57*	88	176	171
α-pinene	136	81, 93, 119	136	272*	
isoprene	68				80*,95,107

* basic peak

5.3. Studies with air and argon

Instead of nitrogen also synthetic air and argon were selected as carrier gas, because air is a commonly used drift gas for IMS. Furthermore these two gases have large Joule-Thomson expansion coefficients, 0.1371 and 0.23 for air and argon at 373 K, respectively whereas it is for helium –0.0638 at 373 K [138], any tendencies toward nucleation should be amplified.

Fig. 5-9 shows acetone mass spectra collected with synthetic air, argon and nitrogen as carrier gas individually. The water content in synthetic air, argon and nitrogen are 0.4 ppm, 0.4 ppm and 0.3 ppm respectively. The major ions for all three gases are $(C_3H_6O)H^+$ with m/z ratio of 59, which has an amplitude 5.5 - 6.5 times that for $(C_3H_6O)H_3O^+$ at m/z 77. all the spectra are quite similar, only in argon there are a lot of small peaks maybe because of the impurity. No carrier gas adducts are observed in either of the three gases. Signal magnitude is nitrogen > argon > air.
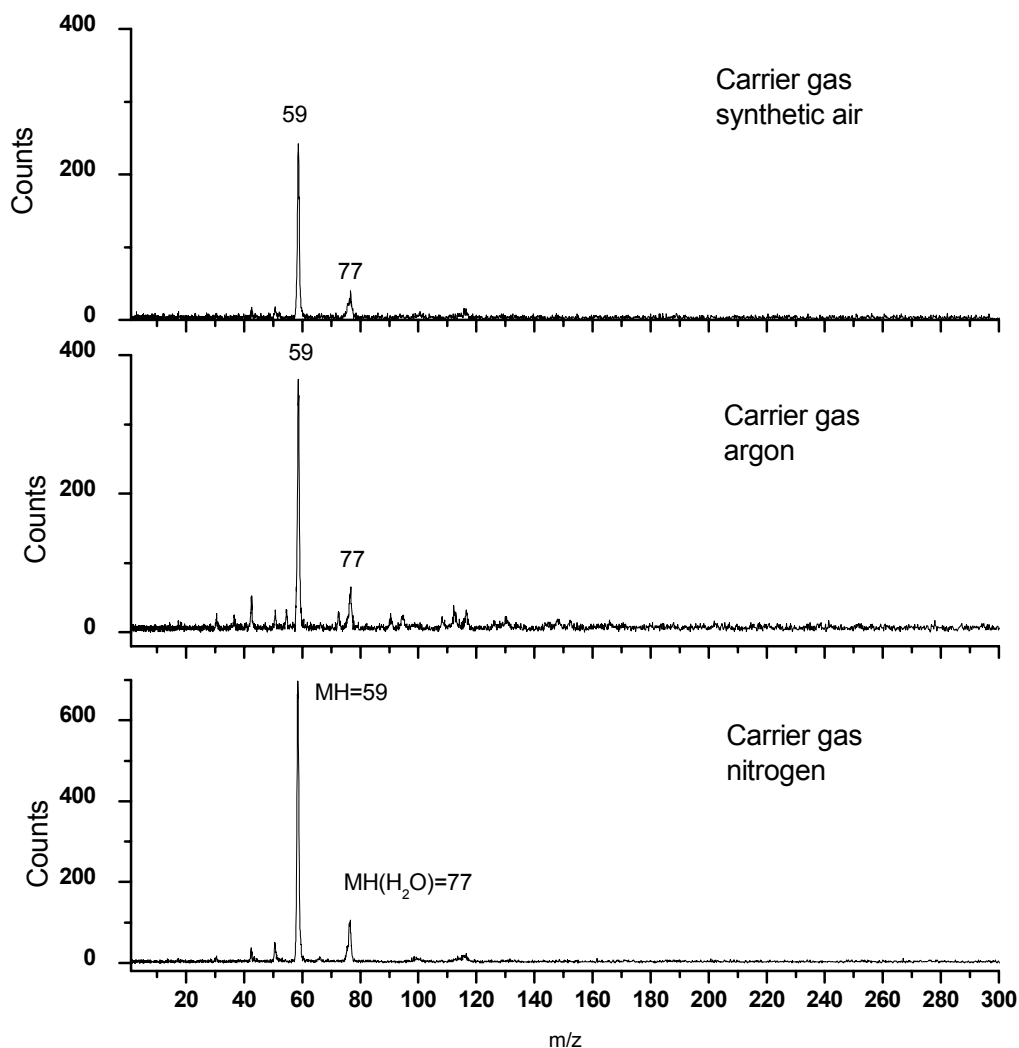
Fig. 5-9 Spectra of acetone using synthetic air, argon and nitrogen as carrier gas (from above to bottom) with optimal voltages on interface of TOF.

5.4. Influence of the distance between sampler and skimmer

Acetone was detected with the distance between the sampler and skimmer set at 4 mm, 5 mm and 6 mm, respectively. The peak distributions are the same as illustrated in Fig. 5-10, the major peak is at m/z 59 which is corresponding to the protonated molecule peak. With regard to the magnitude of the signal, 4 mm and 5 mm are nearly the same and 6 mm is obviously small, this is consistent with the experiments detected with the electrometer.
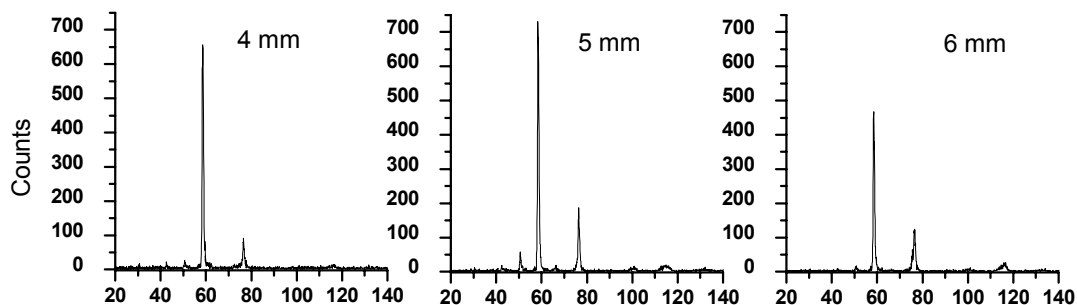
Fig. 5-10 UV-TOF spectra of acetone with different distance between the sampler and skimmer

So it means the second step of the vacuum is not critical for the ion identification, The above illustrated measurement was done with a sampler diameter of Φ 0.35 mm, the vacuum is 6 mbar and 1.3×10^{-2} mbar, respectively, before and after the sampler. According to the above mentioned equation 5-4, the Mach disc was located before 5 mm downstream of the sampler. The ions distribution remained regardless of the Mach disc position, only the signal intensity changed. Consequently the reactions leading to misunderstanding of ions status occur in the first step when ions go through first orifice from atmospheric pressure into vacuum.

5.5. Influence of the other parameters of interface

The other parameters such as the diameter of the sampler were investigated. The signal magnitude was reduced to half of the value when the sampler diameter in 0.35 mm decreased to 0.25 mm as showed in Fig. 5-11. The highest peak of acetone are identical at m/z 59.
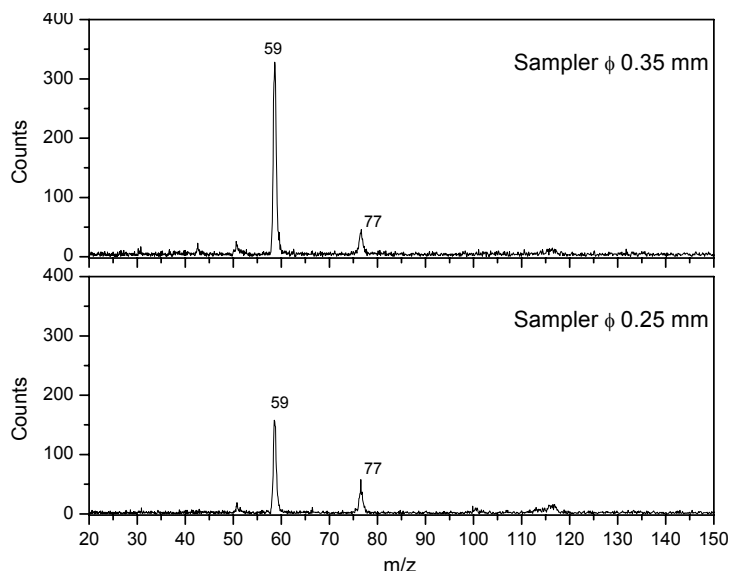
Fig. 5-11 UV-TOF spectra of acetone with different diameters of the sampler. The distance between the sampler and skimmer was 4mm.

As demonstrated in Fig. 5-12, the voltage on the pre-sampler can influence the signal magnitude greatly, the peak height at 59 m/z with the pre-sampler on 90 V is 4.4 times of that of pre-sampler set at 125 V, although the peak at 77 m/z is only 1.5 times correspondingly.
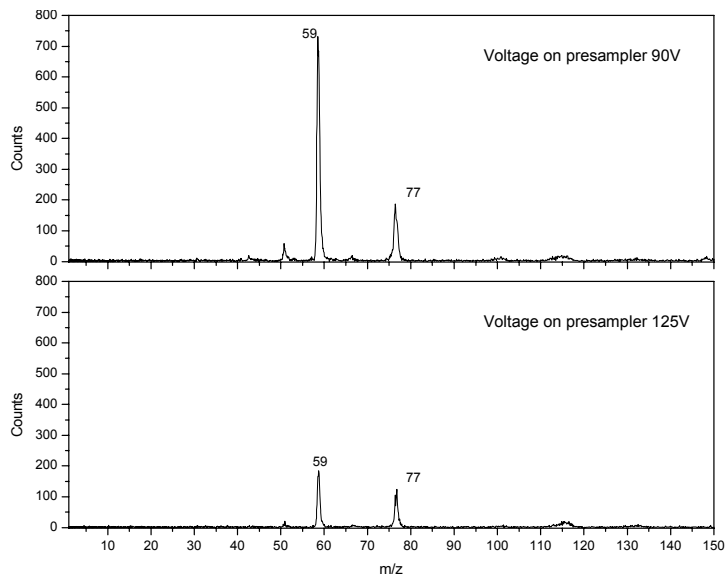
Fig. 5-12 UV-TOF spectra of acetone with different voltage on pre-sampler, the other parameters are the same.

The major peak of acetone on both conditions are composed of protonated monomers, the voltage on the pre-sampler can not affect it.

6. <u>Material and Methods</u>

6.1. Chemicals

acetone, for spectroscopy 99.9%, Merck, Darmstadt

2-butanone, puriss p.a. 99,5% (GC), Fluka, Steinheim

3-pentanone, for synthesis 99% (GC), Merck, Hohenbrunn

cyclohexanon, puriss p.a. 99,5% (GC), Fluka, Steinheim

2-hexanone, purum 98% (GC), Fluka, Steinheim

2-Heptanone, purum 98% (GC), Fluka, Steinheim

2-octanone, purum 97% (GC), Fluka, Steinheim

5-nonanone, purum 97% (GC), Fluka, Steinheim

ethanol, for spectroscopy 99.9%, Merck, Darmstadt

1-propanol, 99.8% (GC), Fluka, Steinheim

1-butanol, for UV-spektoskopie, Riedel-de Haen

2-butanol, puriss p.a. 99,5% (GC), Fluka, Steinheim

3-methyl-1-butanol, microselected, 99% (GC), Fluka, Steinheim

3-methyl-1-butanol, purum, 99% (GC), Fluka, Steinheim

2-pentanol, purum, 98% (GC), Fluka, Steinheim

1-hexanol, puriss p.a. 99% (GC), Fluka, Steinheim

3-octanol, puriss p.a. 99% (GC), Fluka, Steinheim

benzene, G.R. 99.7%, Merck, Darmstadt

toluene, puriss 99,7% (GC), Fluka, Steinheim

o-xylene, puriss p.a. 99% (GC), Fluka, Steinheim

m-xylene, puriss p.a. 99% (GC), Fluka, Steinheim

ethylbenzene, puriss p.a. 99% (GC), Fluka, Steinheim

1,3 – dichlorobenzene, puriss p.a. 99% (GC), Fluka, Steinheim

pyridine, puriss p.a. 99% (GC), Fluka, Steinheim

lutidine, puriss p.a. 99% (GC), Fluka, Steinheim

All reagents are used without further purification.

6.2. Sample gas preparation

A large range of test gas concentrations were required for the measurements, so the exponential dilution as well as the generation of gases using a permeation septum

were exploited. The schematic diagrams for the permeation and the exponential dilution device are shown in Fig. 6-1.

6.2.1. Membrane inlet permeation device

For the UV-IMS-TOF main measurements using UV-IMS-TOF, a 1mL vial (CS-Chromatographie Service GmbH, Langerwehe) is partially filled with the pure liquid of the compound of interest and was then sealed with a central hollow cap, where a PDMS (polydimethylsioxane) membrane (thick: 1mm; Reichelt Chemietechnik GmbH + Co., Heidelberg) was seated, variation of the test gas concentration was achieved by using other membranes, such as sealing disc made from nature rubber and PTFE G8-S, G8-1.0, G8-1.3 (CS-Chromatographie Service GmbH). The vial was put in a big bottle maintained at a constant temperature while passing a flow of 1 L/min nitrogen gas (99.999%) over it. The resulting test gas concentration was determined by weighing the remaining mass of the vial within certain time interval. It can be expressed by

$$C_g = \Delta m / t v_c \qquad\qquad 6\text{-}1$$

where Δm is the mass difference (µg), t is the time interval (min) and v_c is the carrier gas flow rate (L/min). In this way, the constant concentration of test gas was generated.
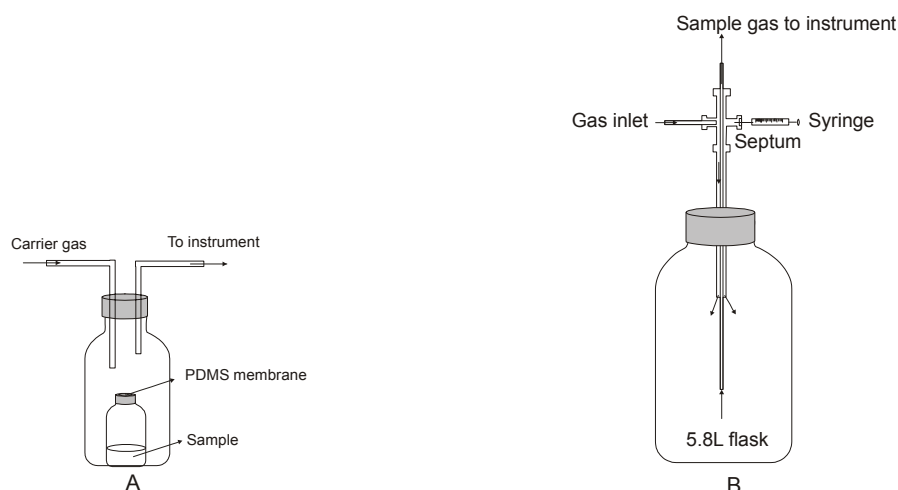
Fig. 6-1 A: Schematic of permeation device,   B: Schematic of exponential dilution device.

6.2.2. Exponential dilution device

for the calibration and LOD detections, exponential dilution was employed [131]. the pure solutes of 5-10 µL were injected with syringe into a 5.8 L flask through a septum

and fully vaporized and diluted by a constant nitrogen gas flow of 1 L/min. the resulting test gas concentration was calculated with

$$C_g = C_0 e^{-\varepsilon t}$$
6-2

in this expression C_0 is the initial concentration, with

$$\varepsilon = v_c / V_g$$
6-3

where v_c is the carrier gas flow rate and V_g is the volume of the dilution flask.

6.2.3. Carrier gas humidity generator

For the measurement of the influence of the carrier gas humidity, well defined relative humidity (RH) values of the sample carrier gas were generated by mixing two gas flows with mass flow controller (MFC — MKS, mass-flow® controller). One was dry nitrogen (0% relatively humidity), the other passing through two serial bottles with water and expected to be saturated (100% relatively humidity), as shown in Fig. 6-2. With different flows of these two gases the relative humidity of the carrier gas can be controlled. Calibration of the system using a standard RH sensor showed excellent agreement of measured and expected RH.

Fig. 6-2 schematic diagram of the humidifier to generate given RH in carrier gas

6.3. Ketones detection with UV-IMS-TOF

The study of eight aliphatic ketones (acetone, 2-butanone, 2-pentanone, 2-hexanone, 2-heptanone, 2-octanone, 3-octanone, 5-nonanone) and one cyclic ketone (cyclohexanone) was undertaken in order to study systematically the processes of photoionization and reactions in UV-IMS.
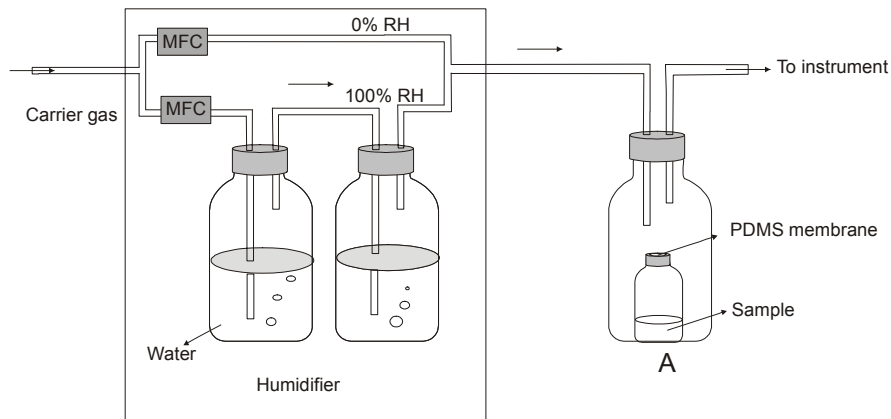
6.3.1. UV-IMS and UV-TOF measurements of pure substances

Pure ketone samples were measured using the membrane inlet permeation system. Different concentrations were achieved according to the volatility of the substance and the type of membrane. The UV-IMS spectra are showed in Fig. 6-3, Acetone, butanone, 2-pentanone consisted of one major peak and the drift times increase continuously from 18.9 ms for acetone to 23.1 ms for 2-pentanone. When the concentration are very high, a small peak appeared after the first peak. For 120 µg/L acetone there is an additional peak at 22.3 ms.
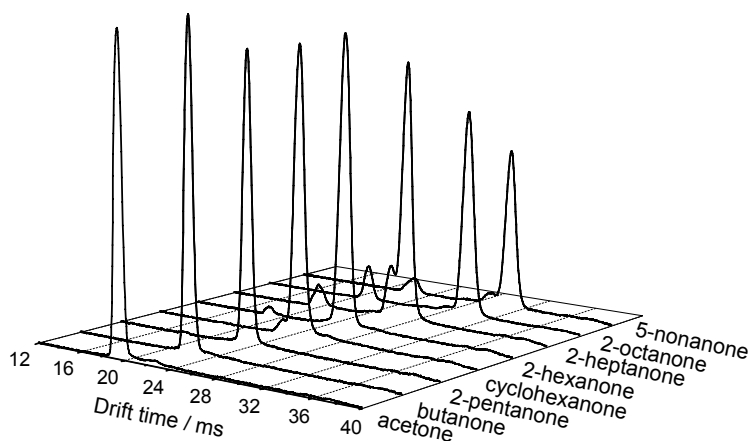
Fig. 6-3 Ion mobility spectra for acetone (120 µg/L), butanone (173 µg/L), 2-pentanone (52 µg/L), 2-hexanone (240 µg/L), cyclohexanone (93 µg/L), 2-heptanone (35 µg/L), 2-octanone (112 µg/L) and 5-nonanone (98 µg/L)

Beginning from 2-hexanone, in front of the major peak there are 1 or 2 other peaks. This fragment peaks increase too according to the number of carbons. The K_0 of 2-hexanone fragment is 1.91 $cm^2V^{-1}s^{-1}$ which is even faster than that of acetone (1.80 $cm^2V^{-1}s^{-1}$).

The trend in the drift times for acetone, 2-butanone, 2-pentanone, 2-hexanone, 2-heptanone, 2-octanone and 5-nonanone reflected the size difference consistent with molecular mass for each compound. From the drift time, the reduced mobilities of the ketones are calculated and listed in Table 6-1. The reduced mobility for the major

peak is decreased from 1.80 $cm^2V^{-1}s^{-1}$ for acetone to 1.13 $cm^2V^{-1}s^{-1}$ for 5-nonanone. In addition, 2-octanone ($K_0=1.17$ $cm^2V^{-1}s^{-1}$)and 3-octanone ($K_0=1.20$ $cm^2V^{-1}s^{-1}$) can also be separated by UV-IMS. In order to identify the peaks in the UV-IMS, the same pure ketone samples were measured individually with UV-TOF. It yields simple spectra that facilitate analysis as shown together in Fig. 6-4: All the ketones have one major peak corresponding to $[MH]^+$, and one other apparent peak corresponding to $[MH+H_2O]^+$. Those are ions with m/z values for acetone (59,77), 2-butanone (73,91), 3-pentanone (87,105), 2-hexanone (101, 119), 2-heptanone (115, 133), 3-octanone (129, 147) and 5-nonanone (143, 161). But for cyclohexanone, octanone and nonanone the $[M+H]^+$ peaks are relatively small, because the cyclohexanone, octanone and nonanone have lower vapour pressure, so the concentrations in the gas samples are smaller. The dimer peak appeared for all ketones, too.
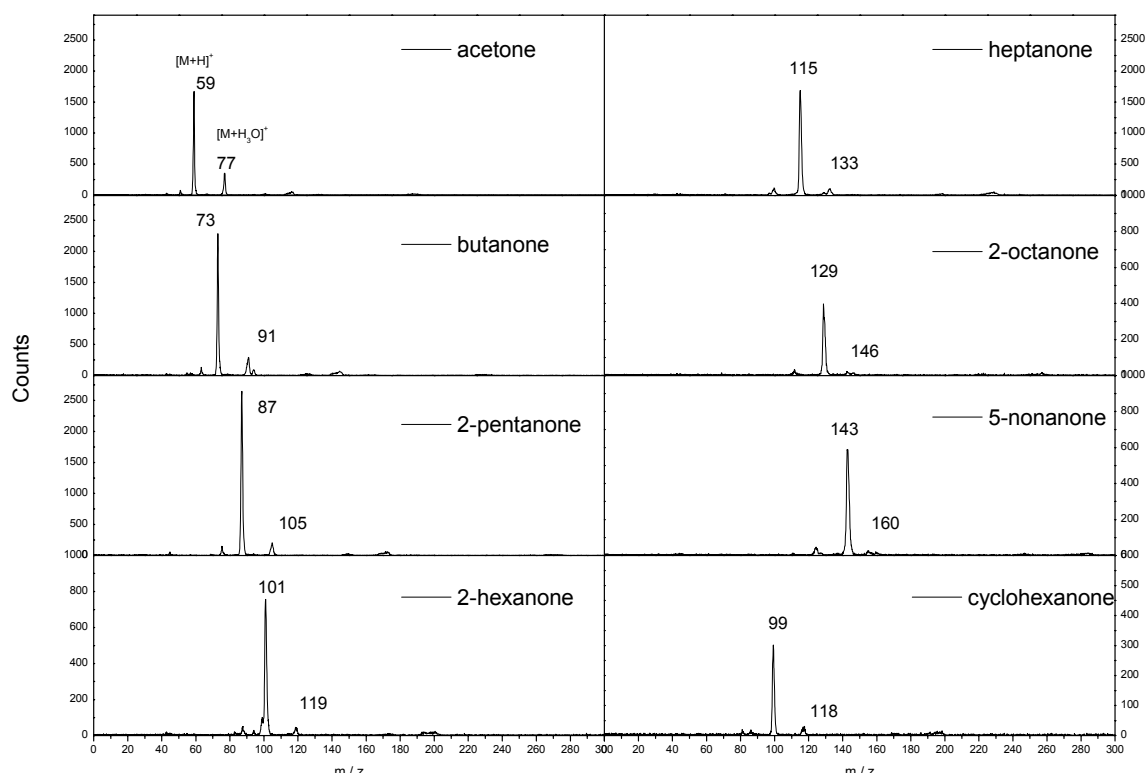
Fig. 6-4 10.6 eV UV-lamp photoionization TOF spectra of acetone (81.7 µg/L), butanone (74.6 µg/L), 3-pentanone (74.8 µg/L), 2-hexanone (37.4µg/L), 2-heptanone (17.0 µg/L), 2-octanone (15.9 µg/L), 5-nonanone (10.4 µg/L), cyclohexanone (12.3 µg/L)

Table 6-1 Reduced mobility K_0 of the ketone ions with UV-IMS

Ketone	MW	IE(eV)	K_0 (cm^2 V^{-1}.s^{-1})		
			Peak 1 (major peak)	Peak 2	Peak 3
acetone	58	9.69 ± 0.02	1.80	1.50	
2-butanone	72	9.52 ± 0.04	1.65	1.39	
2-pentanone	86	9.31 ± 0.02	1.50		
cyclohexanone	98	9.16 ± 0.02	1.41		
2-hexanone	100	9.35 ± 0.06	1.37		1.91
2-heptanone	114	9.33 ± 0.03	1.26	1.33	1.78
2-octanone	128	9.40 ± 0.03	1.17		1.68
3-octanone	128	-	1.20		1.69
5-nonanone	142	9.07	1.13	1.20	1.58

In Fig. 6-5 the relationship between reduced mobility K_0 of the major peaks in the UV-IMS and the mass of [M+H]$^+$ of the ketones are demonstrated.
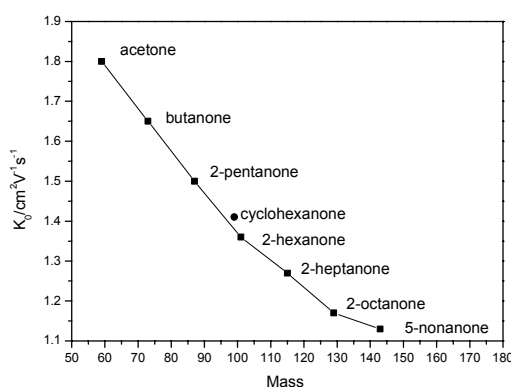
Fig. 6-5 Plots of reduced mobility K_0 of the major peaks in IMS vs. [MH]$^+$of the ketones respectively

It demonstrates that 5-nonanone remarkably deviates from the linear because of the different position of the carbonyl group. 2-hexanone is the turning point which is consistent with the UV-IMS spectra, starting from it there are separable fragment peaks. It can be explained by the UV-TOFMS too. In Table 6-2 all the peaks and their abundances in TOFMS are listed. The peak area of the base peak in TOF was taken as 1, other peaks are calculated according to it. All fragments for acetone, 2-butanone and 2-pentanone are 7%, 12% and 9%, respectively, and the mass of the fragments are similar to those of the molecule ions, so for these three ketones appear only one peak by IMS measurements. The fragment ions of 2-hexanone, 2-heptanone, 2 -octanone, 3-octanone and 5-nonanone constitute respectively 21%, 20%, 24%, 21%, 22% of the total ion current, which is in good agreement with gas phase ion energy data[139]. the mass of the fragments are much smaller than that of

molecule, consequently there are more peaks by IMS. although cyclohexanone has 16% fragment, there is no small fragment, so in IMS there is only one shoulder before the major peak and no separable fragment peak.

Table 6-2 the ion abundances by UV-TOF with sampler voltage of 104 V

Ketone	m/z	Abundance	Ketone	m/z	Abundance
Acetone	59	1.00	5-nonanone	143	1.00
	43	0.02		43	0.04
	51	0.05		69	0.04
	77	0.30		110	0.03
	101	0.04		124	0.11
	117	0.13		155	0.07
	189	0.10		159	0.04
				246	0.06
				284	0.10
2-Butanone	73	1.00	2-heptanone	115	1.00
	43	0.01		30	0.03
	55	0.02		43	0.04
	57	0.03		55	0.02
	63	0.06		71	0.02
	91	0.22		100	0.10
	94	0.06		129	0.04
	127	0.06		133	0.08
	145	0.14		199	0.04
				229	0.10
2-pentanone	87	1.00	2-octanone	129	1.00
	43	0.03		43	0.06
	75	0.06		69	0.04
	105	0.12		85	0.02
	149	0.03		113	0.12
	171	0.09		143	0.08
				146	0.08
				223	0.09
				257	0.13
2-hexanone	101	1.00	3-octanone	129	1.00
	43	0.06		43	0.03
	87	0.08		69	0.03
	83	0.04		94	0.06
	94	0.03		113	0.09
	119	0.11		143	0.07
	173	0.05		146	0.04
	201	0.13		192	0.04
				222	0.21
				256	0.14
			cyclohexanone	99	1.00
				81	0.06
				86	0.10
				117	0.16
				169	0.08
				197	0.21

6.3.2. UV-IMS, UV-TOF measurements of mixture

The mixture of 2-heptanone and 3-octanone were investigated by IMS and TOFMS

individually (Fig. 6-6). With IMS these two ketones can not be separated, The main peaks of 2-heptanone and 2-octanone become combined and the small fragments merged too. With UV-TOFMS 2-heptanone and 2-octanone protonated molecular ion peak at m/z 115 and 129 are the main peaks and well separated. The ionisation energy of 2-heptanone (9.33 eV) and 2-octanone (9.40 eV) are similar. Two molecular peaks can be clearly seen, but for mixture of substances with distinct difference of ionization energy, for example acetone (9.69 eV) and 2-octanone (9.40 eV), due to the charge transfer the peak of acetone is relative small, so the relative signal intensities for each compound in a mixture may not give an accurate representation of the relative abundances, to solve this problem, a chromatographic separation before the test is necessary.
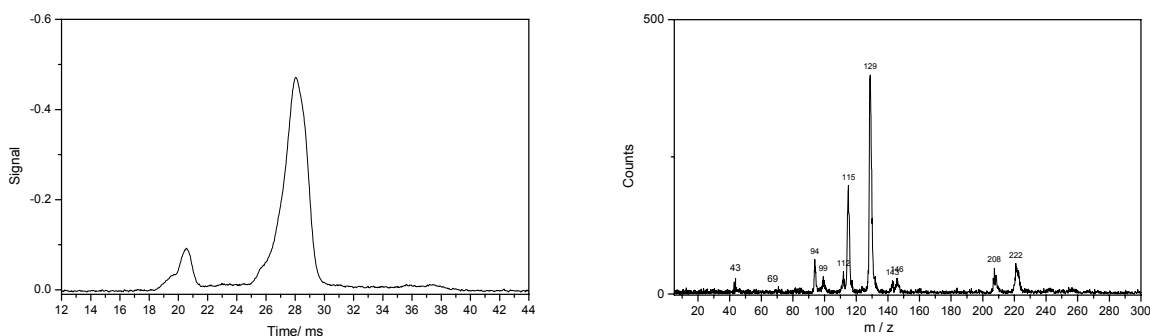
Fig. 6-6 Spectrum of 2-heptanone and 2-octanone mixture using UV-IMS (left) and TOF (right)

6.3.3. Limits of detection and calibration curve

Response vs. concentration was determined individually for acetone and butanone with UV-IMS and UV-TOF, plots of signal (peak area) vs. gaseous concentrations are shown in Fig. 6-7 with a linear range of three orders of magnitude. The detection limits (LOD) with UV-IMS for acetone and butanone are 0.19 µg/L and 0.097 µg/L, respectively, while they are with UV-TOF 0.80 µg/L and 0.42 µg/L, respectively.
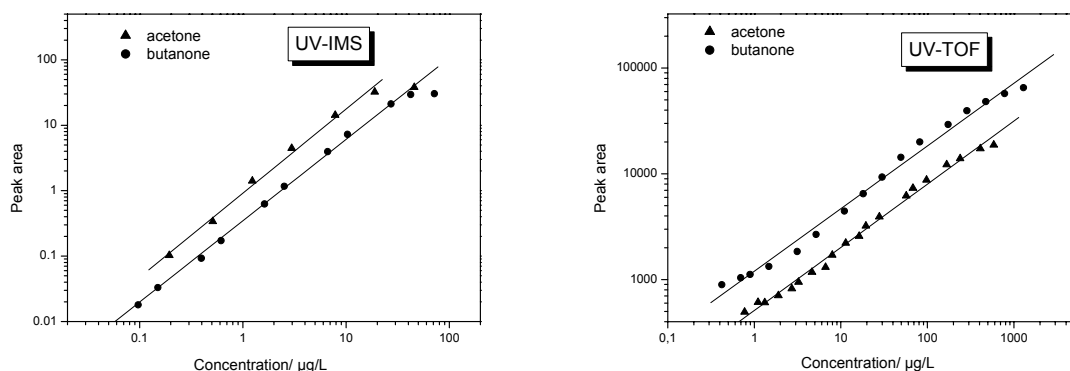
Fig. 6-7 Plot of log peak area vs. log gaseous concentration with (a) UV-IMS (b) UV-TOF

6.3.4. Photo ionisation mechanism of ketones

The principle mechanism for photoionization of ketones is proton absorption and electron ejection to form the molecular ion M^+. In the presence of water vapor (~0.2 ppm humidity in the carrier gas of nitrogen), the molecule ion can extract hydrogen to form MH^+ or even $[MH \cdot H_2O]^+$, because the ketone has a high proton affinity. There are also little abundance of fragmentations, which has not been actively explored previously. It could be formed from protonated monomers rearrangements or decompositions to small fragment ions. All the observed modes of dissociation and reactions are discussed as following, the most abundant ions for all the ketones are protonated molecular ions ([i], [vii]) and all the ketones have $[M+H_3O]^+$ ions too. The fragment ions can attach proton or water molecule too.

$$
\begin{array}{lllllll}
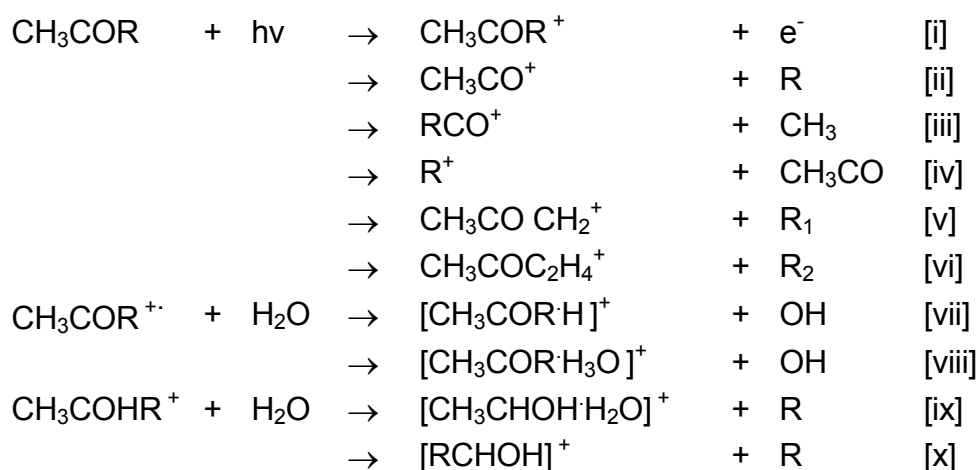CH_3COR & + & h\nu & \rightarrow & CH_3COR^+ & + & e^- & [i] \\
& & & \rightarrow & CH_3CO^+ & + & R & [ii] \\
& & & \rightarrow & RCO^+ & + & CH_3 & [iii] \\
& & & \rightarrow & R^+ & + & CH_3CO & [iv] \\
& & & \rightarrow & CH_3CO\,CH_2^+ & + & R_1 & [v] \\
& & & \rightarrow & CH_3COC_2H_4^+ & + & R_2 & [vi] \\
CH_3COR^{+\cdot} & + & H_2O & \rightarrow & [CH_3COR\,H]^+ & + & OH & [vii] \\
& & & \rightarrow & [CH_3COR\,H_3O]^+ & + & OH & [viii] \\
CH_3COHR^+ & + & H_2O & \rightarrow & [CH_3CHOH\,H_2O]^+ & + & R & [ix] \\
& & & \rightarrow & [RCHOH]^+ & + & R & [x]
\end{array}
$$

For acetone two fragments at m/z 43 and 51 are observed. The abundance are only 2% and 5%, respectively. process [ii] and [iii] are identical which yield $[CH_3CO]^+$ corresponding to 43. It should be noted that fragment at m/z 51 was not mentioned before by other mass spectra, it may be the $CH_3(H_2O)_2^+$. The fragmentation should

occurred in the ionisation source [140]. While the low pressure gas discharge lamp used as ionisation source for IMS and TOF output energy is 10.6 eV and the appearance potential of $[CH_3CO]^+$ is 10.3 eV [141] and the ionisation source was working under atmospheric pressure so the ions can react with moisture in the carrier gas. For butanone, process [ii] and [iii] occur to yield ions at m/z 43 and 57. There is also a anomalous fragment at m/z 63 which is the main fragment. It should through process [iv] to get $[CH_3CHOH \cdot H_2O]^+$. For pentanone the predominant fragment is at m/z 75, it should through process [v] and be assigned as $[CH_3COCH_2 \cdot H_2O]^+$. for these three ketones, the small amount of fragments together with the MH^+ and MH_3O^+ peak consist the major peak in UV-IMS.

For 2-hexanone fragment through [ii] and [x] are predominate. There are 6% amount of $[CH_3CO]^+$ at m/z 43 and 8% amount of $[CH_3CH_2CH_2 CH_2CH_2 OH]^+$ at m/z 87. It exhibit $(MH-18)^+$ peaks from the loss of water too. The major fragment of 2-heptanone and 2-octanone are through process [ii] and [iii] which corresponding to $[MH-CH_3]^+$ (100), $[M-CH_3]^+$ (113) and $[CH_3CO]^+$(43), process [iv] and [v] also take place and $[MH+CH_3]^+$ were observed too.

For 5-nonanone the prominent fragment is the $[M-18]^+$ peak and cyclohexanone has this peak too.

In general, the peaks of ketones appeared in UV-IMS should be the mixture of fragments, protonated and hydrated molecular ions, so when mixtures of ketones are measured by IMS, the ratio of ions or the type of ions in one IMS peak will be changed thus the drift time will be shifted or even new peaks will appear.

6.4. Alcohols detection with UV-IMS-TOF

The series of saturated aliphatic alcohols including ethanol, 1-propanol, 1-butanol, 1-pentanol, 1-hexanol as well as some of the secondary or tertiary alcohols, 2-butanol, 2-pentanol and 2-hexanol, 2-heptanol and 3-octanol and two branched alcohols, 3-methyl-1-butanol, 3-methyl-2-butanol were investigated. These short chain alcohols were selected which were usually measured by UV-IMS. Methanol can not be detected while the ionisation energy is 10.83 eV and the UV-Lampe here used is 10.6 eV. In order to get the best peak shape, the concentration of the alcohols are in the ppm range.

6.4.1. Comparison of UV-IMS and UV-TOF detection

The UV-IMS signal for alcohols are relatively complex. In addition to the main peak, there are one or two peaks in front and after the major peak, so the peak is very broad as shown in Fig. 6-8. For 1-pentanol and 1-hexanol there is a clearly visible peak at the drift time 17.13 ms (K_0=2.01 cm^{2}V^{-1}s^{-1}) and 18.26 ms (K_0=1.90 cm^{2}V^{-1}s^{-1}) (K_0=2.01 cm^{2}V^{-1}s^{-1}) respectively. The drift time (major peak) from ethanol to 1-hexanol increase continuously from 19.73 ms (K_0=1.77 cm^{2}V^{-1}s^{-1}) to 27.57 ms (K_0=1.25 cm^{2}V^{-1}s^{-1}). All the reduced mobilities of the alcohols are listed in.Table 6-3.
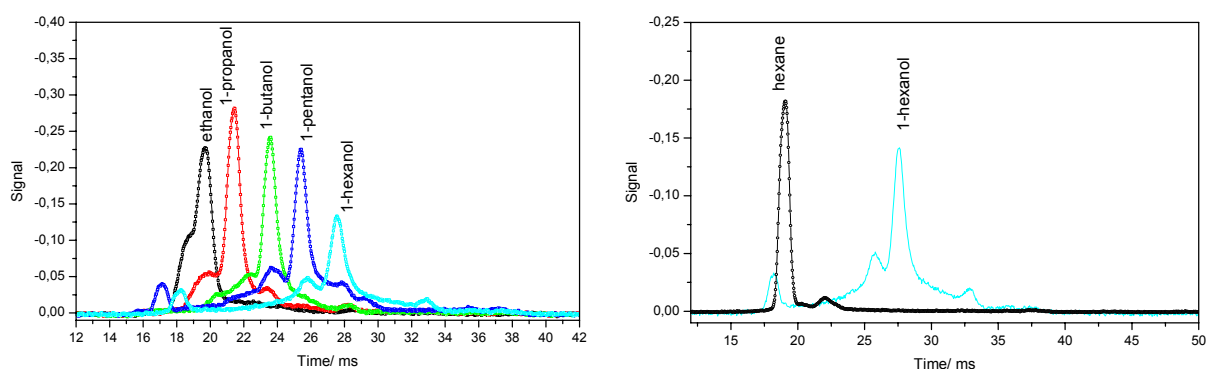
Fig. 6-8 UV-IMS spectra of primary alcohols (left), ethanol (125 µg/L), 1-propanol (125 µg/L), 1-butanol (92 µg/L), 1-pentanol (73 µg/L) and 1-hexanol (72 µg/L). On the right are 1-hexanol (72 µg/L) and 1-hexane (34 µg/L).

Compared the secondary alcohols to the corresponding primary one, they all have a major peak, but secondary alcohol has shorter drift times. K_0 for 1-butanol and 2-butanol are 1.44 cm^{2}V^{-1}s^{-1} and 1.49 cm^{2}V^{-1}s^{-1}. 1-pentanol and 2-pentanol are 1.34 cm^{2}V^{-1}s^{-1} and 1.40 cm^{2}V^{-1}s^{-1}, respectively, but with regard to 1-hexanol (1.25 cm^{2}V^{-1}s^{-1}) and 2-hexanol (1.43cm^{2}V^{-1}s^{-1}), the difference of K_0 is much greater. For

branched alcohol 3-methyl-1-butanol and 3-methyl-2-butanol, the ion mobility spectra are totally different, 3-methyl-2-butanol has only one major peak at 23.90 ms (1.43 $cm^2V^{-1}s^{-1}$) as normal primary and secondary alcohols, 3-methyl-1-butanol has two main peaks at 28.50 ms (1.21 $cm^2V^{-1}s^{-1}$) and 31.27 ms (1.10 $cm^2V^{-1}s^{-1}$). There is also a clearly visible peak at 25.53 ms (1.35 $cm^2V^{-1}s^{-1}$). It demonstrate that the different ions or different ratio of ions are produced. So, UV-IMS is very good instrument for alcohol detection as well as their isomers.
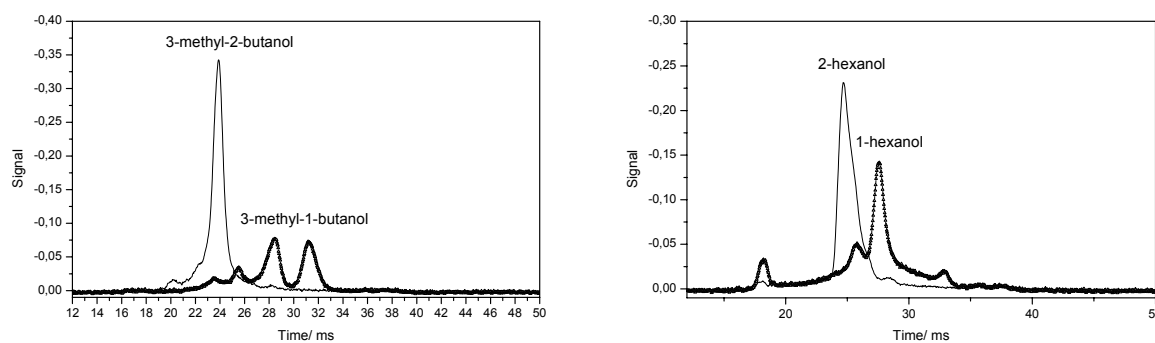
Fig. 6-9 UV-IMS spectra of 3-methyl-2-butanol (148µg/L) and 3-methyl-1-butanol (70µg/L) (left), 2-hexanol (143µg/L) and 1-hexanol (72µg/L) (right)

Table 6-3 Reduced mobility K_0 of measured alcohol ions with UV-IMS

Alcohols	MW (u)	IE(eV)	K_0 $(cm^2/ V.s)$ Peak 1 (major peak)
ethanol	46.07	10.48 ± 0.07	1.77
1-propanol	60.10	10.22 ± 0.06	1.62
1-butanol	74.12	9.99 ± 0.05	1.44
2-butanol	74.12	9.88 ± 0.03	1.49
1-pentanol	88.15	10.42 ± 0.03	1.34
2-pentanol	88.15	9.78 ± 0.03	1.40
1-hexanol	102.17	10.35 or 9.89	1.25
2-hexanol	102.17	10.24 or 9.89	1.43
2-heptanol	116.2	10.4 ± 0.1	1.20
1-octanol	130.23	—	1.18
3-octanol	130.23	—	1.15
3-methyl-1-butanol	88.15	—	1.21 / 1.10
3-methyl-2-butanol	88.15	9.75 ± 0.05	1.43

All these alcohols have been measured by TOF to recognize the peaks in UV-IMS. The TOF spectra of primary alcohols are given in Fig. 6-10 and all of them have protonated molecular ions, hydrated molecular ions and fragments at m/z = [M-17]. The relative high intensity of the dimer ions in the spectra are because of no drift gas

to collide with them to decompose clusters as the conditions in IMS. For ethanol the hydrated molecular ions intensity is 63% to the base peak when the area of base peak was taken as 100%. 1-propanol is 53%. This can result from the hydroxyl group in alcohols. It connects water with hydrogen bond which is relatively strong, the hydrated molecule ions can not decompose by the collision with drift gas in IMS, resulting in peaks after the main peak together with other clusters and dimers. For 1-butanol, 1-pentanol and 1-hexanol the base peaks are fragments at m/z [M-17].
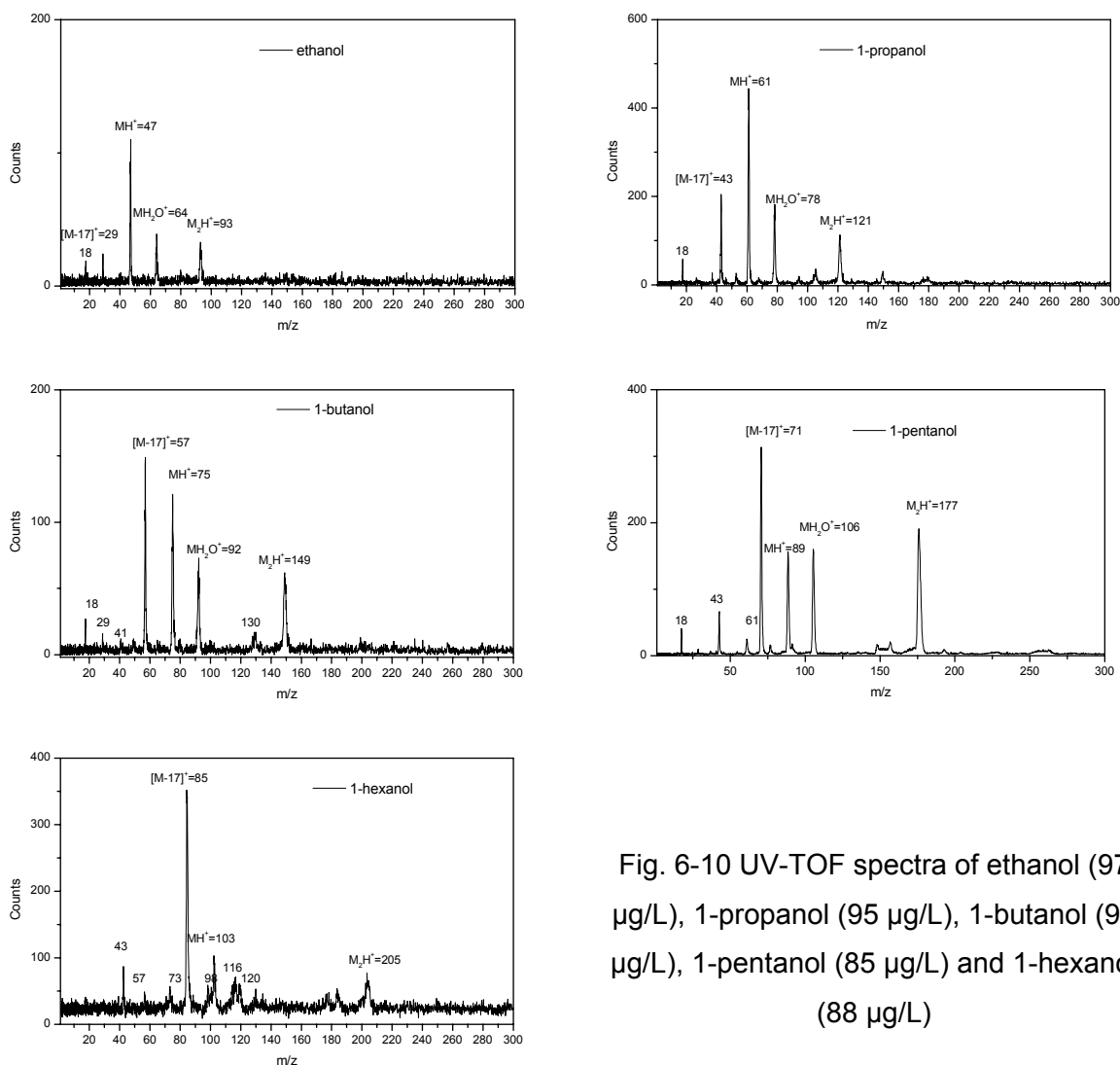
Fig. 6-10 UV-TOF spectra of ethanol (97 µg/L), 1-propanol (95 µg/L), 1-butanol (92 µg/L), 1-pentanol (85 µg/L) and 1-hexanol (88 µg/L)

It may come from the lose of the hydroxyl group. For 1-propanol, 1-butanol, 1-pentanol and 1-hexanol it is possible while the ionisation energy to yield corresponding alky ions are 10.56 eV, 10.18 eV, 10.04 eV and 9.89 eV respectively, which are under 10.6 eV of the UV-lamp energy. For ethanol small amount of ions at m/z 29 corresponding to $CH_3CH_2^+$ may come from the interface system. While for such a decomposition an energy of 12.7 eV is required, and that is much higher than

the lamp energy. The abundance of $C_nH_{2n+1}^+$ fragmentation increase with the number of carbons. The construction of alkyl ions is totally different compared to alcohol ions, because the collision cross section are much smaller. As for hexane, the reduced mobility K_0 is 1.81 $cm^2V^{-1}s^{-1}$, while for 1-hexanol K_0 is 1.25 $cm^2V^{-1}s^{-1}$ as showed in Fig. 6-9.

The secondary alcohol UV-TOF spectra are given in Fig. 6-11, the abundance of the fragment at m/z [M-17] is relatively smaller compared to corresponding primary alcohols. For 1-butanol, 1-pentanol and 1-hexanol, the base peaks are with m/z ratio of [M-17], while for 2-butanol, the base peak is the protonated molecule ion peak. The abundance of [M-17] is only 49% of base peak. For 2-pentanol the ratio of protonated ions and fragment at m/z [M-17] are quite the same. 2-hexanol is not as other alcohols, the base peak is at m/z 99, corresponding to M-3 and the peak at m/z 85 is very small. It is reflected in UV-IMS spectra (Fig. 6-9) where 2-hexanol has only a small peak, so the ion at m/z 85 should be due to $C_6H_{13}^+$.
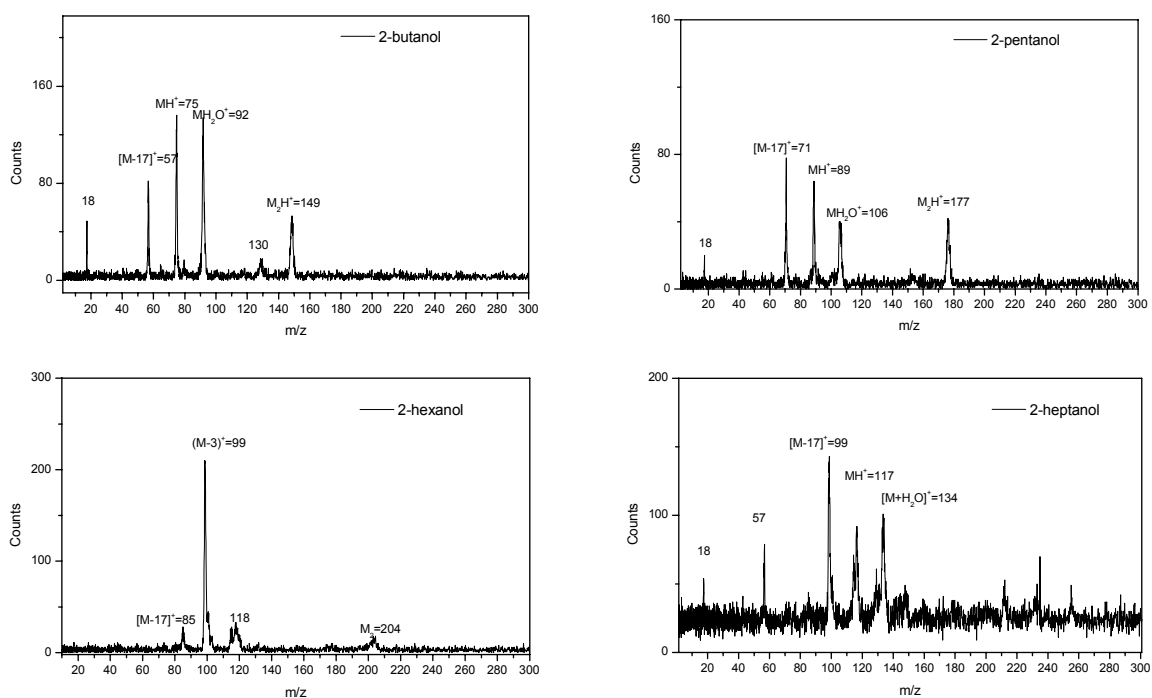
Fig. 6-11 UV-TOF spectra of 2-butanol (98 µg/L), 2-pentanol (91 µg/L), 2-hexanol (93 µg/L) and 2-heptanol (60 µg/L)

Because the UV-IMS spectra of 3-methyl-1-butanol and 3-methyl-2-butanol are totally different, they should have different decomposition. It was proved in TOF as showed in Fig. 6-12, there are two major peaks at m/z 106 and 71 in TOF for 3-methyl1-butanol,due to the [M-17] and [M+H$_2$O], for 3-methyl-2-butanol, the base

peak is at m/z 60 corresponding to [M-C_2H_4]. so the main peak in UV-IMS spectra consists of fragment ions instead of normally considered monomer for 3-methyl-2-butanol.
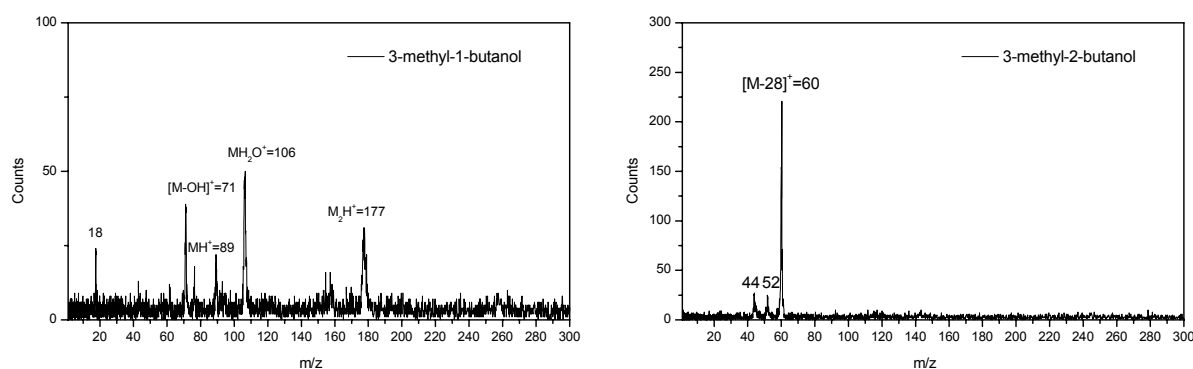
Fig. 6-12 TOF spectra of 3-methyl-1-butanol (86 µg/L) (left) and
3-methyl-2-butanol (166 µg/L) (right)

6.4.2. Photoionization mechanism of alcohols

One of the most characteristic aspects of the mass spectra of alcohols is that the base peak is not always the molecular ion or protonated molecule ion through reaction [I] and [III], the loss of m/z 17 giving a peak at m/z [M-17] as fragment ion is for higher primary alcohols most abundant [II]. Another common peak occur at m/z [M+18] [IV], due to the adducts of water molecule. The dimer peak is also evidently visible by most alcohols in high concentration [V] because of the strong hydrogen bond of hydroxyl in alcohols. All the following processes of photoionization of alcohols may occur in UV-IMS.

$$ROH \quad + \quad h\nu \quad \rightarrow \quad ROH^+ \quad + \quad e^- \quad \quad [I]$$
$$\rightarrow \quad R^+ \quad + \quad OH \quad \quad [II]$$
$$ROH^+ \quad + \quad H_2O \quad \rightarrow \quad [ROH_2]^+ \quad + \quad OH \quad \quad [III]$$
$$\rightarrow \quad [ROH + H_2O]^+ \quad \quad [IV]$$
$$ROH_2^+ \quad + \quad ROH \quad \rightarrow \quad [(ROH)_2 H]^+ \quad \quad [V]$$
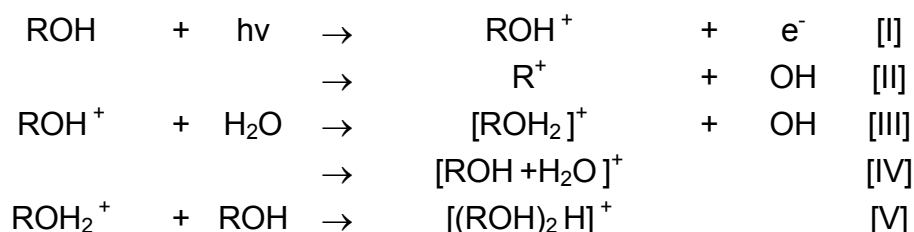
Additionally, the TOF spectra of 2-hexanol also exhibit base peak corresponding to the loss of three hydrogen atoms (M-3) and this fragment is much more intense than the molecular ions.
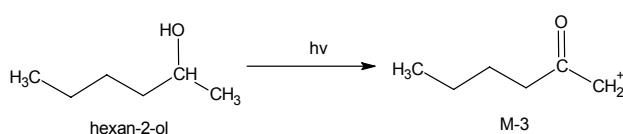
6.4.3. Limits of detection and calibration curve

Response vs. concentration was determined individually for ethanol and 1-propanol using UV-TOF. The plots of the signal (peak area) vs. the gaseous concentrations are shown in Fig. 6-13 with a linear range of three orders of magnitude. The detection limits (LOD) with the UV-TOF are 8.6 µg/L and 3.0 µg/L, respectively.
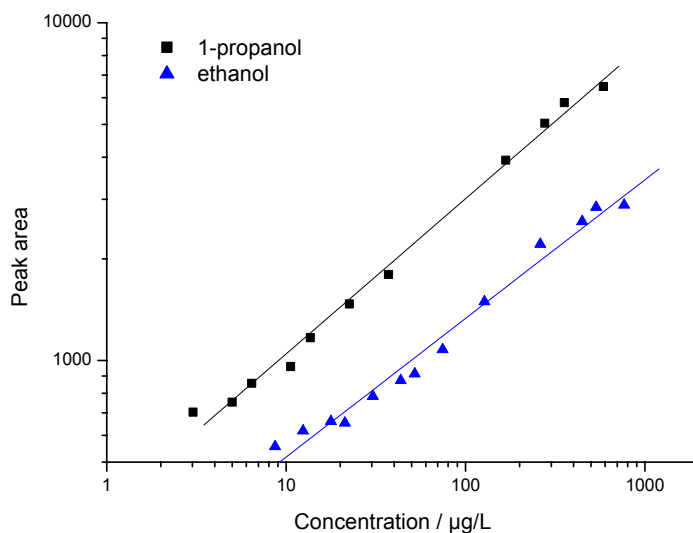
Fig. 6-13 Calibration curve for ethanol and 1-propanol

In Fig. 6-14 the spectra of ethanol with 764 µg/L and 8.6 µg/L are illustrated. In high concentrations, additional to the ethanol molecular ion, the ethanol dimer ion at m/z 93 and water cluster at m/z 64 are present while in low concentration there only appeared the molecular ion.
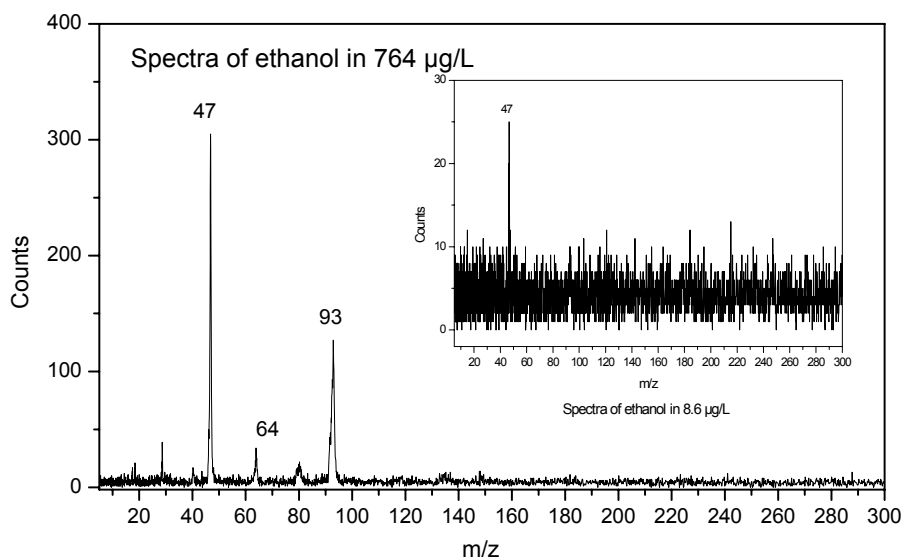
Fig. 6-14 Spectra of ethanol with 764 µg/L and 8.6 µg/L

6.5. Aromatic hydrocarbons detection with UV-IMS-TOF

Aromatic compounds such as benzene, toluene, and xylene are key targets of importance with respect to environment monitoring and currently normal analytical methods are gas chromatography (GC) and gas chromatography coupled with mass spectrometry (GC-MS). The use of a UV-IMS to detect aromatic hydrocarbons is sensitive and reliable [142, 143].

6.5.1. Comparison of UV-IMS and UV-TOF detection.

Fig. 6-15 shows the UV-IMS spectra of compounds benzene, toluene, o-xylene and ethylbenzene, normally all the substances have one peak.
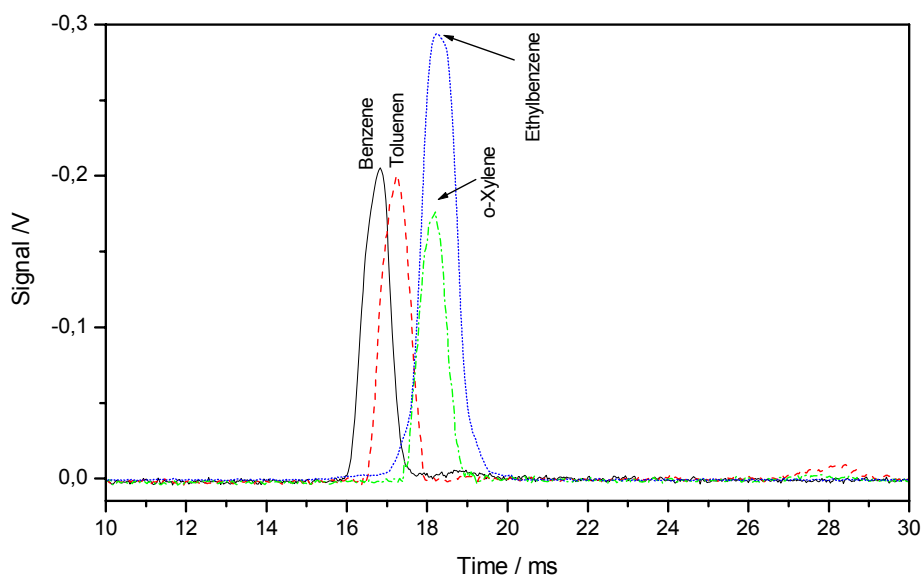
Fig. 6-15 Ion mobility spectra for benzene, toluene, o-xylene and ethylbenzene

The reduced mobilities calculated for these peaks are summarized in Table 6-4. The K_0 value for benene, toluene and o-xylene are 2.09, 1.98, 1.89 $cm^2V^{-1}s^{-1}$, respectively, showing a decrease with an increase of the mass of the molecule.

Table 6-4 Reduced mobility K_0 of measured aromatic ions with UV-IMS

Alcohols	MW (u)	IE (eV)	K_0 (cm^2 $V^{-1}s^{-1}$)
			Peak
Benzene	78.11	9.24	2.09
Toluene	92.14	8.83	1.98
o-Xylene	106.17	8.56	1.89
Ethylbenzene	106.17	8.77	1.92
Propylbenzene	120.19	8.71	1.77
Chlorobenzene	112.56	9.07	1.95
Aniline	93.12	7.72	--

Ethylbenzene has the K_0 of 1.92 $cm^2V^{-1}s^{-1}$ and there is no distinct difference to that of o-xylene. Their reduced mobility is relatively greater compared to those of ketones and alcohols, while they have the ring construction.

The corresponding UV-TOF spectra given in Fig. 6-16 illustrate that the major ions for benzene, toluene, o-xylene and ethylbenzene are molecule ions which are at m/z 78, 91, 106, 106, respectively. For benzene and toluene, the fragments are very small, o-xylene shows more fragmentation with peak at m/z of 91, which is resulting from the loss of methyl group. This peak with m/z ratio of 91 has a magnitude of 41% compared to the main peak at m/z 106. even more fragmentation shows ethylbenzene with peaks at m/z 91 and 77. the fragment ion at m/z 91 rises even to 56% to the ratio of major molecule ion at m/z 106. and the cluster ion at m/z 121 is much greater, it has a magnitude of 25% to that of the major peak of molecule ion.
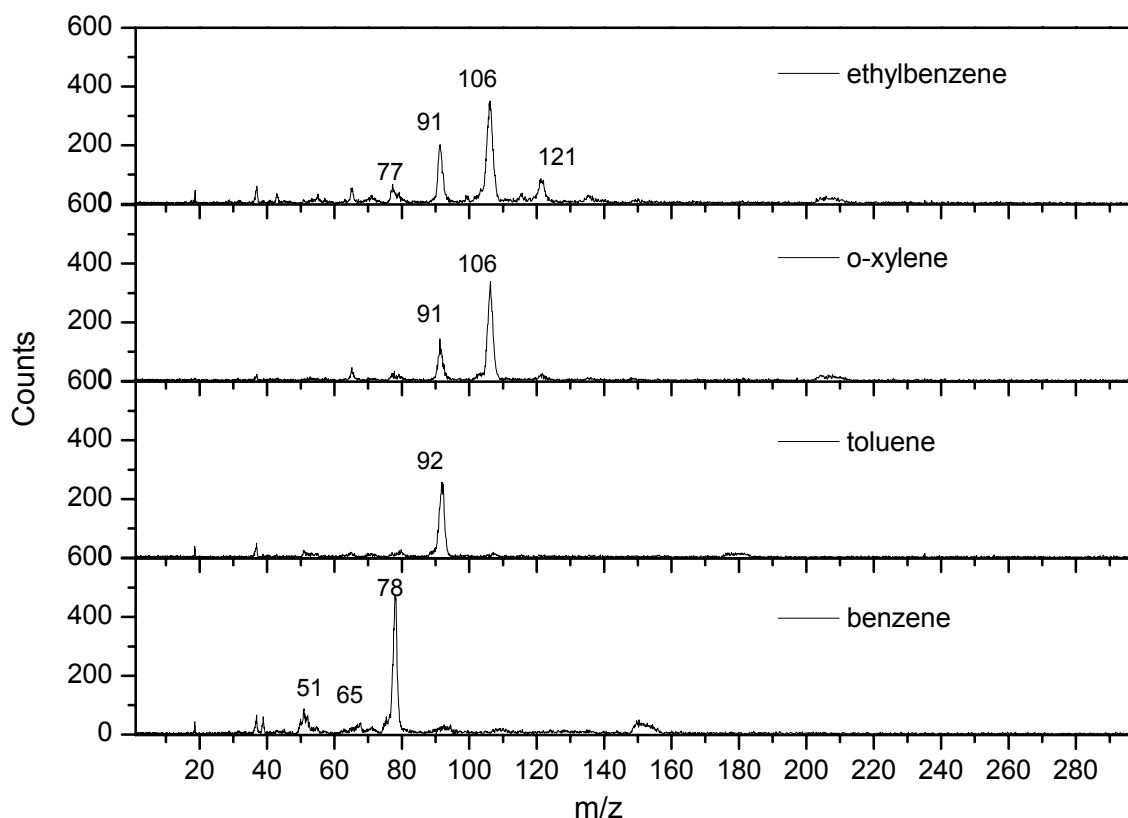
Fig. 6-16 Spectra of benzene, toluene, o-xylene and ethylbenzene with UV-TOF

Other aromatic substances such as aniline has been studied by UV-TOFMS. Aniline exhibits a very pronounced molecular ion (major peak), which can be explained by stabilization of the radical .
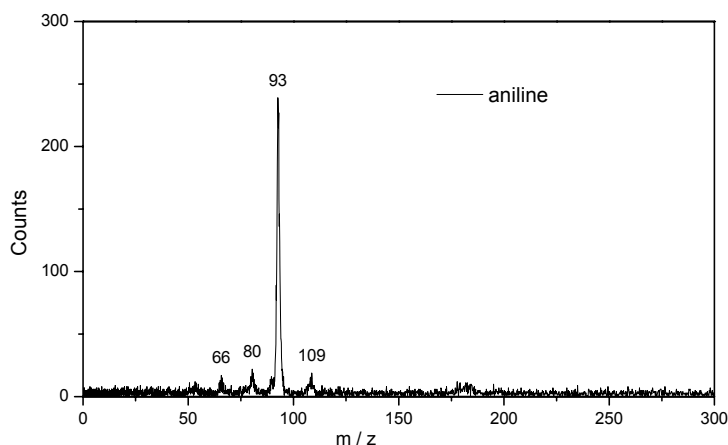
Fig. 6-17 UV-IMS-TOF spectra of aniline

6.5.2. Separation of mixtures of compounds

The UV-TOF spectra has been shown to allow the identification of mixture of aromatics. In Fig. 6-18 shows the TOF spectra of mixture of 134 µg/L benzene, 56 µg/L toluene and 43 µg/L o-xylene. All three molecular ions can be seen without separation using a GC column.
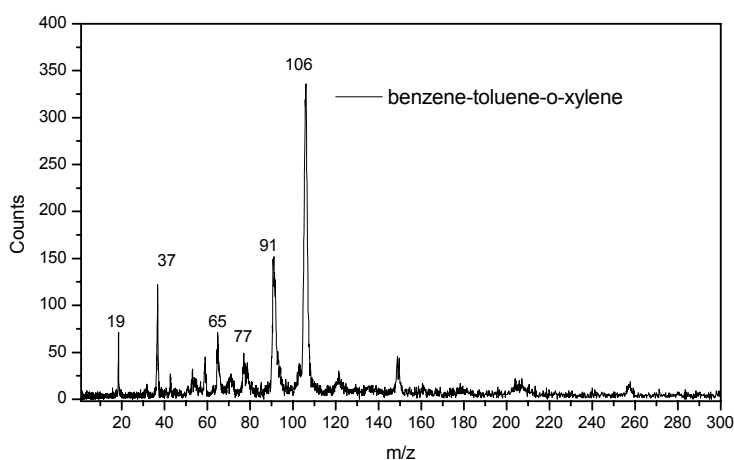
Fig. 6-18 TOF spectra of mixture of 84 µg/L benzene, 56 µg/L toluene and 43 µg/L o-xylene

6.5.3. Limits of detection and calibration curve

In Fig. 6-19, the calibration curves for benzene and toluene are shown, respectively. The linear range for benzene and toluene are 17.2 µg/L to 1576 µg/L and 2.5 µg/L to 200 µg/L. As demonstrated in Fig. 6-20 with the lowest concentration toluene exhibits only one molecular ion peak near the detection limit and in high concentrations there are some fragments at m/z 51, 65, 77 and clusters with a m/z ratio of 107,

121,149,176, but the abundances are very small.
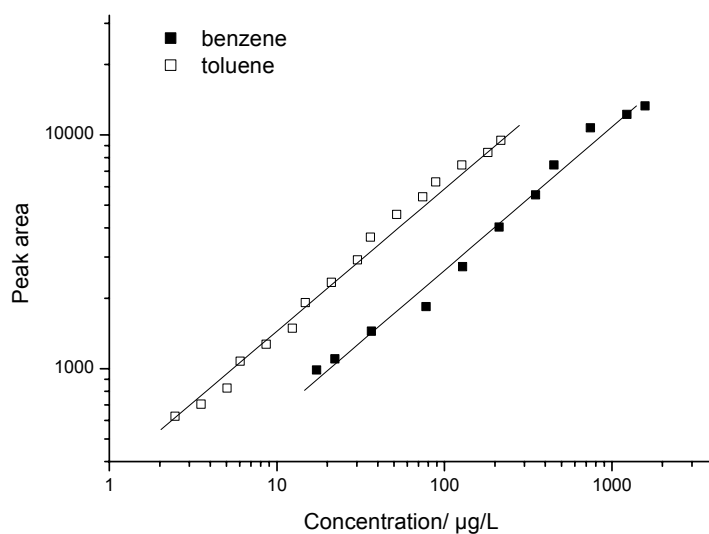
Fig. 6-19 Calibration curves for benzene and toluene
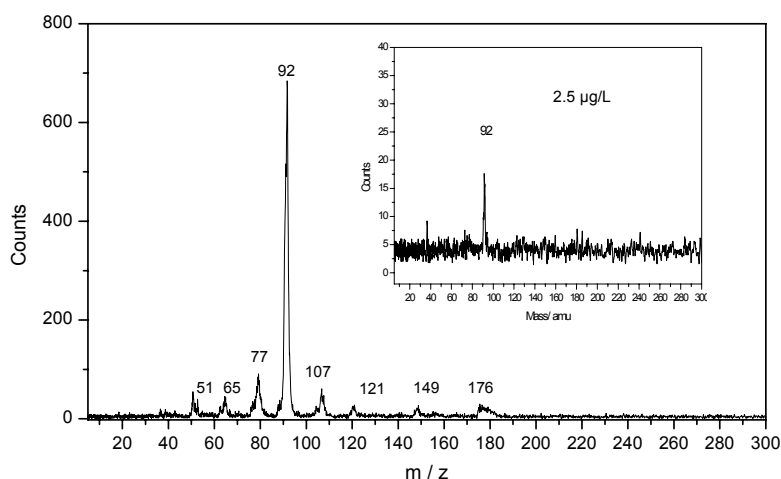
Fig. 6-20 Spectra of toluene with 200 µg/L and 2.5 µg/L

6.5.4. Photo ionization mechanism of aromatics

As shown in spectra a typical TOF spectrum of aromatics is dominated by the molecular ion. For benzene the following process may occurred. The small amount of fragments at m/z 65 and 51 can be seen in TOF spectra in Fig. 6-16.
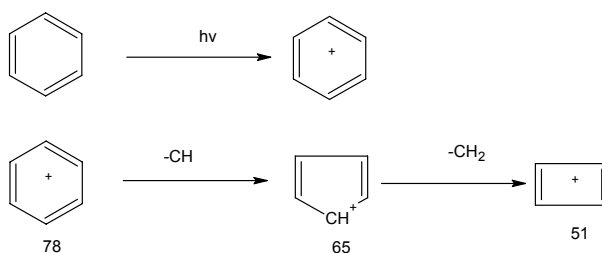
for ethylbenzene, the molecule ion with the mass of 106 is ionized by UV light and the fragment ion $C_7H_7^+$(91) and $C_6H_5^+$ (77) are formed by loss of one and two methyl group. The cluster ion at m/z 121 formed through adduct of a methyl group. All the processes are as demonstrated below.
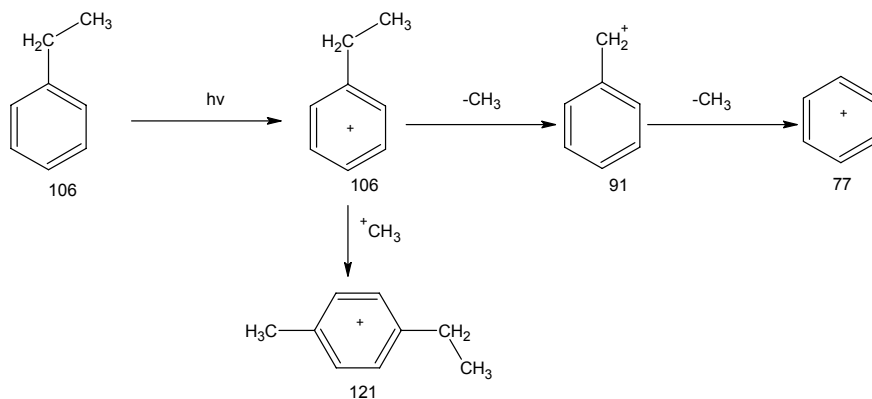
These fragments and clusters can be seen in the spectra in Fig. 6-16, it shows good consistent with the experiments.

6.6. Measurements of applications to real samples

6.6.1. Measurements of CWA simulants

Since the introduction of ion mobility spectrometry in the early 1970s, the IMS has been used to detect chemical warfare agents (CWA). Individual CWA simulants including dimethyl methylphosphonate (DMMP), usually used as a simulant for Sarin and diisopropyl methylphosphonate (DIMP), a chemical by-product resulting from the manufacture and detoxification of Sarin are investigated by UV-TOF due to the high toxicity of the CWA.

UV-TOF yield a predominant molecular ion. Minimum fragmentation was the most benefit for this method compared with normal electron ionization (EI) mass spectrometry as demonstrated in Fig. 6-21. These results show a considerable reduction in complexity of the ion signals.
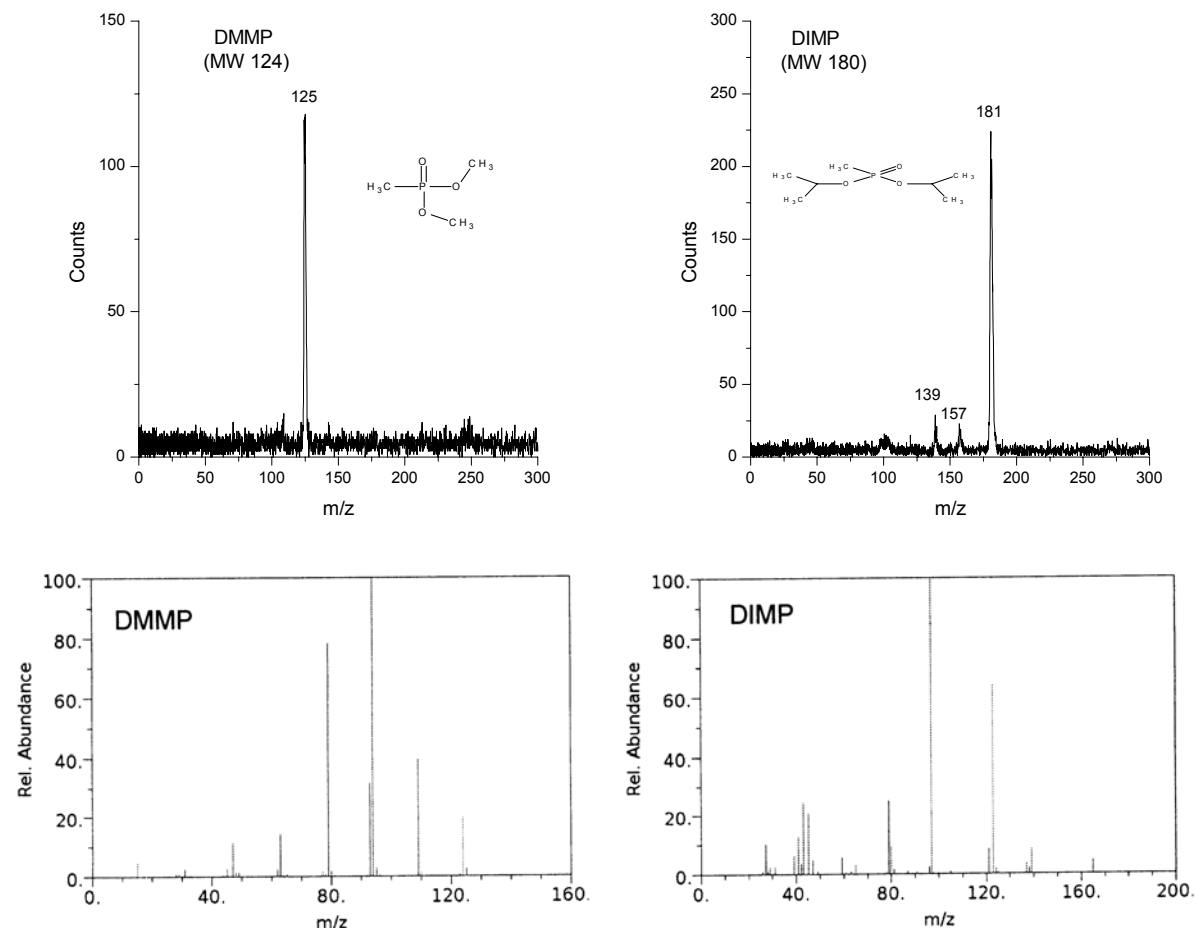
Fig. 6-21 Comparison of UV-TOF (above) vs EI (bottom, from NIST chemistry webbook) for dimethyl methylphosphonate (DMMP) and diisopropyl methylphosphonate (DIMP)

6.6.2. Sulfur-free odorant for nature gas

For other esters like ethyl acrylate, which is used as a synthetic flavouring substance and fragrance adjuvant in nature gas as S-free odorant illustrated in UV-TOF spectra evidently one peak at m/z 101, too.
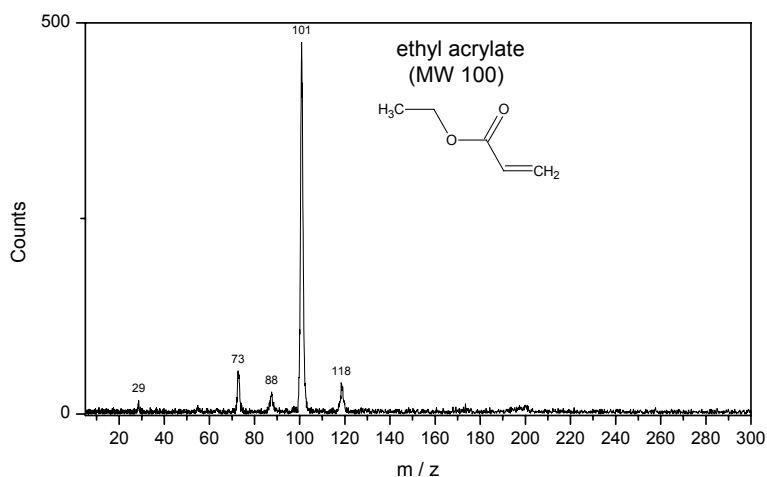
Fig. 6-22 UV-TOF spectrum of 25 µg/L ethyl acrylate

6.6.3. Diesel oil marker

The utility of UV-TOF for high speed and high throughput analysis of 5-nonanone in diesel oil matrix was also investigated. 5-nonanone is used as a marker substance for the identification of the diesel oil. Fig. 6-23 shows the comparison of diesel oil and 50 ppm 5-nonanone in diesel oil, there are two peaks at m/z 143 and 160, which obviously came from the 5-nonanone molecular ion and the water cluster ion.
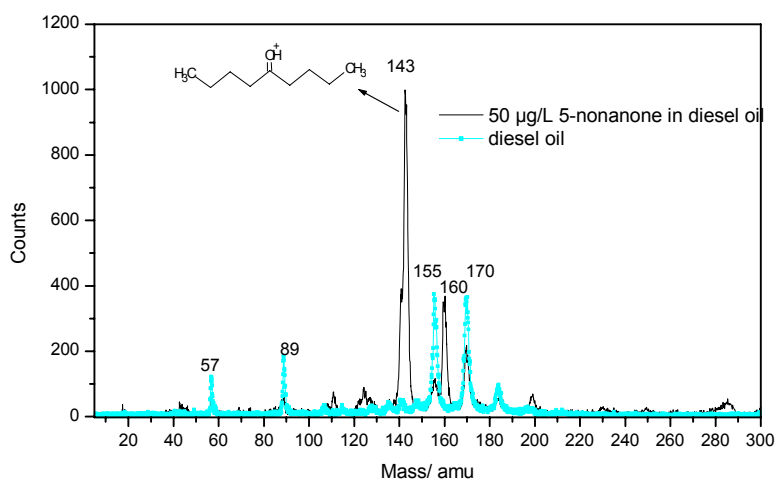
Fig. 6-23 UV-TOF spectra of 50 µg/L 5-nonanone in diesel oil

Additionaly the dynamic range of 5-nonanone was investigated. Signal level versus concentrations of the analytes are shown in Fig. 6-24. The measurements show a linear range of 3 decades with a LOD of 5 ppm$_v$.

The linear dependence is relatively insensitive to the presence of other compounds in a mixture. This property is useful for conducting quantitation of a target compound in mixtures and becomes very useful for high-throughput applications because it minimizes the need to conduct chromatography separation in some cases. Some other usually used soft ionisation methods such as APCI and ESI are susceptible to competition for charge effects, which makes them less reliable for conducting quantitative measurement in the absence of a separation step.
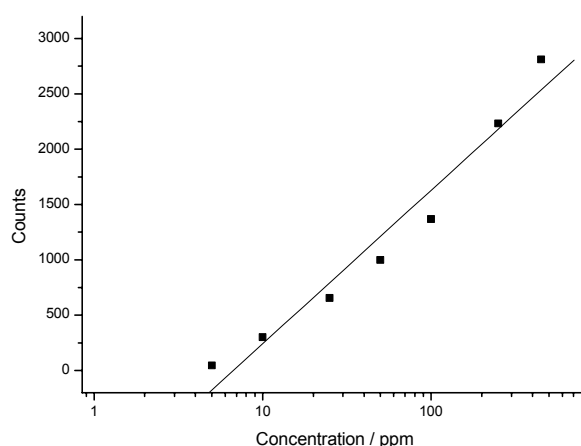
Fig. 6-24 Plot showing linearity of signal vs concentration of 5-nonanone added in diesel oil

6.6.4. Mould (fungi) analysis with UV-IMS-TOF

Microbial volatile organic compounds (mVOC) include alcohols, ketones, terpenes, aldehydes, esters and aromatics produced as metabolic by-products of bacteria and fungi and are detectable before any visible signs of microbial growth appear. They play an important role as indoor allergens, and may be responsible for a large variety of health problems such as skin irritation, headaches, and asthma symptoms. The monitoring of these substances is a tool for diagnosis of the presents of micro-organisms and helps to reduce the health risks.

The emissions of bread mould cultures were measured as a practical application of real samples using UV-IMS-TOF. Two pieces of bread were put in a closed beaker flask and after several days the headspace air was introduced directly into the UV-IMS-TOF by a carrier gas in 300 mL/min. Fig. 6-25 shows the spectra of the emissions after 2 and 5 days culture. After 2 days there are 3 peaks at m/z 47, 64, 93

which are corresponding to protonated ethanol molecule ion and its water adduct and dimer. After 5 days also the protonated acetone ion with m/z ratio of 59 appeared,. Additionally there is a peak at m/z 138, which could be the trimer ion of ethanol or other substances which should be analysed with MS-MS. Compared this method with the UV-IMS combined with a capillary gas chromatographic colum or with a multi capillary column (MCC) [144], it is very fast and convenient to operate and the whole measurement was completed in 2 minutes and didn't need to be separated before.
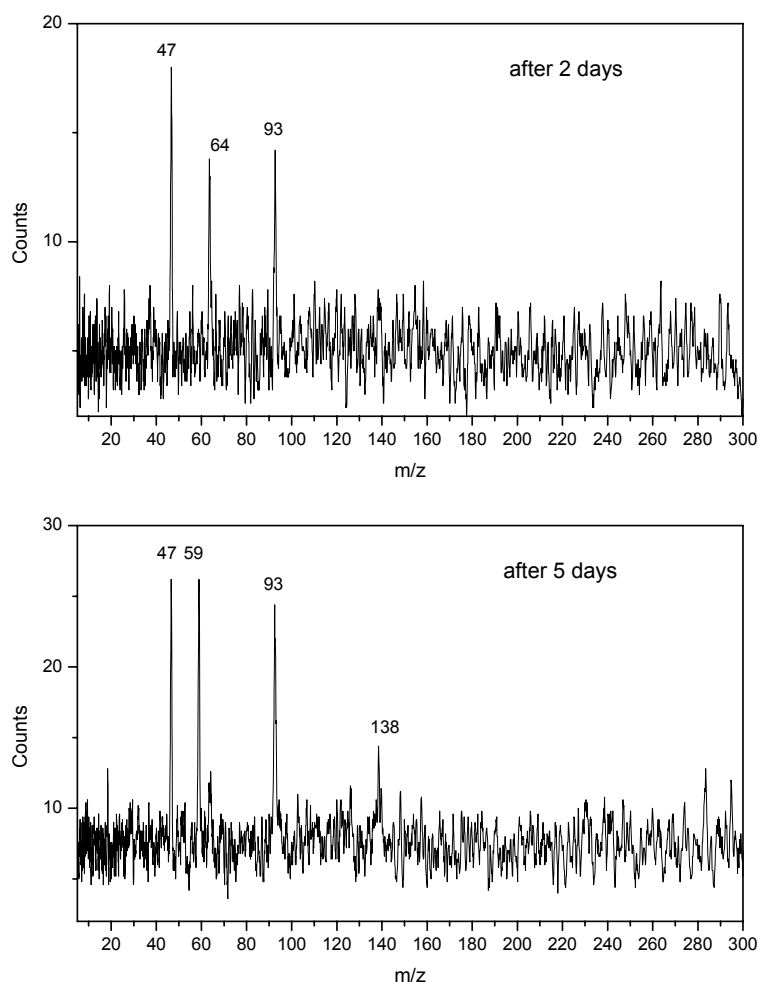
Fig. 6-25 UV-IMS-TOF spectra of bread mould culture after 2 and 5 days
with headspace introduction

6.7. Influence of the moisture in UV-IMS-TOF

Moisture in the sample gas causes the major problem using ion mobility spectrometers. It makes spectra change and sensitivity as well as selectively decrease [145]. Therefore, the influence of humidity on the UV-IMS-TOF signal was investigated.
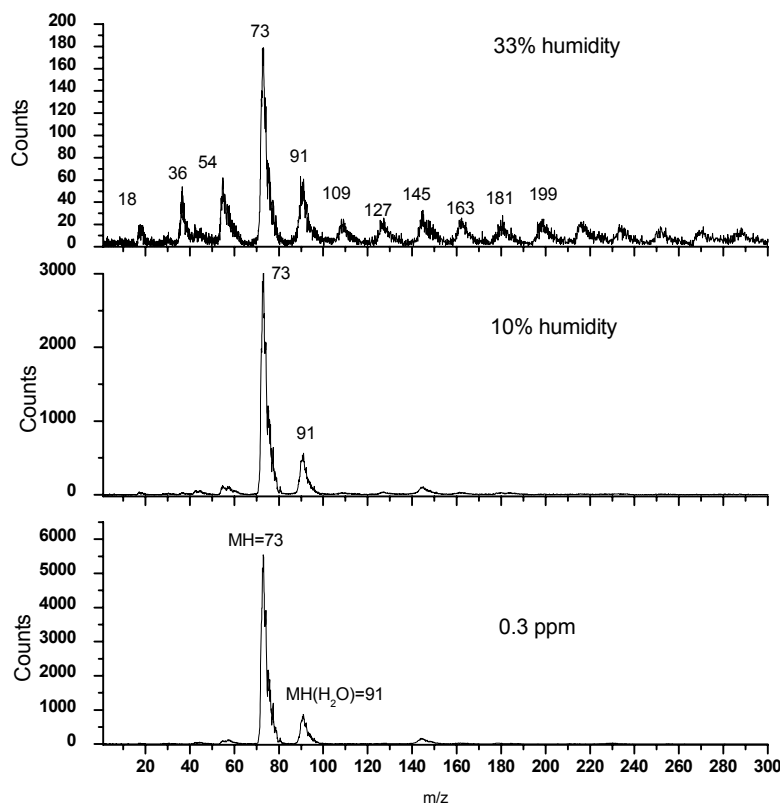
Fig. 6-26 UV-IMS-TOF spectra of 100 µg/L butanone with different humidity of the sample gas. Above the relative humidity is 33%, in the middle 10%, and bottom 0.3 ppm absolute humidity in sample gas.

Absolute humidity (AH) in ppm are measured by the Panametrics moisture monitor series 35, the relative humidity (RH) was measured with a standard RH sensor.

In the present of water hydrated monomer $M^+(H_2O)_n$ or $MH^+(H_2O)_n$ can be formed as shown in Fig. 6-26. When butanone in normal dry sample gas of 0.3 ppm absolute humidity the major peak is at m/z 73 (MH). There is only one additional hydrated ion at m/z 91 ($MH^+(H_2O)$) with a magnitude of 13% to that of the molecule ion. When the sample gas relative humidity increases to 10% (25°C), the signal of molecule ion's height decreases to the half of that before, and the ion at m/z 91 rises to 19% of that of molecule ion. When the moisture increases even to 33% relative humidity (25°C), peak at m/z 73 is only 1/30 to that in dry gas. Besides one water bound protonated ion at m/z 91, which has magnitude of 33% of that of the base molecule peak, additional peaks of molecule ion plus water clusters appear at m/z 109, 127, 145, 163, 181, 199 and so on, they have the intensities of about 13% of that of the base molecule peak. Water peaks at m/z 18, 36, 54 are relatively higher, they have the

magnitude of 11%, 28% and 33%, respectively of that of the molecule ion.

Further investigations with different analytes, selected from different chemical groups including ethanol and benzene were investigated. They all show water cluster ions in a making high humidity. Those additional peaks decreasing the sensitivity of UV-IMS-TOF sensitivity as showed in Fig. 6-27. The reason for the different behavior of benzene could be the nonpolar structure and the related lower reactivity with water molecules.
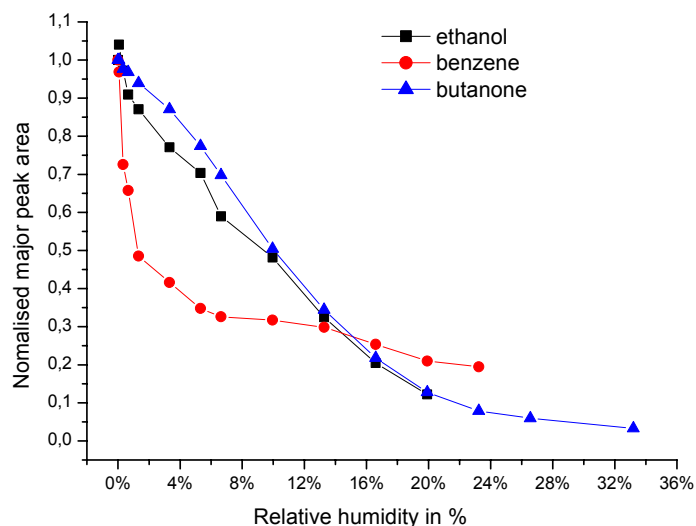
Fig. 6-27 Decrease of the signal area of UV-IMS-TOF spectra for ethanol, benzene and butanone with increasing relative humidity. The major molecular ion peak area was normalized for all analyte.

Detection limits of benzene, ethanol and butanone were determined using exponential dilution under 20% RH and 0% respectively. As listed in Table 6-5, in the case of 20% RH in nitrogen as carrier gas, the detection limits are about 10 times higher than those using dry gas as carrier gas.

Table 6-5 Detection limits of benzene, ethanol and butanone with different relative humidities

	Detection limits (µg/L)	
	0% RH	20% RH
Benzene	2.5	30
Ethanol	8.6	120
Butanone	0.4	6

7. <u>Conclusions and outlook</u>

Ion mobility spectrometry is a separation technique based on the average cross-section of ions. When interfaced to mass spectrometer, additional mass information of the ions could be collected. As shown by theoretical and experimental results in this thesis, a carefully designed UV-IMS[PID] coupling with oa-TOFMS was successfully self-made. It offers high transmission, simple spectrum, high speed and it is able to record the whole mass spectrum quasi simultaneously. These features make it attractive to identify ions, fragments or ion clusters in IMS and to conduct high-throughput molecular analysis of large libraries for compound confirmation and purity assessment.

The pinhole interface system to the UV-IMS [PID]-TOF was characterized by studying a two and a three stage interface. For the two stage pumped interface the effect of the distance between two skimmers on pressure and variations of potentials and dimensions of the pinhole on ion yield were explored. It is proved that with a diameter of 0.25 mm for the sampler, a diameter of 0.3 mm of the skimmer and a distance between them set to 6 mm, the vacuum can reach 8.2×10^{-6} mbar, but it is not desirable for TOF. With the construction of the 3 pinhole system, the vacuum can go down to 10^{-7} mbar and the signal can also be detected with different dimensions of the pinhole. As regard to the compromise of ion yield and vacuum, the best configuration is with a diameter of 0.5 mm for the pinhole of the pre-sampler, a diameter of 0.2 mm for the pinhole of the sampler and a diameter of 0.4 mm for pinhole of the skimmer, and the distance between the sampler and skimmer set to 5 mm.

By simulation with SIMION v. 7.0 it was proved that the configuration of the three stage differential pump system and the Einzel lens was suitable for an orthogonal design of an interface between atmospheric pressure and the TOFMS. The results from SIMION modeling suggested that the beam could be made parallel by the Einzel lens in the region of the TOFMS extraction region, and it will be affected by initial energy of the ion beam. The ions can reach the microchannel plate when the initial energies K_e are not too high or with an additional deflector. The voltages on the repeller and the acceleration region have much more effects compared to the

number of field guard rings and length of the acceleration region.

The pinhole interface systems are optimized and proved to be able to identify ions that has been ionized in IMS. Although reactions downstream of the Mach disc can create sampling errors that distort measured ion distributions, it was shown that it can be adjusted by the voltage on the sampler of the interface of the instrument. The identity of the ions observed in this work are pretty much as expected and agree with literatures.

This device has been proved to have unique benefits for volatile organic compounds analysis. The utility of the UV-IMS[PID]-TOF for high-speed and high throughput analysis of different groups of chemicals, including ketones, alcohols and aromatics were studied. The detection limits are in the range of 0.8 µg/L for acetone, 8.6 µg/L for ethanol and 17.2 µg/L for benzene with direct permeation sampling. The instrument has a dynamic range of about 3 decades for all detected compounds. A wide range of applications including chemical weapon simulation substances detection as well as fungal analysis were achieved with this device. It yields simple spectra that facilitate analysis.

Compared with the most commonly used ionization methods such as atmospheric pressure chemical ionization (APCI) and electrospray ionization (ESI), the UV photoionization works on a different principle. The excitation of a molecule by a photon can directly eject an electron if the photon energy exceeds the ionization potential of the molecule. This process is independent of the surrounding molecules, therefore reducing ion suppression effects. So it is possible to analyze mixtures without resorting to GC to separate the components and itoffers better quantitation accuracy in mixtures. Sample preparation is simple, no additives are needed. The generality of the photoionization condition make it possible for near-universal soft ionization of a wide variety of compounds.

Compared the results of TOF spectra with UV-IMS spectra, most VOCs appearing in UV-IMS are monomer or protonated monomer ions. For the selected ketones from acetone to nonanone, the most abundant ions are protonated molecular ions and beginning from hexanone, the fragmentation is evident and can be detected in IMS. In the case of selected alcohols, not all of them have base peak corresponding to

protonated molecule ions. Some of them such as 3-methyl-2-butanol and 2-hexanol the fragment ion are most abundant. These two groups of compounds all have obvious water adducts peaks because of high proton affinities. For aromatic substances the major ion is the molecular ion.

As enumerated above, the UV-IMS[PID]-TOF could be a powerful means for the rapid analysis of a wide variety of environmental, industrial and biological sample mixtures by benefits of minimal fragmentation, simple sample preparation and near-universal detection efficiency for a wide class of compounds.

In order to assign the peaks in UV-IMS better, in the future, a real time two dimensional separation of simultaneous drift time in IMS and flight time in TOF should be set up. Ions can be gated for 1 ms into the drift region at a frequency of 10 Hz, which is normally used by our UV-IMS made in ISAS. This provided maximum of 100 ms for the TOFMS to collect about 2000 spectra with a maximum length of 50 μs when operated at a frequency of 20 kHz. The UV-IMS gate and TOFMS oa-extractor could be both triggered by a pulse generator and data acquisition should be delayed with respect to both UV-IMS gate and TOFMS extraction, to reduce the size of data array. Two dimensional acquisition software should also be developed.

To increases ion transmission efficiency, gas-filled RF-quadrupole provides a perfect interface between atmospheric pressure ionisation source and the TOF mass analyser, which is working in a high vacuum condition. The cooling property of the gas-filled quadrupole can be served as a tool to confine an ion beam in order to obtain a smaller space volume, which is important to improve MS resolving power.

The mass resolving power of the instrument can be improved in the future by using reflector time-of-flight analyser (ReTOF), which almost doubles the flight path and hence the dispersion in time of flight, but this effect is of lower importance than its capability to compensate for initial energy spread.

8. <u>Acknowledgements</u>

I would like to express my most sincere acknowledgement to Dr. Jörg Ingo Baumbach for giving me the opportunity to study in ISAS - Institute for Analytical Sciences in Dortmund under a constant financial support. All my research work and the writing of this thesis were supervised by him.

I would like to express my gratitude to Prof. Dr. A. Manz for instructive advices and correction of the thesis.

Special thanks are given to Prof. Gary A. Eiceman, in the Department of Chemistry and Biochemistry, New Mexico State University. His profound knowledge and the fruitful discussion about experiments as well as amiable personality will always be impressed in my memory.

Dr. Eiermann is gratefully appreciated for his help on the electronic technique. J. Lonzynski and his colleagues in the mechanical department of ISAS are gratefully appreciated for their rapid high quality work and enthusiastic help. No matter how difficult or how much work I assigned to them, they always make it perfect.

I would like to express my sincere gratitude to Mrs. Luzia Seifert and Stefanie Guessgen for their concern about my life in Germany and their support during this work. Dr. Stefanie Sielemann and Hartwig Schmidt, Vera. Ruzsany and Dr. Wolfgang Vaulz are gratefully appreciated for the helpful scientific discussions and instructive advices. To Dr. Thomas Horvath I wish to appreciate his help on TOF setup problems.

I would give thanks to all the colleagues in ISAS for their help to orient to the work in institute and the discussions during the work.

Finally, I want to thank my husband, Gang Chen, who uncomplainingly sacrificed himself to support my studies and was always giving me moral support and encouragement. And my parents, my son, without their support, it would have been impossible for me to work in ISAS.

9. <u>References</u>

1.   Cohen, M.J. and F.W. Karasek, *Plasma chromatograph - a new dimension for gas chromatography and mass spectrometry.* J. Chromatogr. Sci., 1970. **8**: p. 330-337.

2.   Eiceman, G.A., *Advances in ion mobility spectrometry: 1980-1990.* Crit. Rev. Anal. Chem., 1991. **22**: p. 471-490.

3.   Spangler, G.E., et al., *Developments in ion mobility spectrometry.* ISA Trans., 1984. **23**: p. 17-28.

4.   Roehl, R.E., *Environmental and process applications for ion mobility spectrometry.* Appl. Spectrosc. Rev., 1991. **26**: p. 1-57.

5.   Eisman, M., M. Gallego, and M. Valcarcel, *Automatic Continuous-Flow Method for the Determination of Cocaine.* Anal. Chem., 1992. **64**: p. 1509-1512.

6.   Fytche, L.M., et al., *Ion mobility spectrometry of drugs of abuse in customs scenarios: concentration and temperature study.* J. Forensic Sci., 1992. **37**: p. 1550-1566.

7.   Spangler, G.E., J.P. Carrico, and D.N. Campbell, *Recent advances in ion mobility spectrometry for explosives vapor detection.* J. Test. Eval., 1985. **13**: p. 234-240.

8.   Atkinson, D.A. and A.B. Crockett, *Field screening of solis contaminated with explosives using ion mobility spectrometry.* Fifth Int. Workshop on IMS, Jackson, Wyoming, 1996: p. 399-408.

9.   Ewing, R.G., et al., *A critical review of ion mobility spectrometry for the detection of explosives and explosive related compounds.* Talanta, 2001. **54**(3): p. 515-529.

10.   Buxton, T.L. and P.d.B. Harrington, *Rapid mutivariate curve resolution applied to identification of explosives by ion mobility spectrometry.* Anal. Chim. Acta, 2001. **434**: p. 269-282.

11.   Garofolo, F., et al., *Rapid quantitative determination of 2,4,6-trinitrotoluene by ion mobility spectrometry.* Rapid Commun. Mass Spectrom., 1996. **10**(11): p. 1321-1326.

12.   Eiceman, G.A., et al., *Ion mobility spectrometry of halothane, enflurane, and isoflurane anesthetics in air and respired gases.* Anal. Chem., 1989. **61**: p. 1093-1099.

13. Lawrence, A.H., R.J. Barbour, and R. Sutcliffe, *Identification of wood species by ion mobility spectrometry.* Anal. Chem., 1991. **63**: p. 1217-1221.

14. Schmidt, H., et al., *Detection of chlorinated and fluorinated substances using partial discharge ion mobility spectrometry.* Int. J. Ion Mobility Spectrometry, 2000. **3**(1): p. 8-14.

15. Bacon, T., *Real time monitoring of chlorine dioxide without interference from chlorine.* Paper 326P at the Pittsburgh Conference, New Orleans, 1992, 1992.

16. Karpas, Z. and Y. Pollevoy, *Ion Mobility Spectrometric Studies of Organophosphorus Compounds.* Anal. Chim. Acta, 1992. **259**: p. 333-338.

17. Eiceman, G.A., et al., *Ion mobility spectrometry for continuous on-site monitoring of nicotine vapors in air during the manufacture of transdermal systems.* J. Hazard. Mater., 1995. **43**: p. 13-30.

18. Przybylko, A.R.M., et al., *The determination of aqueous ammonia by ion mobility spectrometry.* Anal. Chim. Acta, 1995. **311**: p. 77-83.

19. Soppart, O., et al. *Partial Discharge Ion Mobility Spectrometry for Rapid Quality Assessment of SF6 used in high Voltage Substations*. in *Field Screening Europe*. 1997. Karlsruhe, Germany.

20. Soppart, O., et al., *Ion Mobility Spectrometry for On-site Sensing of SF6 Decomposition.* IEEE Transactions on Dielectrical and Electrical Insulation, 2000. **7**(2): p. 229-233.

21. Budde, K.J. and W.J. Holzapfel, *Detection of volatile organic surface contaminations arising from wafer boxes and cleaning processes.* Proc. - Electrochem. Soc., 1992. **92-7**: p. 271-286.

22. Kotiaho, T., F.R. Lauritzen, and H. Degn, *Membrane Inlet Ion Mobility Spectrometry for On-Line Measurement of Ethanol in Beer and in Yeast Fermentation.* Anal. Chim. Acta, 1995. **309**: p. 317-325.

23. Allinson, G., *Application of Hand-Held Mobility Spectrometres as Sensors in Manufacturing Industries.* J. Autom. Chem., 1998. **20**: p. 1-7.

24. Ogden, I.D. and N.J.C. Strachan, *Enumeration of Escherichia coli in cooked and raw meats by ion mobility spectrometry.* J. Appl. Bacteriol., 1993. **74**: p. 402-405.

25. Bernard, C., et al., *Instrumental detection of coliform bacteria for industrial control of drinking water quality.* Water Sci. Technol., 1988. **20**: p. 185-191.

26. Karpas, Z., et al., *Novel application for ion mobility spectrometry: diagnosing*

vaginal infections through measurement of biogenic amines. Anal. Chim. Acta, 2002. **224073**: p. 1-9.

27.   Snyder, A.P., et al., *Detection of bacteria by ion mobility spectrometry.* Anal. Chem., 1991. **63**: p. 526-529.

28.   Tabrizchi, M., *Ion mobility spectrometry of alkali salts.* Int. J. Ion Mobility Spectrom., 2001. **4 (2)**(2): p. 74-76.

29.   Dion, H.M., K.L. Ackerman, and H.H. Hill Jr., *Detection of inorganic ions from water by electrospray ionizatio-ion mobility spectrometry.* Talanta, 2002. **57**: p. 1161-1171.

30.   Turner, R.B. and J.L. Brokenshire, *Hand-Held Ion Mobility Spectrometers.* Trend Anal. Chem., 1994. **13**: p. 275-280.

31.   Eiceman, G.A., A.P. Snyder, and D.A. Blyth, *Monitoring of aiborne organic vapors using ion mobility spectrometry.* Int. J. Environ. Anal. Chem., 1989. **38**: p. 415-425.

32.   Eiceman, G.A., et al., *Ion mobility spectrometry as flow-injection detector and continuous flow monitor for aniline in hexane and water.* Talanta, 1992. **39**: p. 459-467.

33.   Tuovinen, K., M. Kolehmainen, and H. Paakkanen, *Determination and identification of pesticides from liquid matrices using ion mobility spectrometry.* Analytica Chimica Acta, 2001. **429**: p. 257-268.

34.   Sielemann, S., et al., *Quantitative Analysis of Benzene, Toluene, and m-Xylene with the Use of a UV-Ion Mobility Spectrometer.* Field Anal. Chem. Technol., 2000. **4**(4): p. 157-169.

35.   Leasure, C.S., et al., *Photoionization in air with ion mobility spectrometry using a hydrogen discharge lamp.* Anal. Chem., 1986. **58**: p. 2142-2147.

36.   Baumbach, J.I., et al., *Detection of the Gasoline Components Methyl tert-Butyl Ether, Benzene, Toluene, and m-Xylene Using Ion Mobility Spectrometers with a Radioactive and UV Ionization Source.* Anal. Chem., 2003. **75**: p. 1483-1490.

37.   Borsdorf, H., et al., *Rapid on-site determination of chlorobenzene in water samples using ion mobility spectrometry.* Anal. Chim. Acta, 2001. **440**: p. 63-70.

38.   Borsdorf, H., et al., *Corona discharge ion mobility spectrometry of aliphatic and aromatic hydrocarbons.* Anal. Chem. Acta, 2000. **403**: p. 235-242.

39.   Borsdorf, H., et al., *Determination of n-alkanes and branched chain alkanes by Corona discharge ion mobility spectrometry.* Int. J. Ion Mobility Spectrom., 1999. **2**(1): p. 9-14.

40.   Eiceman, G.A., et al., *Effects of laser beam parameters in laser-ion mobility spectrometry.* Anal. Chem., 1986. **58**: p. 1690-1695.

41.   Young, D., et al., *Laser desorption–ionization of polycyclic aromatic hydrocarbons from glass surfaces with ion mobility spectrometry analysis.* Anal. Chim. Acta, 2002. **453**: p. 231-243.

42.   Gormally, J. and J. Phillips, *The performance of an ion mobility spectrometer for use with laser ionization.* Int. J. Mass Spectrom. Ion Processes, 1991. **107**(3): p. 441-51.

43.   Buryakov, I.A., et al., *A New Method of Separation of Multi-Atomic Ions by Mobility at Atmospheric Pressure Using a High-Frequency Amplitude-Asymmetric Strong Electric Field.* Int. J. Mass Spectrom. Ion Proc., 1993. **128**: p. 143-148.

44.   Wu, C., et al., *Surface Ionization Ion Mobility Spectrometry.* Anal. Chem., 1999. **71**(1): p. 273-278.

45.   Wittmer, D., et al., *Electrospray ionization ion mobility spectrometry.* Anal. Chem., 1994. **66**: p. 2348-2355.

46.   Hoaglund, C.S., ValentineS.J., and D.E. Clemmer, *An ion trap interface for ESI-ion mobility experiments.* Anal. Chem., 1997. **69**(20): p. 4156-4161.

47.   Purves, R.W., D.A. Barnett, and R. Guevremont, *Separation of protein conformers using electrospray-high field asymmetric waveform ion mobility spectrometry-mass spectrometry.* Int. J. Mass Spectrom., 2000. **197**: p. 163-177.

48.   Miller, R.A., et al., *A novel micromachined high-field asymmetric waveform-ion mobility spectrometer.* Sensors and Actuators B-Chemical, 2000. **67**(3): p. 300-306.

49.   Eiceman, G.A., et al., *Miniature radio-frequency mobility analyzer as a gas chromatographic detector for oxygen-containing volatile organic compounds, pheromones and ohter insect attractants.* J. Chromatogr. A, 2001. **917**: p. 205-217.

50.   Teepe, M., et al. *Miniaturized Ion Mobility Spectrometer*. in *Proc. Intern. J. Ion Mob. Spectrom. 9th Int. Conf. Ion Mob. Spectrom.* 2001.

51.   Wiley, W.C. and I.H. McLaren, *Time-of-Flight Mass Spectrometer with Improved Resolution.* Rev. Sci. Inst., 1955. **26**(12): p. 1150-1157.

52.   Stephens, W.E., *A Pulsed Mass Spectrometer With Time Dispersion.* Phys. Rev., 1946(69): p. 691.

53.   Wolff, M.M. and W.E. Stephens, *A Pulsed Mass Spectrometer with Time Dispersion.* Rev. Sci. Instrum., 1953. **24**: p. 616-617.

54.   Wiley, W.C. and I.H. McLaren, *Time-of-Flight Mass Spectrometer With Improved Resolution.* J.Mass Spectrom., 1997. **32**: p. 4-11.

55.   Gohlke, R.S. and F.W. McLafferty, *Gas Chromatography / Mass spectrometry.* J. Am. Soc. Mass Spectrom., 1993. **4**: p. 367-371.

56.   Harrington, D.B., *The Time-of-Flight Mass Spectrometer, in Advances in Mass Spectrometry.* Pergamon Press: Oxford, 1959: p. 249-265.

57.   Guilhaus, M., *The Return of Time-of-Flight to Analytical Mass Spectrometry.* Adv. Mass Spectrom., 1995. **13**: p. 213-226.

58.   Guilhaus, M., V. MLynski, and D. Selby, *Perfect Timing: TOF-MS.* Rapid Commun. Mass Spectrom., 1997. **11**: p. 951-962.

59.   Dawson, J.H. and M. Guilhaus, *Orthogonal-acceleration Time-of-flight Mass Spectrometer.* Rapid. Commun. Mass Spectrom., 1989. **3**: p. 155-159.

60.   Dodonov, A.F., I.V. Chernushevich, and V.V. Laiko, *Time-of-flight mass spectrometry.* editor: R.J. Cotter, Washington DC: ACS: p. 108-123.

61.   Chernushevich, I.V., W. Ens, and K.G. Standing, *In electrospray ionization mass spectrometry.* Cole R.B., Ed., John Wiley & Sons, New York, 1997: p. 203-234.

62.   Gerhard, P.H., S. Loffler, and K.H. Homann, *Polyhedral carbon ions in hydrocarbon flames.* Chem. Phys. Lett, 1987. **137**(4): p. 306-310.

63.   Olthoff, J.K., I.A. Lys, and R.J. Cotter, *A pulsed time-of-flight mass spectrometer for liquid secondary ion mass spectrometry.* Rapid. Commun. Mass Spectrom., 1988. **2**: p. 171-175.

64.   Kennedy, R.A., C.Y. Kung, and J.P. Miller, *Ion and Cluster Ion Spectroscopy and Structure.* Editor Maier J.P., Elsevier: Amsterdam, 1989: p. 213-219.

65.   Sin , C.H., E.D. Lee, and M.L. Lee, *Atmospheric pressure ionization time-of-flight mass spectrometry with a supersonic ion beam.* Anal. Chem, 1991. **63**: p. 2897-2900.

66.   Myers, D.P., et al., *An inductively coupled plasma—time-of-flight mass spectrometer for elemental analysis. Part I: Optimization and characteristics.* J.

Am. Soc. Mass Spectrom., 1994. **5**(11): p. 1008-1016.

67. Chapman, J.R., *'ionization method', in Encyclopedia of Analytical Science.* ed. Townsend A., Academic Press, London, 1995. **5**.

68. Macfarlane, R.D. and D.F. Torgerson, *Californium 252 Plasma Desorption Mass Spectrometry.* Science, 1976. **191**(4230): p. 920-925.

69. Benninghoven, A. and W.K. Sichtermann, *Detection, identification, and structural investigation of biologically important compounds by secondary ion mass spectrometry.* Anal. Chem., 1978. **50**(8): p. 1180-1184.

70. Lorenz, S.A., E.P. Maziarz, and T.D. Wood, *Electrospray Ionization Fourier Transform Mass Spectrometry of Macromolecules: The First Decade.* Appl. Spectrosc., 1999. **53**(1): p. 18A-36A.

71. Zenobi, R. and R. Knochenmuss, *Ion formation in MALDI mass spectrometry.* Mass Spectrom. Rev., 1998. **17**(5): p. 337-366.

72. Byrdwell, W.C. and W.E. Neff, *Dual parallel electrospray ionization and atmospheric pressure chemical ionization mass spectrometry (MS), MS/MS and MS/MS/MS for the analysis of triacylglycerols and triacylglycerol oxidation products.* Rapid Commun. Mass Spectrom., 2002. **16**(4): p. 300-319.

73. Griffin, G.W., et al., *Ion mass assignments based on mobility measurements.* Anal. Chem., 1973. **45**: p. 1204.

74. Carroll, D.I., et al., *Identification of positiv reactant ions observed for nitrogen carrier gas in plasma chromatograph mobility studies.* Anal. Chem., 1975. **47**: p. 1956-1959.

75. Kim, S.H., K.R. Betty, and F.W. Karasek, *Plasma chromatography of benzene with mass identified mobility spectra.* Anal. Chem., 1978. **50**: p. 1784-1788.

76. Carr, T.W., *.If.Plasma chromatography of isomeric dihalogenated benzene.* J. Chrom. Sci., 1977. **15**: p. 85-88.

77. Karasek, F.W., S.H. Kim, and H.H. Hill, Jr., *Mass identified mobility spectra of p-nitrophenol and reactant ions in plasma chromatography.* Anal. Chem., 1976. **48**: p. 1133-1137.

78. Lawrence, A.H. and A.A. Nanji, *Ion mobility spectrometry and ion mobility spectrometry/mass spectrometric characterization of dimenhydrinate.* Biomed. Environ. Mass Spectrom., 1988. **16**: p. 345-347.

79. Lawrence, A.H., *Ion mobility spectrometry/mass spectrometry of some prescription and illicit drugs.* Anal. Chem., 1986. **58**: p. 1269-1272.

80.	Karasek, F.W. and H.H. Hill, Jr., *Plasma chromatography of heroin and cocaine with mass identified mobility spectra.* J. Chromatogr., 1976. **117**: p. 327-336.

81.	Wu, C., et al., *Electrospray Ionization High-Resolution Ion Mobility Spectrometry-Mass Spectrometry.* Anal. Chem., 1998. **70**(23): p. 4929-4938.

82.	Matz, L.M., G.R. Asbury, and H.H. Hill, *Two-dimensional separations with electrospray ionization ambient pressure high-resolution ion mobility spectrometry/quadrupole mass spectrometry.* Rapid Communications in Mass Spectrometry, 2002. **16**(7): p. 670-675.

83.	Asbury, G.R., et al., *Separation and identification of some chemical warfare degradation products using electrospray high resolution ion mobility spectrometry with mass selected detection.* Anal. Chim. Acta, 2000. **404**: p. 273-283.

84.	Asbury, G.R., J. Klasmeier, and H.H.J. Hill, *Analysis of explosives using electrospray ionization/ion mobility spectrometry (ESI/IMS).* Talanta, 2000. **50**: p. 1291-1298.

85.	Wu, C., et al., *Separation of Isomeric Peptides Using Electrospray Ionization/High Resolution Ion Mobility Spectrometry.* Anal. Chem., 2000. **72**(2): p. 391-395.

86.	Valentine, S.J., S.L. Koeniger, and D.E. Clemmer, *A split-field drift tube for separation and efficient fragmentation of biomolecular ions.* Analytical Chemistry, 2003. **75**(22): p. 6202-6208.

87.	Wu, C., W.F. Siems, and H.H.J. Hill, *Secondary Electrospray Ionization Ion Mobility Spectrometry/Mass Spectrometry of Illicit Drugs.* Anal. Chem., 2000. **72**(2): p. 396-403.

88.	Steiner, W.E., B.H. Clowers, and H.H. Hill, *Rapid separation of phenylthiohydantoin amino acids: ambient pressure ion-mobility mass spectrometry (IMMS).* Analytical and Bioanalytical Chemistry, 2003. **375**(1): p. 99-102.

89.	Guevremont, R., K.W.M. Siu, and J. Wang, *Combined Ion Mobility/Time-of-Flight Mass Spectrometry Study of Electrospray-Generated Ions.* Anal. Chem., 1997. **69**(19): p. 3959-3965.

90.	Purves, R.W., et al., *Mass spectrometric characterization of a high-field asymmetric waveform ion mobility spectrometer.* Review of Scientific Instruments, 1998. **69**(12): p. 4094-4105.

91.	Purves, R.W. and R. Guevremont, *Electrospray Ionization High-Field Asymmetric Waveform In Mobility Spectrometry - Mass Spectrometry.* Anal.

Chem., 1999. **71**(13): p. 2346-2357.

92. Guevremont, R., et al., *Calculation of ion mobilities from electrospray ionization high-field asymmetric waveform ion mobility spectrometry mass spectrometry.* Journal of American Physics, 2001. **114**(23): p. 10270-10277.

93. Barnett, D.A., R. Guevremont, and R.W. Purves, *Determination of parts-per-trillion levels of chlorate, bromate, and iodate by electrospray ionization/high-field asymmetric waveform ion mobility spectrometry/mass spectrometry.* Applied Spectroscopy, 1999. **53**(11): p. 1367-1374.

94. Ells, B., et al., *Trace level determination of perchlorate in water matrices and human urine using ESI-FAIMS-MS.* J. Environ. Monit., 2000. **2**: p. 393-397.

95. Handy, R., et al., *Determination of nanomolar levels of perchlorate in water by ESI-FAIMS-MS.* J. Anal. At. Spectrom., 2000. **15**(8): p. 907-911.

96. Ells, B., et al., *Detection of Nine Chlorinated and Brominated Haloacetic Acids at Part-per-Trillion Levels Using ESI-FAIMS-MS.* Anal. Chem., 2000. **72**(19): p. 4555-4559.

97. Ells, B., et al., *Detection of microcystins using electrospray ionization - High-Field asymmetric waveform ion mobility spectrometry - Mass sectrometry.* EnviroAnalysis 2000, 2000: p. 95-99.

98. Guevremont, R., et al., *Analysis of a Tryptic Digest of Pig Hemoglobin Using ESI-FAIMS-MS.* Anal. Chem., 2000. **72**(19): p. 4577-4584.

99. Barnett, D.A., et al., *Application of ESI-FAIMS-MS to the Analysis of Tryptic Peptides.* J. Am. Soc. Mass Spectrom., 2002. **13**: p. 1282-1291.

100. Barnett, D.A., et al., *Tandem mass spectra of trypic peptides at signal-to-background ratios approaching unity using electrospray ionization highl-field asymmetric waveform ion mobility spectrometry/hybrid quadrupole time-of-flight mass spectrometry.* Rapid Communications in Mass Spectromerty, 2002. **16**: p. 676-680.

101. McCooeye, M.A., et al., *Quantitation of Amphetamine, Methamphetamine, and Their Methylenedioxy Derivatives in Urine by Solid-Phase Microextraction Coupled with Electrospray Ionization - High-Field Asymmetric Waveform Ion Mobility Spectrometry - Mass Spectrometry.* Anal. Chem., 2002. **74**(13): p. 3071-3075.

102. Liu, Y. and D.E. Clemmer, *Characterization Oligosaccharides Using Injected-Ion Mobility Mass Spectrometry.* Anal. Chem., 1997. **69**(13): p. 2504-2509.

103. Valentine, S.J., et al., *Gas-phase separations of protease digests.* Journal of the American Society for Mass Spectrometry, 1998. **9**(11): p. 1213-1216.

104.   Mosier, P.D., et al., *Prediction of peptide ion collision cross sections from topological molecular structure and amino acid parameters.* Analytical Chemistry, 2002. **74**(6): p. 1360-1370.

105.   Valentine, S.J., et al., *Multidimensional separations of complex peptide mixtures: a combined high-performance liquid chromatography/ion mobility/time-of-flight mass spectrometry approach.* International Journal of Mass Spectrometry, 2001. **212**(1-3): p. 97-109.

106.   Taraszka, J.A., A.E. Counterman, and D.E. Clemmer, *Gas-phase separations of complex tryptic peptide mixtures.* Fresenius Journal of Analytical Chemistry, 2001. **369**(3-4): p. 234-245.

107.   Myung, S., et al., *Development of high-sensitivity ion trap ion mobility spectrometry time-of-flight techniques: A high-throughput nano-LC-IMS-TOF separation of peptides arising from a Drosophila protein extract.* Analytical Chemistry, 2003. **75**(19): p. 5137-5145.

108.   Lee, Y.J., et al., *Development of high-throughput liquid chromatography injected ion mobility quadrupole time-of-flight techniques for analysis of complex peptide mixtures.* Journal of Chromatography B-Analytical Technologies in the Biomedical and Life Sciences, 2002. **782**(1-2): p. 343-351.

109.   Gillig, K.J., et al., *Coupling High-Pressure MALDI with Ion Mobility/Orthogonal Time-of-Flight Mass Spectrometry.* Anal. Chem., 2000. **72**(17): p. 3965-3971.

110.   John, M., et al., *Oligonucleotide analysis with MALDI-ion-mobility-TOFMS.* Anal Bioanal Chem, 2002. **373**: p. 612-617.

111.   Bluhm, B.K., K.J. Gillig, and D.H. Russell, *Development of a Fourier-transform ion cyclotron resonance mass spectrometer-ion mobility spectrometer.* Rev. Sci. Instrum., 2000. **71**(11): p. 4078-4086.

112.   Steiner, W.E., et al., *Secondary ionization of chemical warfare agent simulants: Atmospheric pressure ion mobility time-of-flight mass spectrometry.* Analytical Chemistry, 2003. **75**(22): p. 6068-6076.

113.   Syage, J.A. and M.D. Evans, *Photoionization Mass Spectrometery- a powerfull new tool for drug discovery.* Spectroscopy, 2001. **16**(11): p. 14-21.

114.   Sielemann, S., et al., *Detection of alcohols using UV - Ion mobility spectrometers.* Anal. Chim. Acta, 2001. **431**: p. 293-301.

115.   Sielemann, S., et al., *Detection of Trans-1,2-Dichloroethene, Trichloroethene and Tetrachloroethene using Multi-Capillary Columns Coupled to Ion Mobility Spectrometers with UV-Ionisation Sources.* Int. J. Ion Mobility Spectrom., 1999. **2**(1): p. 15-21.

116. Sielemann, S., et al., *Ion mobility spectrometer with UV-ionization source for the determination of chemical warfare agent simulants.* Int. J. Ion Mobility Spectrom., 2001. **4 (2)**(2): p. 81-84.

117. Bradbury, N.E. and R.A. Nielsen, *Absolute Values of the electron mobility in hydrogen.* Phys. Rev., 1936. **49**: p. 388-393.

118. Revercomb, H.C. and E.A. Mason, *Theory of Plasma Chromatography / Gaseous Electrophoresis - A Review.* Anal. Chem., 1975. **47**: p. 970-983.

119. Whealton, J.H. and E.A. Mason, *Transport Coefficients of Gaseous Ions in a Electric Field.* Ann. Phys., 1974. **84**: p. 8-38.

120. Karpas, Z., R.M. Stimac, and Z. Rappoport, *Differentiating between large isomers and derivation of structural information by ion mobility spectrometry/mass spectrometry techniques.* Int. J. Mass Spectrom. Ion Proc., 1988. **83**: p. 163-175.

121. St.Louis, R.H. and H.H. Hill, Jr., *Ion mobility spectrometry in analytical chemistry.* Crit. Rev. Anal. Chem., 1990. **21**: p. 321-355.

122. Freedman, A.N., *The photoionization detector-Theory, performance and application as alow-level monitor of oil vapor.* Journal of Chromatography, 1980. **190**: p. 263-273.

123. Bergman, T., T.P. Martin, and H. Schaber, *High resolution time-of-flight mass spectrometers. Part III. Reflector design.* Rev. Sci. Instrum., 1990. **61**: p. 2592-2600.

124. Schmid, R.P. and C. Weickhardt, *Designing reflectron time-of-flight mass spectrometers with and without grids: a direct comparison.* Int. J. Mass Spectrom., 2001. **206**: p. 181-190.

125. Grotemeyer, J., et al., *Biomolecules in the Gasphase.II. Multiphoton Ionization Mass Spectra of Angiotensin I.* Org. Mass Spectrom., 1986. **21**: p. 595-599.

126. Grotemeyer, J., et al., *Biomolecules in the Gasphase. I. Multiphoton Ionization Mass Spectrometry of Native Chlorophylls.* J. Am. Chem. Soc., 1986. **108**: p. 4233-4239.

127. Gross, J.H., *Mass Spectrometry.* Springer-Verlag Berlin Heidelberg 2004, 2004: p. 120-121.

128. Stevens, C., D.K.W. Jenkins, and D.C. Wilson, *Testing procedure for evaluating codisposal of industrial wastes and municipal refuse with particular reference to pesticides.* ASTM Spec. Tech. Publ., 1983. **805**: p. 111-126.

129. Wiza, J.L., *Microchannel Plate Detectors.* Nucl. Instrum. Methods, 1979. **162**: p. 587-601.

130. Laprade, B.N. and R.J. Labich, *Microchannel Plate-Based Detectors in Mass Spectrometry.* Spectroscopy, 1994. **9**: p. 26-30.

131. Sielemann, S., *Detektion flüchtiger organischer Verbindungen mittels Ionenmobilitätsspektrometrie und deren Kopplung mit Multi-Kapillar-Gas-Chromatographie.* Ph. dissertation, 1999.

132. Wollnik, H., *Ion Optics in Mass Spectrometers.* Journal of Mass Spectrometry, 1999. **34**: p. 991-1006.

133. Boyle, J.G. and C.M. Whitehouse, *Time-of-Flight Mass Spectrometry with an Electrospray Ion Beam.* Anal. Chem., 1992. **64**: p. 2084-2089.

134. Guilhaus, M., *Spontaneous and defleced drift-trajectories in orthogonal acceleration time-of-flight mass spectrometry.* J. Am. Soc. Mass Spectrom., 1994(5): p. 588-595.

135. Spangler, G.E., *Characterization of the ion-sampling pinhole interface for an ion mobility spectrometer/mass spectrometer system.* Int. J. Mass Spectrom., 2001. **208**: p. 169-191.

136. Miller, D.R., *in Atomic and Molecular Beams.* Scoles, G. (Edit), Oxford University Press, New York, 1988. **Vol. 1, Chapter 2,**.

137. ashkenas, H. and F.S. Sherman, *in Rarefied Gas Dynamics, Fourth Symposium IV.* Deleeuw, J.H. (Ed.), Academic Press, New York, 1966. **2, Section 7**.

138. Noggle, J.H., Physical Chemistry, Little, Brown,& company, Boston, 1985.

139. Murad E. and Inghram M.G., *photoionization of aliphatic ketones.* J. Chem. Phys., 1964. **40**(11): p. 3263-3275.

140. Eiceman, G.A., E.G. Nazarov, and J.E. Rodriguez, *Chemical class information in ion mobility spectra at low and elevated temperatures.* Analytica Chimica Acta, 2001. **433**(1): p. 53-70.

141. Trott, W.M., Blais N. C., and W.E. d., *Molecular beam photoionization study of acetone and acetone-d_6.* J. Chem. Phys., 1978. **69**(7): p. 3150-3157.

142. Xie, Z., et al., *Determination of acetone, 2-butanone, diethyl ketone and BTX using HSCC-UV-IMS.* Analytical and Bioanalytical Chemistry, 2002. **372**(5-6): p. 606-610.

143. Sielemann, S., et al., *Quantitative analysis of benzene, toluene, and m-xylene with the use of a UV-ion mobility spectrometer.* Field Analytical Chemistry and Technology, 2000. **4**(4): p. 157-169.

144. Ruzsanyi, V., S. Sielemann, and J.I. Baumbach, *Determination of microbial volatile compounds (MVOC) using IMS with different ionsation sources.* Int. J. Ion Mobility Spectrometry, 2002. **5 (3)**(3): p. 138-142.

145. Vautz, W., S. Sielemann, and J.I. Baumbach, *Determination of terpenes in humid ambient air using ultraviolet ion mobility spectrometry.* Anal Chimica Acta, 2004(513): p. 393-399.

10. <u>Abbreviations index</u>

a_0	speed of sound in the interface
A	analyte molecule
AB	analyte molecule
AB*	excited analytical molecule AB
[AB]	concentration of analytical molecule AB
AH	absolute humidity
APCI	atmospheric pressure chemical ionization
APPI	atmospheric pressure photoionization
b	the length of the modulator in X-direction
ß	radioaktive particles
c	concentration
C	drift gas molecule
C_0	initial concentration of sample gas
C_g	sample gas concentration
[C]	conzentration of drift gas molecule C
CWA	chemical warfare agents
d_1	lengths of the modulator of linear TOF
d_2	lengths of the accelerator of linear TOF
D	lengths of the field-free drift tube of linear TOF
D_o	diameter of the orifice
D_1	distance of the start position of ions in modulator of TOF
ε	exponential coefficient
e	electron
E	Elcetric field
E_1	extracting field in TOF
E_2	Accelerating field in TOF
EI	electron impact
ESI	electrospray ionization
f	mass spectrum repetition rate
f_0	focus length
F	Faraday constant
FAB	fast atom bombardment
FWHM	full-width at half-maximum height
G_0	gas flow rate

G_1	first grid in TOF
G_2	second grid in TOF
h	Planck's constant
i	current
I	transmitted photo intensity
I^0	incident photo intensity
I^0-I	absorbed photo intensity
IMS	ion mobility spectrometer
k	reaction rate constant
k_b	Boltzmann constant
K	Ion mobility
K_0	Ruduced ion mobility
K_e	ion's kinetic energy
ΔK_e	ions energy spread
K_x	ion's initial kinetic energy
K_z	ion's kinetic energy after orthogonal acceleration
L	length of field-free drift tube of TOF
L_d	length of drift tube of IMS
L_i	length of the ionization room
L_m	wavelength of UV lamp
m	analyte ion mass
Δm	mass difference
M	analyte molecule
M^+	analyte molecular ion
M_m	molecular mass
MALDI	matrix assistant laser desorption ionization
MCC	multi capillary column
MCP	microchannel plate
MH^+	protonated analyte molecular ion
MS	mass spectrometer
n_0	source number density
η	photoionization efficiency
ηs	photoionization cross section
n_l	Ionendichte
N	number density of drift gas
N_0	Avogadro constant
Ω	collision cross section of the ion

oa	orthogonal acceleration
P	pressure
P_0	Standard pressure 101,3 kPa
PID	photoionization detector
ppm	percent per million
δ	specific heat ratio
R	reaction rate
R_g	individual gas constant
R_m	resolving power of mass spectrometer
RH	relative humidity
s	Adsorption coefficient
SIMS	secondary ionization
t	time
t_d	drift time of ions in IMS
T	Temperature
T_0	Standard temperature 273 K
TDC	Time-to-digital converter
TOF	time-of-flight mass spectrometer
µ	Reduced mass
UV	ultraviolet
UV-IMS	ISAS UV-IMS
UV-IMS[PID]	ISAS UV-IMS, operated as PID
v_c	carrier gas flow rate
v_d	Velocity of the ions in IMS
V_g	volume of the dilution flask
V_x	Ion's initial velocity in x direction
V_y	Ion's initial velocity in y direction
v_z	Ion's initial velocity in z direction
Δv_z	initial velocity of the ion towards the repeller
z	charge of the ions
Δz	spatial spread of ions

Curriculum Vitae

Name   Fang Li

Day of birth   24.10.1970

Place of birth   Changsha, P.R.China

Marital status   Married, 1 Sohn, 4 years old

Education

09/1977 - 06/1988   Ground school and high school in China

09/1988 - 06/1992   Chemistry department in Hunan University of Science and
                     Technology, P.R. China. Bachelor.

09/1996 - 06/1999   Analytical chemistry in Zhongshan University, V.R. China.
                     Master.

09/2000 – 12/2004   Dissertation in ISAS-institute for analytical sciences, in
                     Dortmund. Supervised by Dr.J.I. Baumbach and Prof. A.
                     Manz.

Work experience

09/1992 - 06/1996   Teachassistant, Chemistry department in Hunan University of

                     Science and Technology, P.R. China.

09/1999 - 06/2000   Lecturer, Chemistry department in Hunan University of
                     Science and Technology, P.R. China.